Composite Higgs models on the lattice

Hungarian Academy of Sciences doctoral thesis

Daniel Nogradi

Eotvos Lorand University

Institute of Physics

Department of Theoretical Physics

2017

Acknowledgments

I would like to thank my collaborators throughout the years with whom I was working on the topics contained in this thesis. It was a pleasure working closely together with Julius Kuti, Zoltan Fodor and Kieran Holland on various aspects of composite Higgs dynamics in the past 10 years and I have learned a lot from all of them. We were joined by several researchers at various stages of our work, Chris Schroeder, Ricky Wong and Santanu Mondal, all of whom were always ready to discuss physics whether related to our work or not.

I also would like to thank Sandor Katz, Szabolcs Borsanyi, Kalman Szabo, Christian Hoelbling, Stefan Krieg, Balint Toth, Norbert Trombitas, Stephan Durr, Simon Mages, Thomas Lippert and Attila Pasztor with whom I have collaborated on the topic of QCD thermodynamics on the lattice. This collaboration also shaped my thinking about strongly interacting gauge theories in general and hence was extremely helpful for our work on composite Higgs dynamics presented in this thesis.

Contents

Chapter 1

Introduction and conclusion

The 2012 discovery of a relatively light Higgs boson with a mass of approximately 125 GeV at the Large Hadron Collider in CERN was a major milestone in our understanding of the Standard Model of particle physics and the electro-weak sector in particular [1, 2]. The discovery provided the last missing piece of the Standard Model which successfully describes the visible Universe with astonishing precision. The high precision achieved is only possible as a result of very precise theoretical calculations based on the Standard Model and very precise measurements at our accelerators, performed over the course of the past 40 years.

Even though the discovery crowned the Standand Model as the most precise and most detailed description of the elementary particles and their interactions, there are a number of shortcomings that are nevertheless present. These shortcomings are not new but gained further prominence by the precise knowledge of the Higgs mass, which was a free parameter prior to 2012. One of these shortcomings is inherent to the Standard Model itself and is usually referred to as the hierarchy problem or fine tuning problem. More specifically, the 125 GeV Higgs mass in the Standard Model is a result of an enormous cancellation between two terms with typical sizes 10^{19} GeV but opposite signs. Technically, this cancellation is necessary to account for the 125 GeV mass because the Higgs particle is described by an elementary spin-0 scalar field whose mass is not protected by any symmetries. The Planck scale 10^{19} GeV comes about as the highest possible scale where the Standard Model can still be valid, beyond that quantum graviational effects certainly kick in. This large hierarchy of scales or the necessary associated fine tuning is highly unnatural and certainly not something we have seen in other phenomena in Nature. The only way to resolve this apparent paradox is to introduce new hitherto unobserved particle sectors well below the Planck scale, i.e. new physics beyond the Standard Model.

The other set of shortcomings of the Standard Model come from cosmological observations and also call for new physics. It is well established by now that only about 5% of the Universe is visible i.e. the Standard Model only applies to this small fraction. The remaining 95% consists of two parts, about 27% dark matter and 68% dark energy, the latter of which may be accounted for by a cosmological constant. The dark matter sector can not be explained by any particle content already present in the Standard Model (such as neutral hadrons or neutrinos) as direct detection experiments [3–6] would have seen it already. The only concievable way to have a description for this approximately 27% of the Universe is to introduce new particles and new interactions to the Standard Model. Any new model of dark matter will be tested by experimental results from dedicated detectors (XENON [3], LUX [4], CDMS [5], among others), the Large Hadron Collider and by cosmological observations.

There are (infinitely) many ways in which the Standard Model can be extended to account for dark matter or any new physics which solves the hierarchy problem. Present and past experimental results set stringent constraints of course, but the possibilities are still vast. The only way forward seems to be reasonable guidelines or general principles which proved useful in particle physics before and are sufficiently well-motivated. One of these guidelines that I find most persuasive is the observation that the mass in the well-understood 5% of the Universe is the result of strong interactions. Even though according to the Standard Model the Higgs particle provides masses to the leptons and quarks (along with the W and Z bosons) the vast majority of the observed mass of stable particles in the visible Universe is originating from the strongly interacting dynamics of Quantum Chromodynamics (QCD) [7]. In QCD the elementary building blocks, quarks and gluons, are not observed directly as stable particles but rather only their composits, baryons or potentially glueballs. Incidentally, QCD is free from any fine tuning problems and is truely a fundamental theory. Hence it is natural to assume that viable theories beyond the Standard Model will be based on strongly interacting models and the observable particles will be composits of more elementary building blocks. This is especially likely for dark matter since about the only aspect we are certain about it is that it contributes a large fraction of the total mass of the Universe. This approach, if applied to the Higgs sector of the Standard Model, also leads to the possibility that the Higgs boson is a composite particle itself and hence the fine tuning problem is averted for the lack of an elementary spin-0 scalar particle.

A key feature of QCD is that it is an asymptotically free non-abelian gauge theory. Asymptotic freedom guarantees the lack of a fine tuning problem, although the more lax requirement of asymptotic safety would also be sufficient. The very nature of non-abelian gauge theories is that they are generically strongly interacting and hence are notoriously difficult to study quantitatively. The experience from QCD and more recently strongly interacting extensions of the Standard Model nevertheless suggests that numerical simulations will be able to allow for robust and quantitative conclusions regarding specific models for physics beyond the Standard Model.

Our class of extensions replaces the essentially weakly coupled Higgs sector by strong coupling dynamics, the idea being guided by analogies from QCD [8,9]. Electroweak symmetry breaking in the Standard Model is then the analog of spontaneous chiral symmetry breaking in QCD and hypothetical new particles called technifermions and technigluons are analogs of fermions and gluons in QCD. This analogy is appealing because symmetry breaking becomes a dynamical phenomenon and the fine tuning problem is solved. Models based on this analogy are often called Strong Dynamics models and will of course only be viable if all constraints given by the known and confirmed sectors of the Standard Model are fulfilled.

One such constraint is that the coupling constant of the model should not change much over a considerable energy range and should be large, i.e. the coupling constant should walk. The reason for walking is that without it a tension exists between the observed smallness of Flavor Changing Neutral Currents and the fermion masses [10, 11]. Walking behavior is expected to occur for theories just below the conformal window, i.e. below the range of flavor number N_f where the model possesses an infrared fixed point. A model just below the conformal window is expected to be "almost" conformal and hence the coupling constant is expected to be slowly changing over a large energy range.

Another strong constraint from electro-weak precision data is the smallness of the S-parameter, related to the spectrum of vector and axial resonances of the model [12]. Perturbation theory suggests that it is proportional to N_f which would indicate that scaled-up QCD where N_f needs to be around $10 - 12$ in order to have walking is not compatible with a small S-parameter. There is no reason however to trust perturbation theory close to the lower end of the conformal window due to strong coupling, hence the fundamental model deserves further study. In any case the fermion content of the model can be increased also by increasing the dimension of the fermion representation. This would have the advantageous effect that the conformal window would move to lower N_f values resulting in a hopefully smaller S-parameter [13,14]. This observation suggests the use of the sextet representation for gauge group $SU(3)$ where perturbative estimates indicate $N_f = 2$ might already be walking.

The most recent constraint on model building is the 2012 discovery of a relatively light new boson at the LHC. Its mass of 125 GeV can only be incorporated into an extension of the Standard Model by strong dynamics if the chosen model contains such a light composite particle in its spectrum. The $N_f = 2$ sextet model with gauge group $SU(3)$ is a promising candidate in this respect as well [15]. If the model is close to the conformal window a light dilaton-like particle might exist in the spectrum. In QCD language this would be the scalar flavor singlet f_0 (or σ) meson. In QCD it is heavy and broad but in a theory close to the conformal window it might be light due to the mild breaking of conformal symmetry [16], although a dilaton-like interpretation is far from being clear [17, 18] . In any case it would be a composite particle.

Yet another reason why the $N_f = 2$ sextet model is appealing from a phenomenological point of view is the fact that the pattern of chiral symmetry breaking (if indeed the model is below the conformal window) is $SU(2) \times SU(2) \to SU(2)$, i.e. the same as in QCD. Hence exactly 3 Goldstone bosons are produced, the right number for the W and Z bosons to “eat”.

Since non-abelian gauge theories are strongly coupled just below the conformal window a non-perturbative method is needed in order to test whether the needed properties are indeed present in any given candidate model. The only tool that does not invoke uncontrolled assumptions and is non-perturbative is a lattice field theoretical approach. Chapter 2 contains a review of the necessary field theory concepts. The lattice field theory literature addressing Strong Dynamics beyond the Standard Model in general and of each technique and method in particular is also reviewed there. Several subtle issues are emphasized which are frequently overlooked in the literature but which are necessary for a critical assessment of the progress in our field. We will make use of these techniques in the subsequent chapters.

Chapter 4 includes our results on the sextet composite Higgs model.

Even though I believe the most promising model from a phenomenological point of view is the sextet model, the fundamental representation deserves study on its own, our results are presented in chapter 5. Many of the new techniques were first tested in the fundamental models and hence chronologically the results from chapter 5 were obtained prior to the results in chapter 4.

It should be kept in mind that the main reason we believe that the Standard Model needs to be extended by new sectors not only at the Planck scale but well below is the principle of Naturalness. Even though this principle is a convincing one there is no guarantee that it will not mislead us. It is possible that eventually it will turn out that the Standard Model is valid up to the Planck scale where a quantum theory of gravity combined with the Standard Model takes over. If this scenario is realized in Nature we will not see new physics in Earth based particle accelerators in the forseeable future. I find this outcome unlikely but in any case the current Run 2 program of the LHC and the further physics program beyond that as well as currently planned new accelerators will definitely shed light on this issue at least up to the energy range they are able to push the energy frontier. Those results will either find new physics or not. If not, several extensions of the Standard Model will be ruled out (whether strongly interacting or not). If new physics is unambiguously found the experimental results need to be compared with theoretical calculations in order to rule out or confirm any particular model. In my work in the past 8 or so years I have studied a class of strongly interacting extensions and a particular realization in detail (the sextet model) in order to have the theoretical results in the event new physics is indeed found.

Chapter 2

Review of the field, techniques and methods

2.1 Introduction

Even though the Standard Model and its electroweak sector in particular are extraordinarily successful in terms of both experimental and theoretical precision the idea of dynamical symmetry breaking came about already in the late 70's [8–10]. The main motivation was and continues to be naturalness and the associated fine tuning problem. In the early technicolor paradigm, scaled up QCD with $\Lambda \sim O(TeV)$ was envisioned to take the place of the Higgs sector, and spontaneous chiral symmetry breaking would be responsible for electroweak symmetry breaking. The resulting Goldstone bosons or techni pions would be eaten by the W and Z bosons and hence the latter would become massive. In particular the model would be either Higgsless or would feature a heavy composite Higgs, analogous to the σ or f_0 meson of QCD, at least according to early expectations.

The initial proposal faced numerous problems including a potentially large S-parameter [12] and the tension between the observed fermion masses and potentially large flavor changing neutral currents [19]. The idea of walking [20,21] was introduced to circumvent some of these issues by assuming that the renormalized coupling was running slowly between two well separated energy scales Λ_{TC} and Λ_{ETC}, where ETC stands for extended technicolor [10,22]. In addition a large mass anomalous dimension was assumed to be generated along the renormalization group trajectory. The large anomalous dimension would guarantee that flavor changing neutral currents remain small while the mass of the top quark is the correct one. At the same time the precise mechanism for fermion mass generation, dubbed extended technicolor, is pushed to a high scale Λ_{ETC} and essentially decouples from the mechanism of electroweak symmetry breaking. Hence the techni gauge sector responsible for electroweak symmetry breaking is thought to be an effective theory only, even though in principle it could be a fundamental theory as QCD.

A natural way to look for models with a coupling that walks is by considering non-abelian gauge theories in the parameter space (G, N_f, R) where G is the gauge group and N_f the number of massless fermion flavors in representation R. In the original technicolor proposals, usually $G = SU(N)$ and the fundamental representation was considered. More generally, once G and R are fixed, N_f may be viewed as a variable and the model may be in one of three phases depending on the value of N_f. Clearly, if N_f is too high asymptotic freedom is lost because the first β-function coefficient will cease to be negative and the theory is trivial. The requirement of asymptotic freedom limits $N_f < N_f^{AF}$ from above and the bound N_f^{AF} is obtained exactly by the 1-loop β-function. Just below this upper bound the model has a Banks-Zaks fixed point with a coupling that is small and can be obtained from a 2-loop calculation [23, 24]. Consequently such a model is a weakly coupled conformal field theory at long distances and all of its properties such as anomalous dimensions, etc., are calculable perturbatively in a reliable way. As N_f is decreased further the fixed point coupling grows. At some critical value N_f^* the coupling becomes strong enough to generate spontaneous symmetry breaking and a dynamical scale like in QCD. Further decreasing N_f towards zero does not change the infrared dynamics in a substantial way although as we will see the detailed properties will be very sensitive to the difference $N_f^* - N_f$. The range $N_f^* < N_f < N_f^{AF}$ is called the conformal window and of course depends on the gauge group G and the representation R. In contrast to the upper end of the conformal window N_f^{AF}, the lower end of the conformal window N_f^* is not calculable in perturbation theory.

It should be noted that the above picture assumes that the flavor number can change continuously which is obviously not the case. For fixed G and R there is only a discrete set of flavor numbers below the upper end of the conformal window N_f^{AF} and the arguments based on a continuous change in N_f may or may not be a good guide. This state of affairs also calls for non-perturbative lattice calculations which in principle can scan all available flavor numbers $N_f < N_f^{AF}$ and determine the infrared properties for each.

A relatively recent development was the realization that higher dimensional representations R have a lower N_f^* and hence lower fermion flavor number would be needed for the theory just below the conformal window. As a result the S-parameter can be hoped to be lower, relative to the fundamental representation, and potentially consistent with electroweak precision data [13, 25, 26]. Compatibility of LHC data and a composite Higgs of the type considered here, including its couplings to the W and Z gauge bosons was scrutinized recently in detail [27].

The present review has a very limited scope and focuses on a selection of topics mostly related to lattice studies. The literature on the subject of dynamical electroweak symmetry breaking, technicolor in its many variants and IR-conformal gauge theories is vast. Extensive reviews on the phenomenological, experimental and formal aspects are available [11, 28–32] as well as more extended reviews of the lattice aspects [33–35].

In section 2.2 we discuss the possibility of a light scalar in strongly coupled gauge theories. In section 2.3 a pedagogical and elementary introduction to the main differences between chirally broken and conformal gauge theories is given, focusing on the scaling properties of the mass spectrum. In section 2.4 we discuss some lattice specific issues and we review the main results on the spectrum for a number of models. In section 2.5 we discuss different definitions of the running coupling, and review related lattice results. Finally in section 2.6 we end with an outlook.

It should be noted that due to the lack of space various very useful approaches of distinguishing conformal and chiral symmetry broken models and studying their properties on the lattice are not discussed in the present review. These include finite temperature studies [36–41], finite size scaling [42–48], radial quantization [49,50], non-degenerate fermion masses for many flavors in order to interpolate between different flavor numbers [51, 52] and the spectral properties of the Dirac operator [54–58].

2.2 Strong dynamics and a light scalar

Even though the original technicolor paradigm of the late 70's envisioned a Higgsless electroweak sector or one with a heavy Higgs, the possibility of a light composite Higgs was nevertheless actively debated [17,18]. It is important to note that the scalar isosinglet mass, naturally, needs to be measured against some other mass scale and its lightness will depend on what scale it is compared to. From a phenomenological point of view the relevant comparison is the mass ratio of the scalar, m_σ, and some other massive state (for instance the vector isotriplet meson m_ϱ) which also stays non-zero in the chiral limit, assuming the model breaks chiral symmetry. This ratio would indicate how far the light scalar is separated from the tower of other massive particle states.

Recent lattice simulations in the (G, N_f, R) parameter space of non-abelian gauge theories show that as the model approaches the conformal window from below the scalar isosinglet meson in fact becomes light, relative to the vector meson, ϱ in QCD. The lattice evidence comes primarily from simulations of $SU(3)$ gauge theory. In the $N_f = 8$ fundamental model with $SU(3)$ lattice calculations indicate that approximately $m_\sigma/m_\varrho \sim 1/2$ can be reached with the available lattice volumes and fermion masses [91–93]. Another model which seems to be close to the conformal window, $SU(3)$ with $N_f = 2$ sextet fermions, also features a light scalar according to lattice calculations. In this model approximately $m_\sigma/m_\varrho \sim 1/4$ was observed [94–96] predicting an even larger separation between the scalar and the rest of the spectrum. These observations make it plausible that a composite Higgs may emerge from a near-conformal gauge theory with its 125 GeV mass obtained after electro-weak corrections are taken into account, most notably the contribution of the top quark [97].

The generation of the Standard Model fermion masses is still left to higher scales and the models are still thought of as effective theories only.

The natural question is what mechanism produces a light scalar out of a strongly interacting non-abelian gauge theory. Again it is important to note what we mean by light. Since just below the conformal window chiral symmetry is broken, all states have masses $\sim \Lambda$ except the Goldstones. What is required is that the ratio of the scalar mass and all other massive states is small. Clearly, there is no small parameter in the theory for fixed (G, N_f, R). One could think of $N_f^* - N_f$ as a small parameter, if one approaches the conformal window from below (leaving aside the issue that N_f is discrete). Then one would be tempted to further argue that as $N_f^* - N_f$ goes to zero, the theory becomes conformal and the β-function vanishes. Hence, as this line of argumentation would go, the mass of the scalar must go to zero as $N_f^* - N_f$ goes to zero, since inside the conformal window it is massless. Therefore if $N_f^* - N_f$ is non-zero but small, the mass of the scalar will be small as well. However, this argument, based on restoration of conformal symmetry, applies equally well to all massive states, like the vector meson discussed above. All massive states become massless as $N_f^* - N_f$ goes to zero but we have no information on the ratios. Depending on the rate at which the masses go to zero, the ratios may stay constant, may go to zero or may go to infinity. Hence there is no a priori reason for the scalar to be light relative to for example the vector meson even if $N_f^* - N_f$ is small.

2.3 Gauge theories inside and outside the conformal window

The first goal of any lattice simulation of a given model is to determine whether chiral symmetry is spontaneously broken or not. There are many phenomena that are markedly different in the two cases and a pedagogical overview of the basic differences is given in this section.

The phenomenological motivation limits our interest to conformal gauge theories where a suitably defined β-function is not identically zero, but rather has an isolated zero of first order. Hence the prototypical example of $\mathcal{N}=4$ SUSY Yang-Mills theory with an identically zero β-function is outside the scope of our discussion. The main difference between an identically zero β-function and one with an isolated zero is that in the former case a theory can be constructed at any value of the coupling such that correlation functions fall off as power-laws on all scales whereas in the latter case there is a single value of the coupling where this is possible.

2.3.1 Infinite volume, zero mass

The behavior of a spontaneously broken or QCD-like gauge theory at short distances can be described by perturbation theory. A dynamical scale Λ is generated and correlation functions behave as in free theories with logarithmic corrections,

$$\langle \mathcal{O}(x)\mathcal{O}(0)\rangle = \frac{1}{x^{2p}}\left(\frac{A}{\log^{2\alpha}(x\Lambda)}+\dots\right)\,, \qquad\qquad |x| \ll \Lambda^{-1} \tag{2.1}$$

with some constants, A, α and where p is the engineering or naive dimension of the operator $\mathcal{O}$. The constant α is zero if the anomalous dimension of $\mathcal{O}$ is zero, for instance if it is a conserved current. In writing eq. (2.1) we assume that operators are already renormalized in a suitable scheme at scale $\mu \sim \Lambda$.

The particle spectrum consists of the massless Goldstone bosons originating from the spontaneous breaking of chiral symmetry as well as a tower of massive bound states. The mass of the non-Goldstone bound states are all proportional to Λ. Consequently, deep in the large distance regime, more precisely for $\Lambda^{-1} \ll |x|$ only power-laws originating from the pions survive. In this regime interaction between the pions can also be neglected and all correlation functions take on the form of a free theory of pions. This deep infrared limit can formally be realized by $\Lambda \to \infty$, explicitly taking the mass of all massive bound states to infinity hence decoupling them from the low lying spectrum of massless (non-interacting) pions. In this sense chirally broken gauge theories are infrared free. Note however that the weakly interacting degrees of freedom at short distances (gluons and fermions) are different from the weakly interacting degrees of freedom at large distances (pions).

A gauge theory inside the conformal window, on the other hand, may behave in one of two distinct ways, see figure 2.1. Note that the Lagrangian is the same in the two cases. A suitably defined renormalized running coupling may be constant on all scales, or may reach the fixed point for large distances only. We will call the former case *conformal* and the latter *IR-conformal* for definiteness. For a detailed discussion on the running coupling and its behavior both inside and outside the conformal window see section 2.5.

In the IR-conformal case a dynamically generated scale Λ is present and correlation functions at short distances behave similarly to a chirally broken theory given by (2.1).

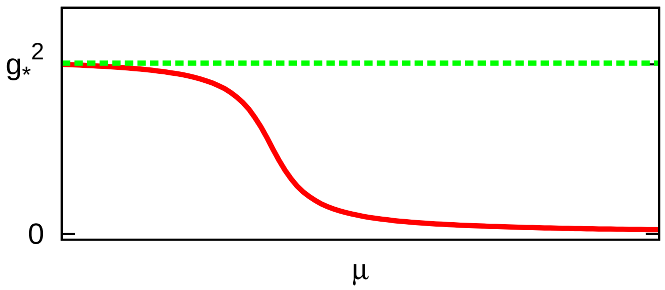

Figure 2.1: Two realizations of the running coupling inside the conformal window. The Lagrangian is the same in the two cases. The n-point functions fall off as power-laws on all scales (green) or fall off as power-laws for large distances but their behavior for short distances is described by asymptotic freedom (red). In order to make the difference clear we will refer to the former (green) as *conformal* and the latter (red) as *IR-conformal*.

At large distances correlation functions behave as power-laws,

$$\langle \mathcal{O}(x)\mathcal{O}(0)\rangle = \frac{A}{x^{2p}(x\Lambda)^{2\gamma}} + \ldots\ , \qquad\qquad |x| \gg \Lambda^{-1}\ , \tag{2.2}$$

where again p is the engineering or naive dimension and γ is the anomalous dimension of the operator $\mathcal{O}$.

Clearly, in (2.2) one may rescale the coordinate x and operator $\mathcal{O}$ by Λ to get rid of the dynamical scale at large distances. Hence if,

$$\begin{aligned} z &= x\Lambda \\ \mathcal{O}_{IR}(z) &= \frac{\mathcal{O}(z/\Lambda)}{\Lambda^p} \end{aligned} \tag{2.3}$$

then in the infrared 2-point functions are simply,

$$\langle \mathcal{O}_{IR}(z)\mathcal{O}_{IR}(0)\rangle = \frac{A}{z^{2p+2\gamma}} + \ldots\ , \qquad\qquad z \gg 1\ . \tag{2.4}$$

In the above equation everything is expressed in dimensionless quantities and the dynamical scale Λ indeed dropped out.

In the second realization of a gauge theory inside the conformal window, where correlation functions are power-laws on all scales an arbitrary dimensionful scale Λ may nevertheless be introduced from dimensional analysis of the classical theory. Then in this case correlation functions behave as equations (2.2) and (2.4) without corrections represented by $\ldots$, i.e. for all x and z.

One may imagine regularizing a gauge theory inside the conformal window by a UV-cutoff Λ_{UV} or a^{-1} in which case all quantities can be measured from the start in Λ_{UV} or a^{-1} units and one would automatically end up with dimensionless quantities. This slight difference in computation, keeping the dynamical scale Λ and only getting rid of it in the infrared by rescaling, or working with dimensionless quantities from the start is clearly irrelevant as far as the infrared behavior is concerned, but in order to distinguish the conformal and IR-conformal scenarios depicted in figure 2.1 the dynamical scale Λ needs to be kept.

In any case the lack of exponentially falling correlation functions at large distances indicates that all channels are massless. Note that there is a smooth limit between the two realizations inside the conformal window by formally taking $\Lambda \to \infty$, i.e. $\Lambda|x| \to \infty$ while $|x|$ is fixed. This limit will turn all correlation functions into power-laws on all scales. Even though the lack of a dimensionful scale will of course not make it possible to measure absolute distance scales, measuring distances relative to each other is still meaningful. The $\Lambda \to \infty$ limit, as defined here, inside the conformal window simply extends the power-law IR behavior to all scales but does not alter the (un)particle [98] content. On the other hand, in a chirally broken gauge theory, this limit corresponds to removing all massive states and ending up with only massless pions, i.e. it reduces the number of particle species.

2.3.2 Finite volume, non-zero mass

The previous discussion was valid in infinite volume and zero fermion mass. A finite volume and non-zero fermion mass are both useful tools in lattice calculations as well as unwanted effects that make the distinction between a gauge theory inside and outside the conformal window more blurred. The chief reason is that massive fermions introduce massive particle states and exponentially falling correlation functions even inside the conformal window and finite volume limits the direct ability to probe the system at large distances.

Nevertheless a finite volume and fermion mass can indeed be used as useful tools since the behavior of a gauge theory inside or outside the conformal window differ markedly in well defined regimes. First let us discuss the still massless but finite volume setup, i.e. the theory is formulated on $T^3 \times R$ with a linear size L for the spatial volume. One naturally has to impose boundary conditions for both the gauge fields and fermions in the spatial directions and it is expected that in small volumes, $L\Lambda \ll 1$, the boundary conditions are relevant and may alter the behavior of the theory substantially whereas for large volumes, $L\Lambda \gg 1$, their influence is expected to be small (either algebraic or exponential, depending on the quantity in question).

Asymptotic freedom ensures that at small volume, $L\Lambda \ll 1$, perturbation theory is applicable. In this regime, often called "femto-world", chirally broken and IR-conformal theories behave very similarly. A perturbative Hamiltonian framework can be set up in a straightforward manner and in this case all eigenvalues of the Hamiltonian and hence all masses behave as

$$M(L) = \frac{1}{L}\left(A + \frac{B}{\log^{2\alpha}(L\Lambda)} + \dots\right) \qquad L \ll \Lambda^{-1}\,, \tag{2.5}$$

where the constants A, B and α depend on the quantum numbers of the state and on the boundary conditions. If the boundary conditions are chosen such that the vacuum is degenerate, tunnelling events will produce splittings which are small relative to the logarithmic corrections above but are nevertheless reliably calculable for small volume [99, 100].

For large volumes, on the other hand, masses inside and outside the conformal window behave very differently. In the IR-conformal case we have,

$$M(L) = \frac{1}{L}\left(A + \frac{B}{(L\Lambda)^{\omega}} + \dots\right) \qquad L \gg \Lambda^{-1}\,, \tag{2.6}$$

where the exponent ω may be obtained from the β-function of the theory, see section 2.5.

On the other hand, if the theory is chirally broken the large volume spectrum, $L \gg \Lambda^{-1}$, will behave markedly differently. In this regime, familiar as the δ-regime of chiral perturbation theory [101], there are modes whose volume dependence is

$$M(L) = \frac{1}{L(L\Lambda)^2} \left(A + \frac{B}{(L\Lambda)^2} + \ldots \right) \qquad\qquad L \gg \Lambda^{-1} \tag{2.7}$$

which will ultimately become the pions at infinite volume and there are also modes whose volume dependence is rather

$$M(L) = \Lambda \left(A + \frac{B}{(L\Lambda)^2} + \ldots \right) , \qquad\qquad L \gg \Lambda^{-1} \tag{2.8}$$

which at infinite volume become the tower of massive bound states.

Now let us turn to the situation of infinite volume, but finite (bare) fermion mass, m. In this case particle states will be massive even in the conformal case and correlation functions will have an exponential fall off for large distances. The masses of gauge singlet particles are of course physical quantities and as such are renormalization group invariant, however the fermion mass m is not. Let us choose a renormalization scheme for the fermion mass and denote by $\tilde{m}(m)$ an RG invariant mass. Then the physical masses of particles states will behave as

$$M(m) = A\Lambda \left(\frac{\tilde{m}}{\Lambda} \right)^{\frac{1}{1+\gamma}} + \ldots \tag{2.9}$$

for $\tilde{m}/\Lambda \ll 1$ in conformal theories with γ the mass anomalous dimension [102, 103]. The coefficient A as well as the function $\tilde{m}(m)$ depends on the renormalization scheme but the exponent γ does not.

In the chirally broken case the fermion mass dependence of the Goldstone bosons is determined by the p-regime of chiral perturbation theory [104],

$$M(m) = \Lambda \left(\frac{\tilde{m}}{\Lambda} \right)^{1/2} \left(A + B\frac{\tilde{m}}{\Lambda} + C\frac{\tilde{m}}{\Lambda} \log \frac{\tilde{m}}{\Lambda} + \ldots \right) \tag{2.10}$$

and the fermion mass dependence of all other states is

$$M(m) = \Lambda \left(A + B \left(\frac{\tilde{m}}{\Lambda} \right)^{\alpha} + \ldots \right) \tag{2.11}$$

with some exponent $\alpha > 0$, typically $\alpha = 1$. It should be noted that the above expressions receive next to leading order corrections in the chiral expansion which can only be assumed to be small if indeed $\tilde{m}/\Lambda$ is sufficiently small. Furthermore, at finite $\tilde{m}/\Lambda$ ratio, or in other words at finite Goldstone mass a further assumption needs to hold, namely that all states are sufficiently heavier than the Goldstone itself. This is because the conventional chiral Lagrangian from which (2.10) and expansions of all other low energy quantities are obtained is only sensitive to the Goldstones as all further states are assumed to be integrated out. However at finite fermion mass it may happen that the mass of further states, which are non-zero in the chiral limit, become comparable to the mass of the Goldstones in which case they must be included as correction terms in the chiral Lagrangian. A potential example is the 0^{++} meson.

Close to the conformal window direct lattice calculations seem to indicate that indeed the scalar meson does not separate from the Goldstones even at the smallest fermion masses accessible to numerical simulations.

Apart from expressions like (2.10) chiral perturbation theory in the p-regime predicts relationships between a host of quantities, like the GMOR relation, as well as the fermion mass dependence of decay constants. In particular the chiral Lagrangian dictates that the decay constant of the Goldstone bosons in the chirally broken case behaves as, at leading order,

$$F(m) = \Lambda \left(A + B\frac{\tilde{m}}{\Lambda} + C\frac{\tilde{m}}{\Lambda} \log \frac{\tilde{m}}{\Lambda} + \dots \right) \tag{2.12}$$

where the A, B, C parameters are different from the similarly named parameters in (2.10), but chiral perturbation theory establishes relationships between them. In the conformal case, on the other hand,

$$F(m) = A\Lambda \left(\frac{\tilde{m}}{\Lambda} \right)^{\frac{1}{1+\gamma}} + \dots \tag{2.13}$$

is expected for small enough fermion mass m.

2.4 Mass spectrum as a probe for IR-conformality

So far our discussion was in the continuum. Any lattice simulation is naturally set up in finite 4-volume and finite lattice spacing. As far as the study of the spectrum is concerned in large volumes the fermion mass also needs to be finite for technical reasons. The first goal of any lattice simulation is to establish whether the simulated theory is inside or outside the conformal window at infinite volume and zero fermion mass. This is a non-trivial task since in order to make use of the continuum expressions which clearly distinguish the two cases, one needs to ensure that both the asymptotic requirements for their validity hold and also that the lattice spacing, a, is sufficiently small. In practice this means that $\Lambda L \gg 1$ and $M(m)L \gg 1$ for the smallest mass $M(m)$ is required in order to have small finite volume effects. Furthermore $a\Lambda \ll 1$ and $aM(m) \ll 1$ needs to hold for small cut-off effects.

2.4.1 Finite volume effects

The most direct way to probe the infrared of a given theory on the lattice is to study its mass spectrum in large volumes keeping the necessary inequalities as well as one can, given the practical constraints of the available computer. Even though this approach is theoretically sound the inequalities are hard to fulfill as one approaches the conformal window from below, as finite volume effects become more and more severe. In practice this means that even though the general rule of thumb in QCD, $M_\pi(m)L > 4$, ensures small finite volume effects in spectral quantities, in theories close to the conformal window $M_\pi(m)L > 5$ or even $M_\pi(m)L > 10$ is required [15, 105]. In addition if one wants to employ infinite volume chiral perturbation theory, for example (2.10) or (2.12), then $F_\pi L \geq 1$ is also needed which condition is analogous to the general $\Lambda L \geq 1$ expression. Note that the latter constraint is particularly hard to maintain close to the conformal window with a small fermion mass because $F_\pi(m)$ varies rapidly as a function of m. The coefficient B is apparently larger just below the conformal window than in QCD in equation (2.12).

For a model inside the conformal window finite volume effects are even more severe and $M_\pi(m)L > 15$ was reported to be necessary to have negligible finite volume effects at finite fermion mass for the $SU(2)$ model with $N_f = 2$ adjoint fermions [106].

Not completely controlling finite volume effects, i.e. having not sufficiently large volumes in the simulations is not only problematic for applying infinite volume chiral perturbation theory or hyperscaling formulae but also more generally. We have seen in the previous section that at small ΛL IR-conformal and chirally broken theories behave very similarly, simply because both are asymptotically free and at not sufficiently large ΛL the simulation can not probe deeply enough in the infrared to distinguish them. The above mentioned general observation that $F_\pi(m)$ drops more steeply as a function of m for small m if the model is closer to the conformal window results in the need for ever larger lattice volumes.

In intermediate volumes, where $\Lambda L \sim 1$ there are no theoretical expectations for the volume dependence or the fermion mass dependence. Increasing the fermion mass in order to increase $F_\pi(m)$ will ensure $F_\pi(m)L \gg 1$ however $M_\pi(m)$ also grows and the asymptotic expressions for small mass will lose their validity both inside and outside the conformal window. As a result simulations with practical constraints on the lattice volume given by the available computer often find themselves between a rock and a hard place: either intermediate volume or intermediate fermion mass, neither of which has a theoretically sound description.

2.4.2 Finite lattice spacing effects

Furthermore, even though the physical volume in a lattice calculation can be increased at fixed lattice volume by increasing the lattice spacing via increasing the bare gauge coupling, this will introduce larger cut-off effects and the $a\Lambda \ll 1$ constraint will hold to a lesser degree. Consequently the conclusions will be less indicative of the continuum theory and perhaps will be specific to the chosen discretization only. In addition there might be bulk phase transitions at some critical bare gauge coupling, which is specific to the given discretization and has nothing to do with the continuum dynamics of the model. In order to draw conclusions which have a chance to describe the continuum theory the bare coupling g_0^2 needs to be smaller than the critical value and this alone might force the simulation into a regime where the physical volume is not large enough, unless very large lattice volumes are used which might not be affordable on a given computer.

2.4.3 Low lying scalar and chiral perturbation theory

A further issue, as mentioned, is that if the scalar meson becomes lighter and lighter, the chiral expansion becomes more and more invalid. Just below the conformal window the scalar meson mass seems to become light indeed. In practice it becomes hard to simulate at light enough masses, such that the pion becomes lighter than the scalar, and this complicates the application of chiral perturbation theory formulae [107–110]. On the other hand, just inside the conformal window one may need to use very small fermion masses in order to fit the data with the leading expression (2.9) and in practice one is forced to use subleading terms in the fits increasing the number of fit parameters. Similarly, the number of fit parameters will grow due to cut-off effects as well, in a chirally broken theory the chiral expansion will have new terms which are vanishing in the continuum but can be sizable at finite cut-off.

2.4.4 Selected lattice results

Since simulations of the mass spectrum close to the conformal window are plagued by the above difficulties, it is all the more important to gather as much evidence as possible, before conclusions are drawn from numerical data. For instance, if for a model chiral symmetry breaking appears to take place it is important to verify this from as many observables as possible. Good chiral fits of the Goldstone mass and decay constant is preferrably complemented by a verification of the GMOR relation and by checking the Random Matrix Theory predictions for the low lying Dirac eigenvalues in the ε-regime. Furthermore there are relations between the various chiral fits in the p-regime since the same low energy constants appear in all of them, allowing for powerful consistency checks. Similarly, it is desirable to complement the conformal scaling tests of the mass spectrum by calculations of the running coupling showing an infrared fixed point (see section 2.5) in the conformal case. Also, the mass anomalous dimension γ from the spectrum should be independent from the channel from which it is extracted. Furthermore it ought to agree with the running mass anomalous dimension at the infrared fixed point, as well as with the one obtained from the scaling of the Dirac spectrum, providing powerful checks in the conformal case too. Note that the study of the Dirac spectrum has its own source of systematic effects, namely definitive conclusions can only be drawn from small eigenvalues as far as the infrared is concerned and this range is particularly distorted by finite volume effects [111].

Despite the above complications, the mass spectra of numerous models were calculated on the lattice keeping the needed inequalities to varying degrees.

As far as $SU(2)$ is concerned there is broad agreement that the $N_f = 2$ model in the adjoint representation is conformal, the mass spectrum in particular was studied in detail [106, 112–117]. The $N_f = 1$ case was also investigated [47] and asymptotic freedom is lost at $N_f = 2.75$. In the fundamental representation asymptotic freedom is lost at $N_f = 11$. Detailed studies of the particle spectrum for $N_f = 2, 4, 6$ are available [105, 118, 119] with $N_f = 6$ being thought to be at around the lower end of the conformal window. Severe finite volume effects at $N_f = 6$ however prohibited a conclusive result as to whether the model is chirally broken or already inside the conformal window.

The gauge group $SU(3)$ was studied on the lattice by many groups. Since the fundamental representation is particularly familiar from QCD applications, this model was the first to be investigated in detail. The $N_f = 6$ model is certainly outside the conformal window. The mass spectrum of the $N_f = 8$ model was studied extensively [91–93, 120–122], results for both $N_f = 9$ [120] and $N_f = 10$ [123] are available as well as $N_f = 12$ [66, 124, 125]. There seems to be disagreement about the $N_f = 12$ model, whether it is already inside or just below the conformal window and the study of the running coupling does not seem to resolve this issue (see section 2.5). Beyond the fundamental representation the most promising candidate model from a phenomenological point of view is the sextet with $N_f = 2$ flavors [13, 25, 26]. The mass spectrum was investigated in detail [15, 94–96, 126], along with various chiral properties. The results seem to be consistent with chiral symmetry breaking although see also [126].

The adjoint of $SU(2)$ or the sextet of $SU(3)$ are the two index symmetric representations and generalizing it further, a first study of $SU(4)$ gauge theory with $N_f = 2$ flavors in the two index symmetric was recently performed [127].

As mentioned in section 2.2 one of the most important conclusions drawn from lattice studies of gauge theories close to the conformal window is the appearance of a light composite scalar meson. Here by light we mean its mass m_σ relative to the mass m_ϱ of the vector meson. In the $SU(3)$ model with $N_f = 8$ fundamental fermions approximately $m_\sigma/m_\varrho \sim 1/2$ was observed, whereas with $N_f = 2$ sextet fermions approximately $m_\sigma/m_\varrho \sim 1/4$. These observations make it plausible that a composite Higgs may emerge from a near-conformal gauge theory with its 125 GeV mass obtained after electro-weak corrections are taken into account [97].

Beyond the unitary gauge group, the mass spectrum of $SO(4)$ was studied [128] with $N_f = 2$ flavors in the fundamental representation, showing consistency with chiral symmetry breaking.

Due to the practical difficulties alternative approaches were also explored in lattice calculations. One area where lot of effort was concentrated is the calculation of the β-function of the models, outlined in the next section.

2.5 Running coupling as a probe for IR-conformality

The basic idea behind the running coupling studies is that an IR fixed point would be characterized by the property that the running coupling goes to a finite value in the limit of zero energy. Typically a very general definition of running coupling is adopted: any observable $g^2(\mu)$ which depends on a single energy scale μ and which admits the following perturbative expansion

$$g^2(\mu) = g_r^2(\mu) + \sum_{n=1}^{\infty} c_n g_r^{2n}(\mu) \ , \tag{2.14}$$

valid for $\mu \to \infty$ is said to be a running coupling. A reference renormalization scheme r has to be assumed in this definition. The $\overline{MS}$ can be considered for definiteness, but other schemes might be used as well. It is worth reminding that the above series is only formal, it does not converge and it does not imply analyticity. We will say that a given coupling $g^2(\mu)$ is a *good probe for IR-conformality* if it diverges in the $\mu \to 0$ limit in theories with spontaneous chiral symmetry breaking (SχSB) and goes to a finite nonzero value in IR-conformal theories. Throughout this section we will assume that we are setting the quark masses equal to zero, and IR-conformality is possibly broken only by a finite volume.

Unfortunately eq. (2.14) is not enough to guarantee that the running coupling $g^2(\mu)$ is a good probe for IR-conformality. It is easy to construct observables $g^2(\mu)$ satisfying (2.14) that *do not* diverge in theories with SχSB. In general, given a running coupling $g^2(\mu)$ that diverges in the $\mu \to 0$ limit, it is always possible to construct another running coupling

$$\tilde{g}^2(\mu) = \frac{g^2(\mu)}{1 + g^2(\mu)} \tag{2.15}$$

that goes to 1 in the $\mu \to 0$ limit. Later on we will show how a coupling defined in terms of the vector-current two-point function does not diverge in the IR limit even if chiral symmetry breaks, exactly because of pion physics.

It is also easy to produce examples of couplings that diverge in the IR limit in case of IR-conformality. Let us assume that $g^2(\mu)$ behaves in the IR limit accordingly to standard Wilsonian RG behaviour

$$g^2(\mu) \simeq g_*^2 - A_\omega (\mu/\Lambda)^\omega + \dots \ , \tag{2.16}$$

where A_ω and ω are positive numbers. In particular ω is related to the anomalous dimension of the first irrelevant operator at the IR fixed point. Define now the following coupling

$$\tilde{g}^2(\mu) = -\frac{b_0 g^6(\mu)}{\mu \frac{\partial g^2(\mu)}{\partial \mu}} , \tag{2.17}$$

where $-b_0$ is the first coefficient of the expansion of the beta function around $g^2 = 0$ and ensures the validity of the representation (2.14). In the IR limit

$$\tilde{g}^2(\mu) \simeq \frac{b_0 g_*^6}{\omega A_\omega} (\mu/\Lambda)^{-\omega} + \dots , \tag{2.18}$$

which shows that $\tilde{g}^2(\mu)$ diverges. This example shows that the standard Wilsonian RG treatment does not work for the coupling $\tilde{g}^2(\mu)$. The reason is that Wilsonian RG assumes regularity properties that might not hold, and in fact one should not expect to be valid especially if the considered theory is strongly coupled. Typically couplings defined at high energies and satisfying eq. (2.14) capture the interaction strength between quarks, and they have nothing to do with large distance physics. Both in the case of spontaneous χSB and IR-conformality the large-distance degrees of freedom are in fact colorless and can be approximated as quark bound states in case of a weakly coupled Banks-Zaks fixed point. [23, 24]

We believe that whenever a coupling $g^2(\mu)$ satisfying eq. (2.14) is proposed to study IR-conformality, then a proof of the property that $g^2(\mu)$ is also a good probe for IR-conformality should be provided which is not based merely on perturbative Wilsonian RG, but maybe on more general effective-theory analysis, before definitive conclusions are drawn. Surprisingly enough this logical issue has been largely ignored in the literature. We will review some possible definitions of running couplings, trying to highlight what we know or we do not know about their IR-behaviour.

2.5.1 Static potential

The force $F(r)$ between static quarks can be defined in terms of rectangular Wilson loops with size $r \times t$ as

$$F(r) = \lim_{t \to \infty} \frac{1}{t} \frac{\partial}{\partial r} \ln W(r,t) . \tag{2.19}$$

We assume for simplicity that we have already taken the zero-mass and infinite-volume limits. At small r the force between static quarks has a perturbative expansion

$$F(r) = -\frac{k\, g_r^2(r^{-1}) + O(g_r^4)}{r^2} , \tag{2.20}$$

where k is a positive constant. A running coupling can be defined as

$$g_F^2(\mu) = -\, k^{-1} r^2 F(r)\big|_{r=\mu^{-1}} . \tag{2.21}$$

The static force provides a physically motivated definition of the running coupling, at least for short distances or in other words in the perturbative regime. If the model exhibits SχSB, the force is governed by the dynamics of the effective string at intermediate distances and $F(r) \simeq -\sigma$. At large enough distances, in theories that generate string-breaking (like QCD), the effective string is broken by generation of a light quark-antiquark pair, and each dynamical quark binds to a static one forming heavy-light mesons. In this regime $F(r)$ becomes the force between these mesons, rather than between static quarks. At asymptotically large distances it is dominated by one-pion exchange. Since we are in the chiral limit, the pion is massless and the induced interaction is Coulombic, i.e. the force vanishes proportionally to r^{-2}. Therefore the coupling $g_F^2(\mu)$ grows quadratically at intermediate distances and goes to a constant at very large distances. It is worth mentioning that this problem is avoided in theories with a residual center symmetry (e.g. confining theories with fermions in the adjoint representation): in this case string breaking does not occur and the running coupling grows quadratically at asymptotically large distances.

In case of IR conformality, the force is expected to be Coulombic at large distance and the coupling $g_F^2(\mu)$ is expected to go to a non-zero finite value. In conclusion, even though in some intermediate regime the quantity $g_F^2(\mu)$ is expected to behave differently in case of IR-conformality and SχSB, its behavior at asymptotically large distance is not sufficient to unambiguously differentiate between the two cases. Empirically one sees that the regime in which the effective string breaks is very hard to reach in typical numerical simulations, and in practice only short and intermediate distances are explored. Earlier results using variations of this scheme include e.g. Creutz ratios [120], or the twisted Polyakov loop (TPL) coupling [129, 130] to investigate IR-conformality. It is instructive to notice that the TPL coupling is expected to go to a constant in the low-energy limit even in pure Yang-Mills theory [131], because of an algebraic cancelation very similar in spirit to the one in eq. (2.15). In the case with dynamical fermions a similar saturation effect is expected [129, 130].

2.5.2 Vector current

We consider the two-point function of the non-singlet vector current, calculated in infinite volume:

$$C_V(x) = \langle V_\mu^a(x) V_\mu^a(0) \rangle \ , \qquad V_\mu^a(x) = \bar{\psi} \tau^a \gamma_\mu \psi(x) \ . \tag{2.22}$$

At small x the two-point function admits a perturbative expansion $x^6 C_V(x) = c_0 + c_1 g_r^2(x^{-1}) + \ldots$ where the c_0 and c_1 coefficients can be analytically worked out (see section 2.3). Therefore one can define a legitimate running coupling as follows

$$g_V^2(\mu) = \left. \frac{x^6 C_V(x) - c_0}{c_1} \right|_{x=\mu^{-1}} \ . \tag{2.23}$$

This running coupling has never been used in studies of the conformal window. However it possesses very interesting features that are worth highlighting. If the theory is IR-conformal, the large distance behaviour is determined by the scaling dimension of the vector current. Since $V_\mu^a(x)$ is a conserved current, its scaling dimension is equal to its engineering one. This means that the vector two-point function decays like x^{-6} at large distances. Therefore the coupling $g_V^2(\mu)$ goes to a constant in the $\mu \to 0$ limit as expected. If chiral symmetry is spontaneously broken, then the vector current couples to two-pion states at large distance. If π is the pion field, at the leading order in chiral perturbation theory, the vector current is represented by the operator $\mathrm{Tr}\, \tau^a \pi \partial_\mu \pi$ up to total derivatives. [104] It is easy to check by power counting that the vector two-point function decays like x^{-6} (one x^{-2} per pion propagator and one x^{-1} per derivative). Therefore the running coupling $g_V^2(\mu)$ goes to a constant in the $\mu \to 0$ limit even if chiral symmetry is spontaneously broken. Notice that this constant is predicted by chiral perturbation theory.

2.5.3 Schrödinger functional (SF) coupling

Most studies which aim at determining IR conformality in gauge theories have used finite-volume renormalization schemes. The idea is to define the running coupling as some observable calculated in a hypercubic box and to identify the renormalization scale μ with the inverse of the box size L. This approach has the advantage to remove or dramatically reduce two sources of systematic errors in typical lattice simulations: *(1)* the infinite-volume extrapolation, and *(2)* the chiral extrapolation. In finite volume, if boundary conditions are properly chosen, the Dirac operator has a gap even in the massless limit and simulations at the chiral point are possible. If fermions with a residual chiral symmetry are employed then one can simulate exactly at zero bare mass. In case of Wilson fermions the chiral limit is reached at an unknown value of the bare mass which can be found by interpolation (rather than extrapolation). In these kinds of calculations one still has systematic errors that come from the continuum extrapolation, on which we will comment later. It is worth noticing that in order to ensure a perturbative expansion of the type (2.14) one needs to use boundary conditions such that the vacuum is unique at tree level. One can relax this condition by choosing boundary conditions such that the vacuum is degenerate at tree-level but the degeneracy is completely lifted at one-loop, provided that more general expansions than (2.14) are considered. [132]

One can consider a hypercubic box with periodic boundary conditions in the three spatial directions, and SF boundary conditions [133, 134] for the gauge field at the boundaries $x_0 = 0$ and $x_0 = L$. Typically one chooses

$$A_k(0,\vec{x}) = \frac{\eta\lambda_1}{L} \ , \quad A_k(L,\vec{x}) = \frac{\lambda_0 - \eta\lambda_1}{L} \ , \tag{2.24}$$

where λ_0 and λ_1 are color matrices and η is a free parameter. Also the fermion fields satisfy some appropriate boundary conditions, whose explicit form plays no role in the present discussion. The boundary conditions induce a background chromomagnetic field. If the background field is properly chosen, uniqueness of the tree-level vacuum is ensured. The variation of the free energy with respect to the boundary fields turns out to be proportional to the inverse of the squared coupling, and can be used to define a running coupling [135], as in

$$\left.\frac{1}{g^2_{\mathrm{SF}}(\mu)}\right|_{\mu=L^{-1}} = k \left.\frac{d}{d\eta}\right|_{\eta=0} \ln Z_{\mathrm{SF}}(\eta) \ , \tag{2.25}$$

where Z_{SF} is the partition function with SF boundary conditions and k is a constant that ensures the correct normalization. The renormalizability of QFT with SF boundary conditions and the existence of the continuum limit of the SF coupling are nontrivial issues and have been discussed in the literature. [135–139]

Empirically one observes that in pure Yang-Mills and QCD the SF coupling diverges at $L \to \infty$. In pure Yang-Mills one can easily argue that this is in fact the case by using the existence of a mass gap. [140] In a theory with spontaneous χSB, the leading contribution to the running coupling at large volume will come from multi-pion exchange between the two boundaries or from pions traveling around the periodic direction. These contributions are powers in L, and depending on the exponent they could lead to a vanishing, finite or divergent behaviour of the running coupling at low energies. In principle this power can be determined by representing the SF running coupling in terms of operators of the chiral Lagrangian. It is interesting to notice that this issue has not been addressed from the theoretical point of view.

In case of IR conformality one would like to argue that the SF running coupling must go to a constant in the $L \to \infty$ limit. This is most probably the case, but the issue is far from being completely trivial. By working out the derivative with respect to the boundary conditions in eq. (2.25) one finds out that the SF running coupling can be represented in terms of expectation values of operators on the boundaries

$$\left.\frac{1}{g_{\mathrm{SF}}^2(\mu)}\right|_{\mu=L^{-1}} = \frac{k_0}{L}\int_{L^3} d^3x\, \langle \mathrm{Tr}\,\lambda_1 F_{0k}(0,\vec{x})\rangle_{\mathrm{SF}} + \frac{k_L}{L}\int_{L^3} d^3x\, \langle \mathrm{Tr}\,\lambda_1 F_{0k}(L,\vec{x})\rangle_{\mathrm{SF}} \ . \tag{2.26}$$

In fact this is the way in which the SF running coupling is calculated in numerical simulations. Notice that the operator $\mathrm{Tr}\,\lambda_1 F_{0k}$ is not gauge invariant, but this is not a problem as the boundary conditions are not invariant under gauge transformations. At the fixed point, the bulk theory is scale invariant. The finite volume breaks scale invariance softly, which means that the trace of the energy momentum tensor is zero in the bulk, but not necessarily on the SF boundary. If no dynamical scale is generated on the boundary, then by dimensional analysis the expectation value of $\mathrm{Tr}\,\lambda_1 F_{0k}$ should be proportional to L^{-2} yielding a finite limit for the running coupling for $L \to \infty$. However notice that the boundary field is not invariant under (3-dimensional) dilations, therefore we expect the trace of the energy momentum tensor to get a non-vanishing contribution at the boundary, and a dynamical scale could be generated if the relevant or marginal operators of the boundary theory get anomalous dimensions. This issue might well turn out to be trivial, but it is surely worth to be analyzed in detail.

In conclusion it looks very plausible that the SF coupling turns out to be a good probe for IR conformality, however more theoretical work is needed in order to understand its low-energy limit. The SF coupling has been widely used to investigate IR conformality in various theories mostly until 2013, and then it has been almost completely replaced by the much more precise gradient-flow coupling. All SF-coupling studies [141–144] agree on the existence of an IR fixed point in $SU(2)$ with 2 adjoint fermions. Concerning $SU(2)$ with N_f fundamental fermions, the SF-coupling runs away for $N_f = 4$ [145], and an IR-fixed point is found for $N_f = 10$ [145]. The case $N_f = 6$ collects evidence in favour of slow running of the SF-coupling [145, 146] and against it [147]. The $SU(3)$ gauge theory with 8 fundamental fermions collected evidence for strong running of the SF-coupling [64,148]. The same studies report evidence for an IR-fixed point in the $SU(3)$ gauge theory with 12 fundamental fermions. Slow running of the SF-coupling has been reported also in the $SU(3)$ theory with 2 sextet fermions [149–151], in the $SU(3)$ theory with 2 adjoint fermions and in the $SU(4)$ theory with 6 antisymmetric two-index fermions [152] and in the $SU(4)$ theory with 2 symmetric two-index fermions [153].

2.5.4 Gradient flow (GF) coupling

The gauge field B_t at positive flowtime t is defined as a function of the fundamental gauge field A through the differential equation

$$\partial_t B_{t,\mu} = D_{t,\mu} G_{t,\mu\nu} \ , \qquad B_{0,\mu} = A_\mu \ , \tag{2.27}$$

where $D_{t,\mu}$ and $G_{t,\mu\nu}$ are respectively the covariant derivative and the field strength tensor built with the gauge field $B_{t,\mu}$. The GF coupling [154, 155] is defined in a finite hypercubic box with some given boundary conditions as

$$g_G^2(\mu) = \mathcal{N}(c)\, t^2 \langle \mathrm{Tr}\, G_t^2 \rangle \big|_{\mu=L^{-1}=c(8t)^{-1/2}} \ , \tag{2.28}$$

where c is some arbitrarily chosen constant and $\mathcal{N}(c)$ gives the correct normalization of the coupling. The boundary conditions are often chosen in such a way that the perturbative expansion is non-degenerate and a representation of the type (2.14) holds, however this is not necessary to define a possible probe for IR conformality. The existence of the continuum limit of the GF coupling is non trivial and we refer to the relevant literature for its proof. [156]

As for the SF coupling, no proof is available of the expectation that the GF coupling diverges in case of SχSB. As for the SF functional one might want to represent the GF coupling in terms of operators in the framework of chiral perturbation theory. This might allow us to understand the IR behaviour of the coupling in terms of pion physics. Notice that operators at some nonzero but fixed flowtime are non-local, but the range of nonlocality is small with respect to the pion Compton length. Therefore they can be represented as local operators in terms of the pion fields [157]. However the IR behavior of the GF coupling is obtained in the $t \to \infty$ limit and it is not obvious *a priori* that this regime is correctly captured by chiral perturbation theory.

In the case of IR-conformality, one can argue that operators at positive flowtime do not get anomalous dimensions, and therefore $\langle \mathrm{Tr}\, G_t^2 \rangle$ vanishes proportionally to t^{-2} in the large t limit. This immediately implies that the GF coupling goes to a constant in the IR limit. In order to see this it is useful to think of the flowtime as a real coordinate [156]. Operators at positive flowtime are mapped into local operators in a 5-dimensional theory with boundary ($t = 0$). At the IR fixed point, the original 4-dimensional theory becomes scale invariant. One would like to understand whether the full 5-dimensional theory is scale invariant as well. Notice that the GF equation is scale invariant which implies that the bulk theory is scale invariant. Moreover the bulk theory is classical so no anomalous dimensions will be generated. Because of the interaction of the 4-dimensional theory with the bulk theory, new boundary operators are generated. In order to estabilish scale invariance of the full 5-dimensional theory, one needs to make sure that no relevant operators are generated on the boundary because of the interaction with the bulk. This is surely true if the fixed point is sufficienlty weakly coupled. It would be interesting to understand whether stronger results could be estabilished, e.g. whether the absence of chirally-invariant relevant operators in the original 4-dimensional theory implies the absence of relevant interaction boundary operators.

The GF coupling has the great advantage over other couplings to come with small statistical errors in numerical simulations. For this reason it has practically become the coupling of choice in studies of IR-conformality. Concerning the $SU(3)$ gauge theory with N_f fundamental fermions, clear indication for fast running has been observed for $N_f = 4, 8$ [158–160]. Slow running has been confirmed for $N_f = 12$ [48] even though the authors observe no compatibility with IR-conformal finite-size scaling. Compatibility with an IR fixed point has been observed for $SU(2)$ with 2 adjoint fermions [161], consistently with previous studies. Studies of the running coupling of $SU(3)$ with two sextet fermions show some tension [162, 163]. Interestingly the studies of the spectrum of this theory seem to point towards SχSB with strong non-QCD like features.

2.5.5 Nucleon mass

Finally we give an example of a possible coupling whose IR behaviour is very easy to predict and is deeply related to the physics that we would like to probe. We consider a generic gauge theory coupled to a number of massless Dirac fermions in some representation of the gauge group, such that twisted boundary conditions à la 't Hooft [164] can be used. We consider a $T^3 \times R$ box with linear spatial size equal to L, and with twisted boundary conditions in some of the spatial planes. In this setup it is possible to extract the mass gap $M(L)$ in the sector at baryon number equal to one from the long-distance behaviour of some properly defined two-point function. At small volume the mass gap has a perturbative expansion:

$$LM(L) = c_0 + c_1\, g_r^2(L^{-1}) + O(g_r^4) \ . \tag{2.29}$$

where the c_0 and c_1 coefficients are calculable analytically. Therefore one can define a running coupling satisfying eq. (2.14) as follows

$$g_M^2(\mu) = \left. \frac{L\, M(L) - c_0}{c_1} \right|_{L=\mu^{-1}} \ . \tag{2.30}$$

If chiral symmetry is spontaneously broken, then the gap is expected to survive in infinite volume and the coupling diverges. If the theory is IR-conformal, the gap is expected to vanish proportionally to $1/L$, and the coupling goes to a constant. A similar construction with the pion mass instead of the nucleon mass would provide a running coupling that behaves in a funny way. In fact in the chiral limit the pion mass vanishes in the infinite-volume limit irrespectively of the long distance properties. The chiral symmetry broken and IR-conformal scenarios are discriminated by how fast the pion mass vanishes. In case of IR-conformality the pion mass would vanish like L^{-1} as any other mass. In contrast the large volume limit in the case of spontaneous chiral symmetry breaking (a.k.a. δ regime) is dominated by the rotor physics and the pion mass vanishes like L^{-3}, as already discussed in section 2.3. A running coupling defined like in (2.30) with the pion mass would go to a non-zero constant in the case of IR-conformality and would *vanish* in the case of spontaneous chiral symmetry breaking, in the $\mu \to 0$ limit. One might be tempted to use other mesonic states other than the pion, for instance the mass of the ground state in the non-singlet vector channel. However notice that in case of chiral symmetry breaking and in large volume, this state is a state of two weakly-interacting pions (and not the ρ resonance). Therefore its energy vanishes as L^{-3}, like for the single-pion state.

2.5.6 Continuum limit of finite-volume couplings

We want to comment on the largest source of systematic error in running coupling determinations, i.e. the continuum extrapolation. The material discussed here is trivial for lattice practitioners, but might be useful for physicists of other communities who try to interpret the meaning and quality of lattice data. We discuss the setup that is usually employed to calculate the running coupling in finite volume schemes. Again, this means that the running coupling is measured in a finite hypercubic box with length L and the renormalization scale is identified with L^{-1}. The primary observable that one measures on the lattice is not the running coupling itself, but rather the so-called step-scaling function $\sigma(u,s)$ defined by the implicit equation

$$\sigma(u,s) = \left. g^2(sL) \right|_{g^2(L)=u} \ , \tag{2.31}$$

in terms of which one can define the discrete beta function e.g. as

$$B(u,s) = \left.\frac{g^2(sL) - g^2(L)}{\ln s}\right|_{g^2(L)=u} = \frac{\sigma(u,s) - u}{\ln s} \ . \tag{2.32}$$

Note that the $s \to 1$ limit reproduces the infinitesimal beta function familiar from continuum perturbation theory. However on the lattice a finite and rational value for s is chosen, since the lattice size in units of the lattice spacing is always an integer. In an asymptotically free theory $B(u,s)$ is always positive. Moreover $B(u,s)$ vanishes when it approaches fixed points. Often in the lattice literature the ratio $\sigma(u,s)/u$ is considered instead of the discrete beta function.

In lattice simulations one measures $\Sigma(u,s,N)$, a discretized version of $\sigma(u,s)$, which is function of the lattice size in lattice units $N = L/a$. The continuum limit $a \to 0$ is reached if $N = L/a$ goes to infinity

$$\hat{g}^2(g_0, N) = u \ , \tag{2.33}$$

determines g_0 as a function of the target value u of the running coupling and the number of points N. We will denote $g_0(N,u)$ this function. Notice that in the continuum the running coupling $g^2(L)$ is actually a function of $L\Lambda$, where Λ is the dynamically generated scale. Assuming that $g^2(L)$ is a monotonous function of $L\Lambda$, fixing the value of the running coupling through eq. (2.33) actually means to fix the box size L in units of Λ^{-1}.

In analogy with eq. (2.31), the step-scaling function is defined in the lattice discretized theory as

$$\Sigma(u,s,N) = \left.\frac{\hat{g}^2(g_0, sN)}{u}\right|_{\hat{g}^2(g_0,N)=u} \ . \tag{2.34}$$

The continuum limit $a \to 0$ is reached if $N = L/a$ goes to infinity while L is kept fixed, i.e. while condition (2.33) is satisfied. This happens at the Gaussian fixed point

$$\lim_{N\to\infty} g_0(N,u) = 0 \ , \tag{2.35}$$

which is the fixed point that defines the continuum limit in asymptotically free theories. Therefore the step-scaling function in the continuum is given by

$$\sigma(u,s) = \lim_{a/L\to 0} \Sigma(u,s,a/L) \ . \tag{2.36}$$

In practice this limit is obtained by fitting the following simple functional form to the data

$$\Sigma(u,s,a/L) = \sigma(u,s) + \alpha(u,s)\frac{a^2}{L^2} \ . \tag{2.37}$$

This is motivated by the Symanzik effective description of the lattice artefacts in an $O(a)$-improved setup. At very small values of a the physics at the cutoff scale is always governed by the Gaussian fixed point, irrespectivily of the existence of an IR fixed point. The truncation in (2.37) assumes that $O(a^4)$ terms are subleading. If the theory is IR conformal and u is close enough to its IR fixed-point value for typical values of a/L, which means $a \gg \Lambda^{-1}$, it is reasonable to expect that higher orders become important. In fact detailed study of the systematic errors due to the truncation of the series in (2.37) typically show that the $O(a^4)$ cannot be neglected and this generally results in very large systematic errors for the continuum extrapolation close enough to the IR fixed point. Clearly the value of the coupling at which the validity of the truncation breaks down depends on the particular discretization of the action. However the general message to take home is that even with step-scaling procedure large lattices are still necessary in order to investigate IR-conformality.

2.5.7 Anomalous dimension of $\bar{\psi}\psi$

Finite volume and the step-scaling procedure can be used also to calculate the renormalization factor of $\bar{\psi}\psi$ (or of the mass), from which one can extract the corresponding anomalous dimension $\gamma(g)$ as a function of the running coupling, or its value γ_* at the fixed point if the fixed-point value of the coupling is known. This technique has been widely used in a variety of theories which we will not review here in detail. [58, 142, 143, 146, 150–153] The $\bar{\psi}\psi$ anomalous dimension can be extracted also from other techniques, which do not require knowledge of the value of the coupling at the fixed point, including fit of infinite-volume masses to hyperscaling relations, finite-size scaling analysis of masses [42–48] and power-law fits of the spectral density of the Dirac operator. [47, 54–58]

2.6 Outlook

Lattice simulations of 4-dimensional non-abelian gauge theories close to the lower edge of the conformal window are difficult. There are systematic effects which are rather mild for QCD but become dominant as the conformal window is approached from below. We have reviewed two approaches in detail (1) study of the mass spectrum at finite fermion mass in infinite volume; and (2) study of the running coupling in the massless case in finite volume. There are numerous other very useful and promising approaches but the no-free-lunch theorem seems to apply: if one aspect of the calculation manages to suppress some unwanted systematic effect, another aspect will unavoidably bring back a different, potentially more severe, one. In order to judge the quality of any given lattice result there is no simple rule of thumb to apply but rather all the potential sources of systematic effects, specific to the given approach used, have to be scrutinized. This is, admittedly, not an easy task. Not fully controlling all systematic effects leads to lattice results which are on occasion not fully consistent, but we believe further work in understanding these both theoretically and algorithmically will eventually provide a mature set of results similar to QCD.

What has nevertheless consistently emerged from the non-perturbative lattice investigations is important for model building and phenomenology. The particle spectrum of models close to the conformal window seems to contain a light scalar (relative to for example the vector meson) which might be interpreted as a composite Higgs particle. How the other composite particles of the spectrum of any potential strongly interacting model fit into the Standard Model or extensions thereof is not entirely clear at the moment. Hopefully further lattice investigations together with progress on the experimental side will provide further constraints to help separate the viable from the non-viable models. In the meantime toy models are extremely important for the unexpected systematic effects that may arise in walking models in other words models which are close to the conformal window [59]. One such toy model is introduced in the next chapter.

Chapter 3

A toy model of confining, walking and conformal gauge theories

3.1 Introduction

Lattice simulations of technicolor inspired models are plagued by known systematic uncertainties [60–63, 120]. Although the models under consideration are QCD-like in that they are four dimensional non-abelian gauge theories coupled to dynamical fermions the systematic effects of the interesting models (those that are either conformal or walking) are much more difficult to control than in actual QCD. As a result currently there are disagreements between various approaches, discretizations, etc, and universality is not immediately evident [64–67, 224]. Clearly the general expectation is that once all systematic effects are controlled and taken into account the results from different approaches and regularizations will agree as they should.

In this paper a toy model is proposed which mimics many of the features of non-abelian gauge theories in the hope that systematic effects can be fully explored. Hopefully these will help controlling the corresponding effects in the much more complicated gauge theories. The proposed model is the two dimensional $O(3)$ non-linear sigma model with a θ term. At $\theta = 0$ the model served as a toy model of QCD for a long time since it is asymptotically free, features instantons, confinement and dimensional transmutation [68]. It is exactly solvable [69] even at finite volume [70–72]. Since the topological term is invisible in perturbation theory the model is asymptotically free for arbitrary θ. The dynamics in the infra red is however expected to be very sensitive to θ.

At $\theta = \pi$ the model is conjectured [73, 74] to have a non-trivial infra red fixed point governed by the $SU(2)$ WZNW model at level $k = 1$ and, if the conjecture holds, is also exactly solvable. Some numerical evidence in support of the conjecture has been presented in [75] and a recent very detailed study confirming it in [76]. The infra red fixed point implies a zero of the β-function. This situation is analogous to gauge theories in the conformal window.

For $0 < \theta < \pi$ exact solvability is lost but based on continuity one expects that for θ not much below π the β-function develops a near zero and the renormalized coupling will walk. This arrangement is analogous to gauge theories just below the conformal window. Hence dialing θ corresponds to dialing the number of flavors N_f in the gauge theory.

In all three scenarios (confining, walking, conformal) one may also introduce an external magnetic field to mimic the effect of a finite quark mass.

Before exploring the analogies further and investigating the origins of the severe systematic effects the first task is to establish non-perturbatively that the θ-term is actually a relevant operator and also what the singularity structure of the theory is for $\theta > 0$. This is not immediately obvious largely because of the unusual scaling properties of the topological susceptibility and a class of similar observables.

It is well known that small size instantons render the topological susceptibility $\chi = \langle Q^2 \rangle / V$ ill defined in the semi-classical approximation [77]. Going beyond the semi-classical approximation fully non-perturbative lattice studies have shown that regardless how one improves the details of the lattice implementation a logarithmically divergent susceptibility is obtained at finite physical volume in the continuum limit. Moreover, all even moments of the total topological charge distribution $\langle Q^{2m} \rangle / V$ have the same property.

However, the model at $\theta = 0$ is exactly solvable and both the exact solution and the continuum limit of lattice simulations agree that correlators of the topological charge density, e.g. $\langle q(x)q(0) \rangle$ are finite. The above two observations, namely that certain statistical properties of the total charge distribution $P(Q)$ are ill defined while at the same time correlators of $q(x)$ are finite, might make one wonder whether the total charge operator Q is an irrelevant operator while $q(x)$ is not. If so, the only consistent continuum value of $\langle Q^{2m} \rangle$ would be zero and the apparent divergences in the lattice calculations would be regarded as artifacts. This scenario would imply that the theory defined on the lattice at non-zero θ leads to an identical continuum theory as the one defined at $\theta = 0$. Equivalently, the total charge operator inserted into any correlation function would be zero in the continuum theory $\langle Q \ldots \rangle = 0$, while correlation functions of the type $\langle q(x) \ldots \rangle$ are finite. This scenario would of course invalidate Haldane's conjecture about the equivalence of the $\theta = \pi$ theory with a non-trivial interacting conformal field theory.

In this work it is shown that there exist quantities built out of the total topological charge operator Q which have well defined continuum limits and are non-zero. These observables are differences of connected correlation functions of the topological charge, in other words the cumulants. Each term is logarithmically divergent but the divergence cancels in the difference and moreover they scale correctly in the continuum limit to non-zero values. Showing correct scaling towards the continuum limit in itself would not be sufficient to prove that the θ-term is a relevant operator because the continuum limit value could be zero. Since all cumulant differences are finite there is only a single UV-divergent parameter in the partition function $Z(\theta)$ but otherwise it is finite.

While preparing this manuscript the preprint [76] appeared also with the conclusion that θ is a relevant coupling. The method was different though, in [76] it was shown to high precision that a well defined observable is different in the continuum limit for three different values of θ implying that θ can not be irrelevant. In the current work all simulations are carried out at $\theta = 0$ and the same conclusion is reached by showing that certain combinations of the topological charge operator are non-zero in the continuum.

3.2 $O(3)$ sigma model with a θ-term

The model in Euclidean continuum notation is defined by the action

$$S = \frac{1}{2g_0^2} \int d^2x \partial_\mu s_a \partial_\mu s_a \tag{3.1}$$

for the unit 3-vectors s, $s_1^2 + s_2^2 + s_3^2 = 1$, where g_0 is the bare coupling. Only a torus geometry will be considered corresponding to a box of finite linear size L which will be regularized by a symmetric lattice.

The corresponding partition function, free energy per unit volume and topological charge distribution of the model at non-zero θ and volume V is given by

$$Z(\theta) = \langle e^{i\theta Q} \rangle = e^{-Vf(\theta)} = \sum_Q P(Q) e^{i\theta Q} \ , \tag{3.2}$$

with the normalization $Z(0) = \sum_Q P(Q) = 1$. Since physics is periodic with period 2π in θ and $\theta \to -\theta$ is a symmetry the free energy per unit volume can be Fourier expanded

$$f(\theta) = \sum_{n=1}^{\infty} (1 - \cos(n\theta))\, f_n \ . \tag{3.3}$$

It has been pointed out in [78] that in the semi-classical or dilute gas approximation all f_n coefficients vanish except for f_1 which is UV divergent due to instantons of size $a \ll \rho \ll \xi$ where a is the lattice cut-off and ξ is the physical correlation length. The remaining coefficients come from interactions between instantons. Semi-classical arguments also suggest that for instantons causing the UV divergence in f_1 the ratio between their size and their average separation goes to zero in the continuum limit. This would imply that the interactions responsible for the $f_{n>1}$ coefficients are small in the continuum limit hence will not cause them to diverge.

To summarize, the semi-classical approximation accounts for a UV divergent f_1 and finite $f_{n>1}$ coefficients. A suitable way of addressing whether this statement is true beyond the semi-classical approximation is to consider observables that can be expressed by the $f_{n>1}$ coefficients only and calculating them fully non-perturbatively. The simplest choice is to take the connected correlation functions of the topological charge,

$$\chi_{2m} = (-1)^{m+1} \left. \frac{d^{2m} f}{d\theta^{2m}} \right|_{\theta=0} \tag{3.4}$$

and consider their differences,

$$\Delta\chi_{2m} = \chi_{2m} - \chi_{2m+2} = \sum_{n=2}^{\infty} f_n n^{2m} (1 - n^2) \tag{3.5}$$

from which f_1 drops out. The first few such correlation functions are

$$\begin{aligned} \chi_2 &= \frac{\langle Q^2 \rangle}{V} \\ \chi_4 &= \frac{\langle Q^4 \rangle - 3\langle Q^2 \rangle^2}{V} \\ \chi_6 &= \frac{\langle Q^6 \rangle - 15\langle Q^4 \rangle \langle Q^2 \rangle + 30\langle Q^2 \rangle^3}{V} \ . \end{aligned} \tag{3.6}$$

All of these are expected to diverge in the continuum limit but their differences are expected to be finite. Some numerical evidence has been presented in [78] in favor of correct scaling behavior for $\Delta\chi_2$ but whether the continuum value is zero or non-zero has not been discussed.

In the following it will be shown to high precision that the expectations from the semi-classical analysis indeed hold non-perturbatively and all moments $\langle Q^{2m}\rangle$ and all cumulants χ_{2m} are logarithmically divergent but the differences $\Delta\chi_{2m}$ are finite. This implies that there is a single ill-defined constant in $f(\theta)$ namely f_1 but otherwise it is finite. The constant f_1 can be removed by an appropriate renormalization condition leading to a finite and universal free energy and partition function for arbitrary θ.

3.3 Numerical simulation

It is convenient to take the continuum limit on a symmetric periodic lattice L^2 of fixed physical volume. Physical length and mass is defined by the second moment correlation length ξ_2 [79],

$$\frac{1}{\xi_2(L)^2} = \left(\frac{\sin\frac{\pi a}{L}}{\frac{\pi a}{L}}\right)^2 \left(2\frac{M_0}{M_2} - \frac{4\pi^2}{L^2}\right) \tag{3.7}$$

where

$$M_{2n} = \left(\frac{L}{2\pi}\right)^{2n} \sum_t \left(2\sin\frac{\pi t}{L}\right)^{2n} C(t) \tag{3.8}$$

is given in terms of the zero spatial momentum projection of the 2-point correlation function $C(t) = \sum_x \langle s_a(t,x) s_a(0,0)\rangle$ of the field s. Let us introduce $m(L) = 1/\xi_2(L)$. Note that in this notation $m(L)$ is not the mass gap in finite volume but rather is simply defined as the inverse of ξ_2 (which for $L \to \infty$ agrees with the mass gap but not for finite L). The physical volume is fixed to $m(L)L = 4$. A novel [80–82] topological lattice action is used for the simulations,

$$S = \sum_{\langle i,j\rangle} S(s_i, s_j) \tag{3.9}$$

where the sum is over all neighboring sites and

$$S(s_i, s_j) = \begin{cases} 0 & \text{if} \quad s_i \cdot s_j > \cos\delta \\ \infty & \text{otherwise} \end{cases} \tag{3.10}$$

In other words the action is zero for two neighboring vectors if their relative angle is smaller than δ and infinite otherwise. The continuum limit is taken by tuning the bare coupling δ towards zero. This action is topological because small perturbations of the field s do not change the action nevertheless it has been shown that it is in the right universality class [82].

If $\delta < \pi/2$ powerful improvements exist for the measurement of the topological charge distribution [75] based on a generalization of the usual cluster algorithms [83, 84]. The topological charge operator from [85] is used assigning an integer charge to each configuration even at finite lattice spacing.

The continuum extrapolation of the cumulant differences will be done through 12 lattice spacings using the parameter values from [82] listed in table 3.1. The measured

L/a	δ/π	$m(L)L$	$L^2\chi_2$	$L^2\chi_4$	$L^2\chi_6$	$L^2\Delta\chi_2$	$L^2\Delta\chi_4$
60	0.48490	4.0017(14)	1.2957(2)	0.8812(8)	-0.019(5)	0.4145(8)	1.069(5)
80	0.47260	4.0032(19)	1.4651(2)	1.0292(8)	-0.011(6)	0.4359(7)	1.143(6)
100	0.46370	4.0007(19)	1.6018(3)	1.1512(9)	-0.035(8)	0.4507(9)	1.186(7)
120	0.45680	3.9939(20)	1.7155(3)	1.257(1)	0.033(9)	0.459(1)	1.224(8)
160	0.44680	4.0011(14)	1.9214(4)	1.444(1)	0.16(1)	0.477(1)	1.28(1)
200	0.43950	4.0015(17)	2.0836(3)	1.596(1)	0.24(1)	0.488(1)	1.35(1)
240	0.43385	3.9998(14)	2.2208(3)	1.729(1)	0.40(1)	0.492(1)	1.33(1)
320	0.42545	4.0010(17)	2.4476(4)	1.946(1)	0.57(1)	0.502(1)	1.37(1)
400	0.41930	3.9983(14)	2.6259(4)	2.118(2)	0.71(2)	0.508(2)	1.41(2)
480	0.41455	4.0014(19)	2.7845(4)	2.274(2)	0.88(2)	0.511(2)	1.39(2)
640	0.40740	4.0021(18)	3.0347(4)	2.521(2)	1.07(3)	0.514(2)	1.45(3)
800	0.40210	3.9952(19)	3.2221(3)	2.704(2)	1.20(3)	0.518(2)	1.50(3)

Table 3.1: Results for the first few cumulants and their differences for fixed physical volume $m(L)L = 4$. The bare parameters δ are taken from [82].

correlation lengths and topological susceptibilities are in agreement with those in [82]. In the present work $O(10^8)$ configurations were generated at each volume and every 10^{th} was measured for the topological charge distribution and correlation length. The large number of configurations was necessary because there are huge cancellations between the various terms in the difference of cumulants, especially for $\Delta\chi_4$. The third difference, $\Delta\chi_6$, was already impossible to obtain with the current statistics.

The results for the cumulant differences $\Delta\chi_2$ and $\Delta\chi_4$ are shown on figure 3.1. Obtaining continuum estimates is not entirely trivial since the precise form of the leading and sub leading cut-off effects is not known a priori. Using the results of [86,87] one may expect the leading corrections to be $O((a/L)^2)$ with possibly large logarithmic corrections. Fits of the form

$$C + (a/L)^2 \left(\sum_{j=n}^{m} A_j \log^j(L/a) \right) \tag{3.11}$$

with $(n,m) = (0,3), (1,3), (2,3), (0,2)$ all work quite well with χ^2/dof values close to unity for $\Delta\chi_2$ and slightly higher, around 1.8 for $\Delta\chi_4$. The continuum extrapolated values agree in both cases among the four fit function choices and the four curves lie almost entirely on top of each other. In both cases the $(n,m) = (0,2)$ choice is shown on the plots leading to continuum estimates $C = 0.523(2)$ and $1.48(2)$ for $L^2\Delta\chi_2$ and $L^2\Delta\chi_4$, respectively. Clearly, both values are non-zero.

3.4 Summary and conclusion

It has been known for a long time that the topological susceptibility in the two dimensional $O(3)$ model is ill-defined in the continuum. Consequently the topological charge distribution $P(Q)$ does not have a finite continuum limit. The semi-classical analysis predicts precisely what part of $P(Q)$ is actually divergent and what part of it is finite. In this work non-perturbative evidence has been presented supporting the semi-classical result. The only divergent quantity is the first Fourier coefficient of the

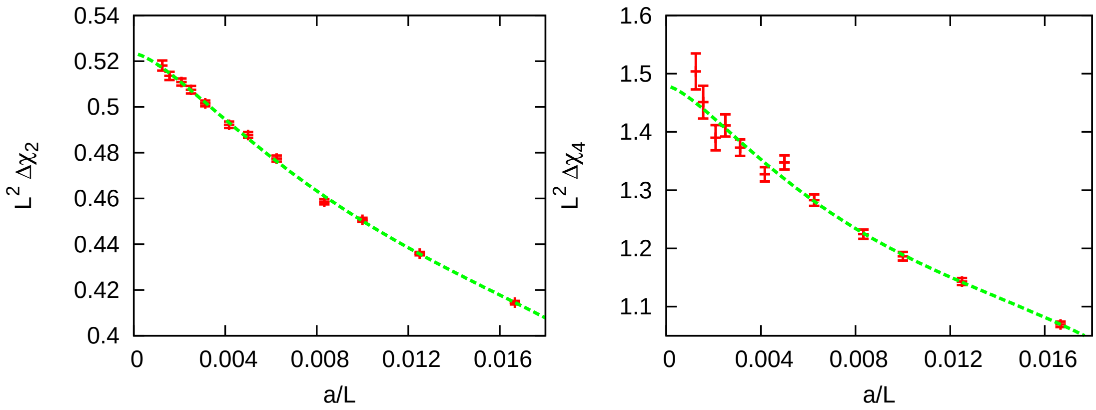

Figure 3.1: Continuum extrapolation for the first two cumulant differences multiplied by the volume, $L^2\Delta\chi_2$ and $L^2\Delta\chi_4$.

free energy density,

$$f_1 = -\int_0^\pi f(\theta)\cos(\theta)\frac{d\theta}{2\pi} \ , \tag{3.12}$$

while the remaining part $\sum_{n>1}(1-\cos(n\theta))f_n$ is finite and non-zero. Hence the quantity

$$f_R(\theta) = f(\theta) - (1-\cos(\theta))f_1 \tag{3.13}$$

is finite and universal and one may consider the subtraction an additive renormalization. Similarly the renormalized partition function $Z_R(\theta) = \exp(-Vf_R(\theta))$ is finite and universal and related to the bare partition function by a multiplicative renormalization. Instead of subtracting f_1 it is sufficient to subtract only its divergent piece. The logarithmic singularity is expected to be volume independent[1]. Let us then denote this singular quantity by f_{1s}. Since $\chi_2 = f_1 + \sum_{n>1} n^2 f_n$ a suitable definition of f_{1s} is the logarithmic singularity in the topological susceptibility which can directly be measured in lattice calculations. A natural renormalization procedure is then the following: one defines the theory for non-zero θ by the action

$$S(\theta) = S(\theta=0) - i\theta Q - (1-\cos(\theta))Vf_{1s} \tag{3.14}$$

and all resulting correlation functions related to topology (i.e. derivatives with respect to θ) become finite. The last term in the full action above is a non-perturbatively generated counter term. It is important to note that the above renormalization does not mean that θ itself gets renormalized, the bare θ is still a physical quantity which does not require renormalization. It would of course be very interesting to check the volume independence of f_{1s} in lattice simulations.

The finite quantities $f_{n>1}$ and $\Delta\chi_{2m}$ are not volume independent and are non-trivial functions of $z = m(L)L$. Since the model is exactly solvable at $\theta = 0$ it would be interesting to derive the first few cumulant differences $\Delta\chi_{2m}(z)$ from the exact solution or at least their value in the infinite volume limit.

[1] I thank Ferenc Niedermayer for pointing this out.

In any case the finite and non-zero cumulant differences naturally lead to the conclusion that θ is a relevant coupling of the theory and the total topological charge operator Q is a relevant operator despite the ill-defined nature of the moments $\langle Q^{2m} \rangle$.

The original motivation was the study of a toy model mimicking confining, walking and conformal behavior in four dimensional gauge theories in order to study the severe systematic effects of the latter. It was proposed that increasing θ is analogous to increasing the number of flavors N_f because as θ goes from zero to π the model goes from confining to walking and to conformal. In the toy model a suitable renormalized coupling is $g_R^2(L) = m(L)L$ which would then run with the finite volume L. A necessary condition for this analogy to hold was establishing precisely the divergence structure of the partition function at non-zero θ.

A particular difficulty of the gauge theory calculation can also be studied in the toy model. It is very difficult to distinguish numerically the following two cases: the theory with zero quark mass just below the conformal window and the theory with a small but non-zero quark mass just inside the conformal window. Both theories walk, the former for the usual reason of being just below the conformal window while the latter because even though it would be conformal for zero quark mass, the non-zero mass drives the coupling away from the would-be fixed point as soon as the running scale goes below the massive fermionic states. This phenomenon can be mimicked in the toy model by considering it at zero external magnetic field and $\theta = \pi - \varepsilon$ and also at a small but non-zero external magnetic field and $\theta = \pi$. Both theories are expected to walk and it would be interesting to explore in the toy model what intrinsic features are different despite the similar behavior of the walking coupling constant.

There are a couple of differences between the toy model and gauge theory though. Less important is the fact that while θ does not enter the perturbative β-function, N_f does. More significant is the fact that due to the $\theta \to -\theta$ symmetry and periodicity by 2π the two values $\theta - \varepsilon$ and $\theta + \varepsilon$ lead to the same continuum theory and it does not have an infra red fixed point (for non-zero ε the coupling walks). This means that the zero of the β-function at $\theta = \pi$ is eliminated by arbitrary perturbations of θ meaning that this zero is a second order zero, unlike in the gauge theory where generically the zero is expected to be first order and is preserved by small perturbations. Hence the $\theta = \pi$ model is really analogous to a gauge theory which is exactly at the lower edge of the conformal window. It would be interesting to find a simple toy model which possesses all essential features and in addition the infra red fixed point is a first order zero of the β-function and disappears by joining with a non-trivial UV fixed point as expected in gauge theory [88–90].

Chapter 4

Sextet composite Higgs model

4.1 Introduction

An important strongly coupled near-conformal gauge theory built on the minimally required SU(2) bsm-flavor doublet of two massless fermions, with a confining gauge force at the TeV scale in the sextet representation of the new SU(3) BSM color gauge group is an intriguing possibility for the minimal realization of the composite Higgs mechanism. Early discussions of the model as a BSM candidate were initiated in systematic explorations of higher fermion representations of color gauge groups [13,25, 26] for extensions of the original Higgsless Technicolor paradigm [8,9]. In fact, the first appearance of the particular two-index symmetric SU(3) fermion representation can be traced even further back to Quantum Chromodynamics (QCD) where a doublet of sextet quarks was proposed as a mechanism for Electroweak symmetry breaking (EWSB) without an elementary Higgs field [165]. This idea had to be replaced by a new gauge force at the TeV scale, orders of magnitude stronger than in QCD, to facilitate the dynamics of EWSB just below the lower edge of the conformal window in the new BSM paradigm [13,25,26]. It should be noted that throughout its early history the important near-conformal behavior of the model was not known and definitive results had to wait for recent non-perturbative investigations with lattice gauge theory methods as used in our work.

Near-conformal BSM theories raise the possibility of a light composite scalar, perhaps a Higgs impostor, to emerge from new strong dynamics, far separated from the associated composite resonance spectrum in the few TeV mass range with interesting and testable predictions for the Large Hadron Collider (LHC). This scenario is very different from what was expected from QCD when scaled up to the Electroweak scale, as illustrated by the failure of the Higgsless Technicolor paradigm. Given the discovery of the 125 GeV Higgs particle at the LHC, any realistic BSM theory must contain a Higgs-like state, perhaps with some hidden composite structure.

Based on our *ab initio* non-perturbative lattice calculations we find accumulating evidence for near-conformal behavior in the sextet theory with the emergent low mass 0^{++} scalar state far separated from the composite resonance spectrum of bosonic and baryonic excitations in the 2-3 TeV energy range [15, 94, 96, 166]. The identification of the light scalar state is numerically challenging since it requires the evaluation of disconnected fermion loop contributions to correlators with vacuum quantum numbers in the range of light fermion masses we explore. The evidence to date is very promising that the 0^{++} scalar is light in the chiral limit and that the model at this stage remains an important BSM candidate.

4.2 Electroweak multiplet structure, gauge anomalies, and baryons

As in the minimal scheme of Susskind [9] and Weinberg [8], the gauge group of the theory is $\mathrm{SU(3)_{bsm}}\otimes\mathrm{SU(3)_c}\otimes\mathrm{SU(2)_w}\otimes\mathrm{U(1)_Y}$ where $\mathrm{SU(3)_c}$ designates the QCD color gauge group and $\mathrm{SU(3)_{bsm}}$ represents the BSM color gauge group of the new strong gauge force. In addition to quarks and leptons of the Standard Model, we include one SU(2) bsm-flavor doublet (u, d) of fermions which are $\mathrm{SU(3)_c}$ singlets and transform in the six-dimensional sextet representation of BSM color, distinct from the fundamental color representation of fermions in the original Technicolor scheme [8, 9]. The formal designation $(\mathrm{u, d})$ for the bsm-flavor doublet of sextet fermions uses a similar notation to the two light quarks of QCD but describes completely different physics. The massless sextet fermions form two chiral doublets $(\mathrm{u,d})_\mathrm{L}$ and $(\mathrm{u,d})_\mathrm{R}$ under the global symmetry group $\mathrm{SU(2)_L}\otimes\mathrm{SU(2)_R}\otimes\mathrm{U(1)_B}$. Baryon number is conserved for quarks of the Standard Model separate from baryon number conservation for sextet fermions which carry 1/3 of BSM baryon charge associated with the BSM sector of the global $\mathrm{U(1)_B}$ symmetry group.

4.2.1 Electroweak multiplet structure

It is straightforward to define consistent multiplets for the sextet fermion flavor doublet under the $\mathrm{SU(2)_w}\otimes\mathrm{U(1)_Y}$ Electroweak gauge group with hypercharge assignments for left- and right-handed fermions transforming under the $\mathrm{SU(2)_w}$ weak isospin group. The two fermion flavors $\mathrm{u^{ab}}$ and $\mathrm{d^{ab}}$ of the strongly coupled sector carry six colors in two-index symmetric tensor notation, $\mathrm{a, b} = 1, 2, 3$, associated with the gauge force of the $\mathrm{SU(3)_{bsm}}$ group. This is equivalent to a six-dimensional vector notation in the sextet representation. The fermions transform as left-handed weak isospin doublets and right-handed weak isospin singlets for each color,

$$\psi_\mathrm{L}^\mathrm{ab} = \begin{pmatrix} \mathrm{u_L^{ab}} \\ \mathrm{d_L^{ab}} \end{pmatrix}, \qquad \psi_\mathrm{R}^\mathrm{ab} = (\mathrm{u_R^{ab}},\ \mathrm{d_R^{ab}}). \tag{4.1}$$

With this choice of representations, the normalization for the hypercharge Y of the $\mathrm{U(1)_Y}$ gauge group is defined by the relation $\mathrm{Y} = 2(\mathrm{Q} - \mathrm{T_3})$, with $\mathrm{T_3}$ designating the third component of weak isospin.

Once Electroweak gauge interactions are turned on, the chiral symmetry breaking pattern $\mathrm{SU(2)_L}\otimes\mathrm{SU(2)_R} \to \mathrm{SU(2)_V}$ of strong dynamics breaks Electroweak symmetry in the expected pattern, $\mathrm{SU(2)_w} \times \mathrm{U(1)_Y} \to \mathrm{U(1)_{em}}$, and with the simultaneous dynamical realization of the composite Higgs mechanism. It is important to note that the dynamical Higgs mechanism is facilitated through the electroweak gauge couplings of the sextet fermions and does not depend on the hypercharge assignments of the multiplets [9]. Recently, we presented a detailed analysis on anomaly constraints of hypercharge assignments [167]. In this report we summarize what is relevant for the sextet baryon analysis of our existing gauge ensembles with dark matter and model viability implications [167].

4.2.2 Anomaly conditions

Anomaly constraints have a long history in Technicolor motivated BSM model building with representative examples in [26, 168–171]. The first condition for model construction with left-handed doublets is the global Witten anomaly constraint which requires an even number of left-handed SU(2) multiplets to avoid inconsistency in the theory from a vanishing fermion determinant of the partition function [172]. In addition, gauge anomaly constraints also have to be satisfied [173]. With vector current $\mathrm{V}^{\mathrm{i}}_{\mu}(\mathrm{x}) = \overline{\psi}\mathrm{T}^{\mathrm{i}}\gamma_\mu\psi(\mathrm{x})$ and axial current $\mathrm{A}^{\mathrm{i}}_{\mu}(\mathrm{x}) = \overline{\psi}\mathrm{T}^{\mathrm{i}}\gamma_\mu\gamma_5\psi(\mathrm{x})$ constructed from fermion fields and internal symmetry matrices T^{i} in some group representation R for fermions, the anomaly in the axial vector Ward identity is proportional to $\mathrm{tr}(\{\mathrm{T}^{\mathrm{i}}(\mathrm{R}), \mathrm{T}^{\mathrm{j}}(\mathrm{R})\}\mathrm{T}^{\mathrm{k}}(\mathrm{R}))$ and must vanish. In the sextet theory fermions are either left-handed doublets or right-handed singlets under the $\mathrm{SU}(2)_{\mathrm{w}}$ gauge group. The matrices T^{i} will be either the τ^{i} Pauli matrices or the diagonal U(1) hypercharge Y. Since the SU(2) group is anomaly free, $\mathrm{tr}(\{\tau^{\mathrm{i}}, \tau^{\mathrm{j}}\}\tau^{\mathrm{k}}) = 0$, we only need to consider anomalies where at least one T^{i} is the hypercharge Y. The non-trivial constraints come from two conditions on hypercharge traces,

$$\mathrm{tr}(\mathrm{Y}) = 0, \quad \mathrm{tr}(\mathrm{Y}^3) \propto \mathrm{tr}(\mathrm{Q}^2\mathrm{T}_3 - \mathrm{Q}\mathrm{T}_3^2) = 0\,, \tag{4.2}$$

where $\mathrm{Y} = 2(\mathrm{Q} - \mathrm{T}_3)$ with electric charge Q, and T_3 as the third component of weak isospin. There are two simple solutions for BSM model building with sextet fermions to satisfy the Witten anomaly condition and gauge anomaly constraints on tr(Y) and $\mathrm{tr}(\mathrm{Y}^3)$ in Eq. (4.2). The first solution with the choice $\mathrm{Y}(\mathrm{f_L}) = 0$ for doublets of left-handed sextet fermions ($\mathrm{f_L}$) leads to half-integer electric charges for composite baryons. The second solution with the choice $\mathrm{Y}(\mathrm{f_L}) = 1/3$ for doublets of left-handed sextet fermions leads to integer electric charges for composite baryons. The hypercharges of right-handed singlets are automatically set from consistent electric charge assignments in both cases. The two choices have very different implications for sextet baryons.

4.2.3 Sextet baryons and the Early Universe

In the sextet BSM theory we do not have direct observations of new heavy baryons to set unique hypercharge assignments for left-handed doublets and right-handed singlets of sextet fermions from two alternate solutions to the anomaly conditions. Viability of the choices $\mathrm{Y}(\mathrm{f_L}) = 0$, or $\mathrm{Y}(\mathrm{f_L}) = 1/3$, is affected by the different electric charge assignments they imply. With heavy sextet baryon masses in the 3 TeV range, as determined from our recent lattice simulations [167], the seemingly minimal solution with $\mathrm{Y} = 0$ for left-handed doublets would lead to intriguing predictions of baryon states with half-integer electric charges for future accelerator searches and relics with fractional electric charges from the early Universe with observable consequences. Problems with half-integer electric charges, from the choice $\mathrm{Y}(\mathrm{f_L}) = 0$ in our case, were anticipated earlier from strong observational limits on stable fractional charges in the early Universe and their terrestrial relics [174, 175]. The non-controversial $\mathrm{Y}(\mathrm{f_L}) = 1/3$ anomaly solution for the sextet model has new dark matter implications [167] which require new lattice calculations proposed here.

4.2.4 Ongoing lattice work on sextet baryons

The lightest baryons in the strongly coupled sextet gauge sector are expected to form isospin flavor doublets (uud, udd), similar to the pattern in QCD. As we noted earlier, baryons in the sextet model should carry integer multiples of electric charges if $Y(f_L) \neq 0$ to avoid problems with the relics of the early Universe. This leads to the simplest choice $Y(f_L) = 1/3$ with gauge anomalies to be compensated. A new pair of left-handed lepton doublets emerged from this choice as the simplest manifestation of the anomalies and the Electroweak extension of the strongly coupled sextet gauge sector [167].

Neutron-like udd sextet model baryons (n_6) will carry no electric charge and proton-like uud sextet model baryons (p_6) have one unit of positive electric charge from the choice $Y(f_L) = 1/3$. The two baryon masses are split by electromagnetic interactions. The ordering of the two baryon masses in the chiral limit of massless sextet fermions will require non-perturbative *ab initio* lattice calculations of the electromagnetic mass shifts to confirm intuitive expectations that the neutron-like n_6 baryon has lower mass than the proton-like p_6 baryon. In QCD this pattern was confirmed by recent lattice calculations [176]. We expect the same ordering in the sextet model so that the proton-like p_6 baryon will decay very fast, $p_6 \to n_6 + ...$, with a lifetime $\tau \ll 1$ second. It is unlikely for rapidly decaying p_6 baryons to leave any relic footprints from dark nucleosynthesis before they decay.

With BSM baryon number conservation the neutral n_6 baryon is stable and observational limits on its direct detection from experiments like XENON100 [3] and LUX2013 [4] have to be estimated. In charge symmetric thermal evolution sextet model baryons are produced with relic number density ratio $n_{B_6}/n_B \approx 3 \cdot 10^{-7}$. For 3 TeV sextet model baryon masses we can estimate the detectable dark matter ratio of respective mass densities ρ_{B_6} and ρ_B as $\rho_{B_6}/\rho_B \approx 10^{-4}$, about $5 \cdot 10^4$ times less than the full amount of unaccounted dark mass, $\rho_{\rm dark} \approx 5 \cdot \rho_B$. We will use this mass density estimate to guide observational limits on relic sextet model baryons emerging from charge symmetric thermal evolution where tests of dark baryon detection come from elastic collisions with nuclei in dark matter detectors [167]. The neutral and stable n_6 baryon can interact several different ways with heavy nuclei in direct detection experiments including (a) magnetic dipole interaction, (b) Z-boson exchange, (c) Higgs boson exchange, and (d) electric polarizability. It turns out that cross sections from (a) and (b) can be parametrized and estimated even without lattice simulations. Cross sections from (c) and (d) require lattice calculations using our existing gauge ensembles and capacity computing from new allocation we request for gpu capacity computing. Based on these estimates we expect to show that the sextet BSM model is consistent with observational limits and stable baryons will contribute a small fraction to the missing dark matter content. New physics implied by gauge anomaly constraints, like new lepton generations with neutrinos [167], can also contribute to the relic abundance of dark matter. These are important and interesting issue for future investigations.

4.3 Mass-deformed chiral perturbation theory and the chiral condensate

One of the most important goals of lattice BSM models is to accurately set the Electroweak scale as a function of the lattice spacing. This allows control on the continuum limit when the cutoff is removed and phenomenologically relevant BSM predictions are made. The chiral $SU(2)_L \times SU(2)_R$ symmetry of the model is dynamically broken to the diagonal vector symmetry $SU(2)_V$ and three associated Goldstone pions facilitate the minimal realization of the Higgs mechanism after the Electroweak interactions are turned on. The Electroweak scale in finite lattice spacing units is set from the decay constant F_π of the Goldstone pion in the chiral limit with F = 250 GeV in continuum physics notation. It can be identified as the fundamental scale of the theory related to the chiral (Higgs) condensate through the GMOR relation.

4.3.1 Taste breaking cutoff effects in the staggered pion spectrum

Since the determination of the Goldstone decay constant F in the chiral limit is critically important for the location of the light scalar mass and the well-separated resonance spectrum in the 2-3 TeV range, we carefully monitor taste breaking effects in the pion spectrum with the goal of removing cutoff effects from physics predictions. This also serves as guidance for our choice of lattice spacings for new configuration generation.

To illustrate cutoff dependent taste breaking effects, spectra of mass-deformed non-Goldstone pion states are shown in Figure 4.1 from our newest data with the definition of the relevant correlators and quantum numbers given in [15,66]. In the fermion mass range of our data set the taste breaking pattern is different from QCD where the residual Δ mass shifts of the non-Goldstome pions are equispaced in the chiral limit with approximately degenerate SO(4) taste multiplets and with parallel slopes for finite fermion mass deformations of Goldstone and non-Goldstone pion states [177]. For example, as part of the equispaced split of degenerate SO(4) multiplets, the observed approximate split $\Delta_{\rm ij} \sim 2\Delta_{\rm sc}$ of two multiplets in QCD appears to have collapsed in the sextet model. The other distinct difference from QCD is the non-parallel slopes which fan out in Goldstone and non-Goldstone mass deformations of the pion spectrum as shown in Figure 4.1. While the Δ additive mass shifts are LO taste breaking effects in the chiral Lagrangian [177,178], the taste breaking slope corrections δ can plausibly be identified with NLO analytic terms in rooted staggered chiral perturbation theory (rsχPT) [179]. The corrected mass relation is $M^2_{\rm NLO} = M^2_{\rm LO}(1+\delta)$ where δ depends on the taste quantum number of the pion state. Several relations constrain the δ taste breaking corrections [179]. The pion spectrum with taste breaking cutoff effects is the input to analyze the fundamental parameters of rsχPT as worked out for the SU(3) group in [178]. Our adaptation to the SU(2) group of rsχPT in the sextet model is straightforward.

4.3.2 Fundamental parameters from rooted staggered chiral perturbation theory (p-regime)

For the SU(2) analysis we adapted the procedure from [178]. There are two fundamental parameters F and B in the SU(2) chiral Lagrangian. The fundamental parameter F of χPT, defined as the chiral limit of the pion decay constant F_π, sets the Electroweak scale and the fundamental parameter B sets the fermion mass deformation of the Goldstone spectrum. With bare fermion mass m, the RG invariant combination $m \cdot BF^2$ is related to the chiral condensate via the GMOR relation.

We apply rooted staggered chiral perturbation theory to the mass-deformed pion spectrum and F_π. The fitting procedure in the p-regime proceeds in several steps. In the first step finite volume correction is applied to the M_π and F_π data from 1-loop continuum χPT. This is sufficient to assure that in the next step the fitting procedure is applied to data free from volume dependence. A linear fit is applied to the quadratic masses of the non-Goldstone pion spectrum to determine their mass shifts and slopes.

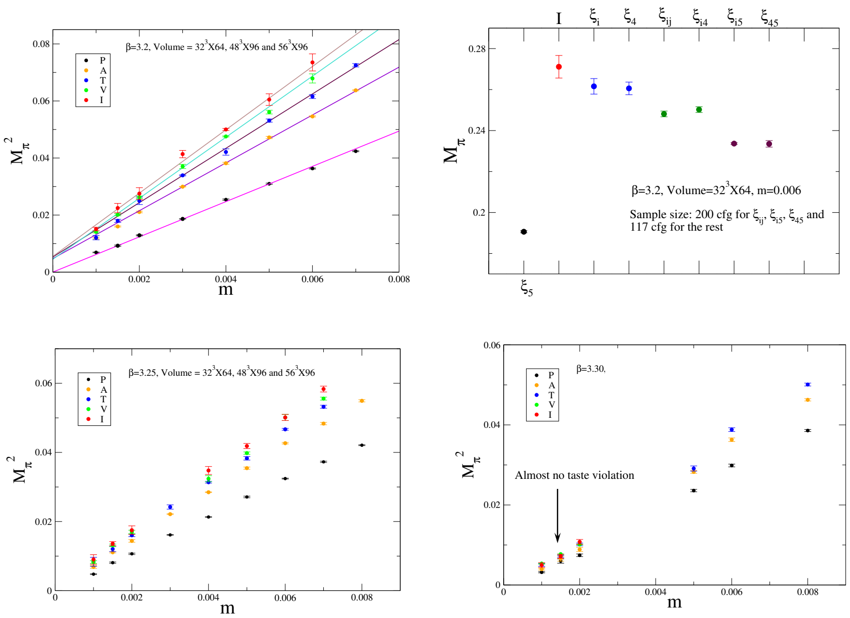

Figure 4.1: To illustrate cutoff dependent taste breaking effects, spectra of mass-deformed non-Goldstone pion states are shown from our newest data with the definition of the relevant correlators and quantum numbers given in [15,66]. In the fermion mass range of our data set the taste breaking pattern is different from QCD where the residual Δ mass shifts of the non-Goldstone pions are equispaced in the chiral limit with approximately degenerate SO(4) taste multiplets and with parallel slopes for finite fermion mass deformations of Goldstone and non-Goldstone pion states [177]. For example, as part of the equispaced split of degenerate SO(4) multiplets, the observed approximate split $\Delta_{\rm ij} \sim 2\Delta_{\rm sc}$ of two multiplets in QCD appears to have collapsed in the sextet model. The other distinct difference from QCD is the non-parallel slopes which fan out in Goldstone and non-Goldstone mass deformations of the pion spectrum as shown. While the Δ additive mass shifts are LO taste breaking effects in the chiral Lagrangian [177,178], the taste breaking slope corrections δ can plausibly be identified with NLO analytic terms in the chiral analysis [179]. The corrected mass relation is $\mathrm{M}^2_{\rm NLO} = \mathrm{M}^2_{\rm LO}(1+\delta)$ where δ depends on the taste quantum number of the pion state. Several relations constrain the δ taste breaking corrections [179].

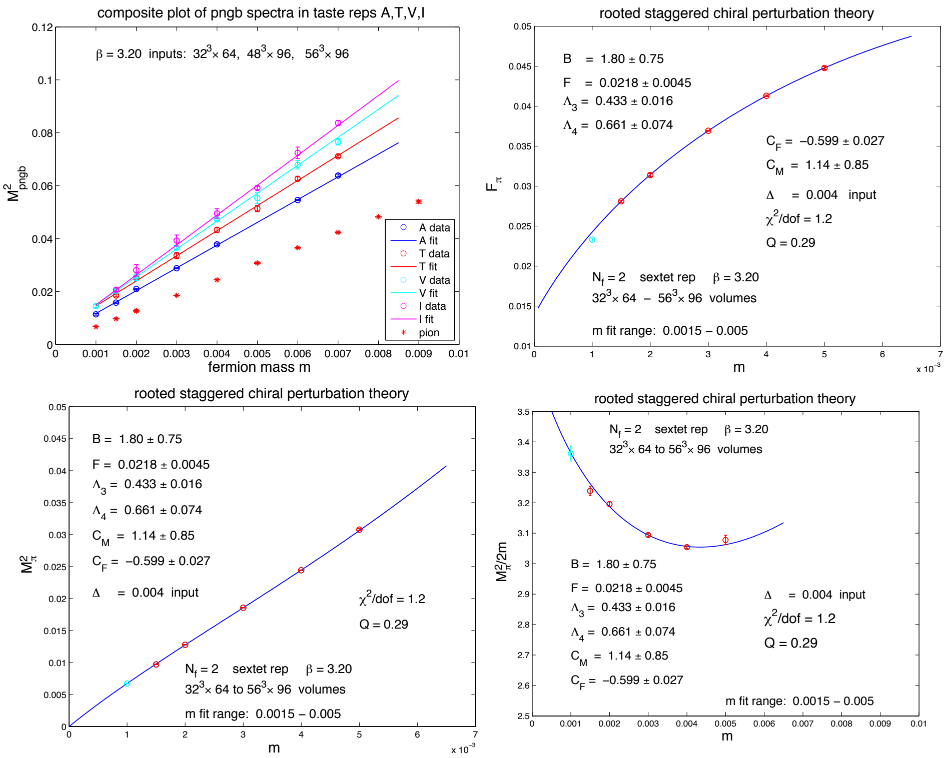

Figure 4.2: Preliminary results from rooted χPT are shown from fits at gauge coupling $\beta = 3.20$ which corresponds to our coarser lattice of the two extended sets of gauge ensembles. The upper left panel shows the linear fits to the quadratic masses of the non-Goldstone pions to determine their mass shifts and slopes as input. The upper right panel shows the rooted χPT fit to F_π as a function of fermion mass deformations away from the chiral limit. The two lower panels show rooted χPT fits to M_π as a function of fermion mass deformations away from the chiral limit. We have similar analysis for M_π^2 and F_π at $\beta = 3.25$.

In the final analysis of rooted chiral perturbation theory, non-Goldstone pion states run in the chiral loops including their mass splittings and fan-out slope structure from taste breaking as determined from the linear fits to the non-Goldstone spectrum. We applied this analysis at two values of the gauge coupling where we have extensive ensembles.

For illustration, preliminary results from rsχPT are shown in Figure 4.2 from fits at gauge coupling $\beta = 3.20$ which corresponds to our coarser lattice of the two extended sets of gauge ensembles. The upper left panel shows the linear fits to the quadratic masses of the non-Goldstone pions to determine their mass shifts and slopes as input. The upper right panel shows the rsχPT fit to F_π as a function of fermion mass deformations away from the chiral limit. The two lower panels show rsχPT fits to M_π as a function of fermion mass deformations away from the chiral limit. Fits at the finer lattice spacing $\beta = 3.25$ are quite similar in quality but with lower confidence level. The unambiguous determination of the cutoff dependent F and B parameters and their continuum limit from rsχPT will require extended analysis. Partial quenching with valence fermions is the first added step to make the ongoing analysis more robust.

Although our results are consistent with chiral symmetry breaking and rsχPT, ongoing work will require considerable extensions for definitive results. Important new work, besides partial quenching includes a solution to the entanglement problem of the light scalar with the low pion spectrum in perturbation theory with comparable masses in the rsχPT regime, crossover analysis from the p-regime to the ϵ-regime and applications of Random Matrix Theory (RMT) in the ϵ-regime. Coupled chiral dynamics of the low mass scalar 0^{++} state with the pions requires new analysis based on an extended effective theory. We are using the modified effective field theory of χPT on existing gauge ensembles but new gauge configuration generation is also needed in the crossover to the ϵ regime. For independent control on the results for the fundamental parameters F and B we developed and apply now mixed actions with improved chiral symmetry without taste breaking in the valence sector of the analysis. Ongoing new efforts in the p-regime and RMT based ϵ-regime in mixed action setting will resolve important aspects of rsχPT with better determination of F and B.

4.3.3 Epsilon-regime, RMT, and mixed action in the valence sector

Safe extrapolation from the entangled regime of the low mass 0^{++} scalar with pions to the massless fermion limit is enabled by crossover to the ϵ-regime of χPT at low enough scales λ where Goldstone dynamics begins to decouple from the scalar state. This is demanding and requires significant resources. To control taste breaking we cannot go to lattice spacings coarser than the one set by $\beta = 3.20$. The uncertainties in the value of $\mathrm{F} \sim 0.018 - 0.025$ with limitations from rooted chiral perturbation theory at this lattice spacing requires large $\mathrm{V} = 56^3 \times 96$ and $\mathrm{V} = 48^3 \times 96$ lattice volumes to control the $\mathrm{F} \cdot \mathrm{L} \geq 1$ condition which is necessary for convergent expansion in all regimes of χPT, including the ϵ-regime. Even for our largest $\mathrm{V} = 56^3 \times 96$ and $\mathrm{V} = 48^3 \times 96$ lattice volumes control with $\mathrm{F} \cdot \mathrm{L} \sim 1$ is just barely sufficient. For the lowest fermion mass $\mathrm{m} = 0.0010$, we have now at these volumes and at this lattice spacing, the scaling variable $\mathrm{m}\Sigma\mathrm{V} \sim 80$ is very large and more appropriate for the p-regime analysis of χPT. Reaching the ϵ-regime requires substantial decrease in the scaling variable $\mathrm{m}\Sigma\mathrm{V}$ targeting $\mathrm{m} = 0.0003$ which presents considerable algorithmic challenge for accelerated inversion methods and also calls for mixed action innovation. We deploy accelerated inverters in configuration generation to the $\mathrm{m} = 0.0010 - 0.0003$ range and analyze these configurations with mixed valence actions of good chiral properties as described below. Our limited resources this year allowed us to test these methods without comprehensive deployment for phenomenologically relevant results like the $\mathrm{M}_{0^{++}}/\mathrm{F}$ ratio in the continuum limit.

The $\mathrm{m} = 0.0010 - 0.0003$ range is in the crossover from the p-regime to the ϵ-regime where known methods of χPT are based on partial quenching and mixed action analysis. For reliable testing, we performed χPT analysis in the crossover to the ϵ-regime with partial quenching and a mixed valence action with improved chiral symmetries. We take the p-regime gauge configurations of the lowest fermion masses on the largest lattice volumes and analyze the fermion condensate and the Dirac spectrum with valence fermion action where the original gauge link variables are replaced with the ones with a fixed number of small stout steps which corresponds to fixed gradient flow time t in lattice spacing units at each gauge coupling. This strategy can be viewed as a mixed action based analysis with very good chiral properties of the fermion valence

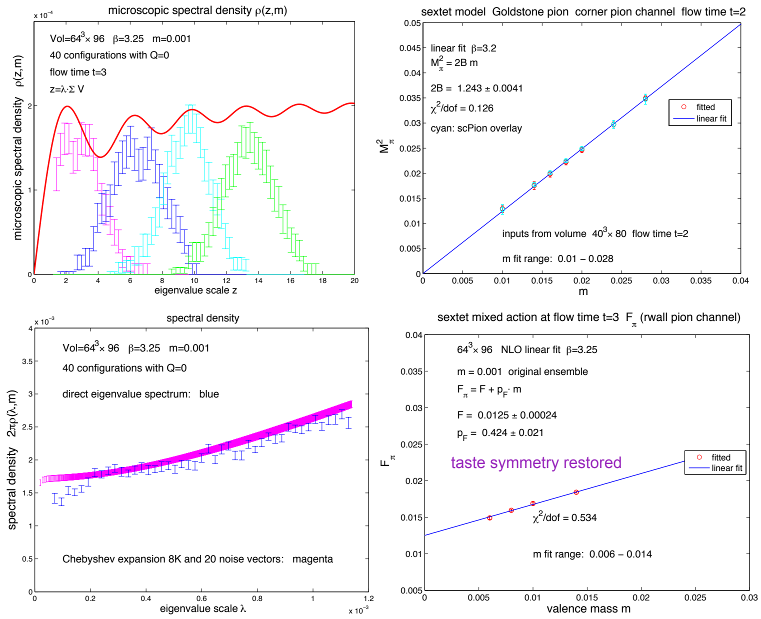

Figure 4.3: The upper left panel shows the RMT distribution of four degenerate quartets showing that the ϵ-regime is reached with the scaling variable $\lambda\Sigma_{\mathrm{mixed}}\mathrm{V} \sim 10$ where the fermion mass is replaced by the scale of the gradient flow defined valence Dirac spectrum ($\mathrm{m} \to \lambda$). The lower left panel shows the infrared part of the directly calculated Dirac spectral density on the gauge configurations and its Chebyshev expansion based approximation. The lower right panel shows the pion decay constant F_π fitted with the mixed action for fixed sea mass as a function of valence masses.

action.

The newest test results are shown in Figure 4.3. The valence action is defined with a large number of very small stout steps which corresponds to gradient flow time $\mathrm{t} = 3$ in cutoff units. We checked the eigenvalues of the Dirac operator which order into nearly degenerate quartets with the smeared gauge links of the gradient flow. The degenerate eigenvalues follow the index theorem count matching the topology of each gauge configuration as measured from the topological charge operator on the gradient flow. The upper left panel shows the RMT distribution of four degenerate quartets showing that the ϵ-regime is reached with the scaling variable $\lambda\Sigma_{\mathrm{mixed}}\mathrm{V} \sim 10$ where the fermion mass is replaced by the scale of the gradient flow defined valence Dirac spectrum ($\mathrm{m} \to \lambda$). The fermion condensate Σ_{mixed}, not RG invariant itself, is consistently determined from the gradient flow defined valence Dirac operator. The upper right panel illustrates the perfect degeneracy of the Goldstone pion with one selected non-Goldstone pion (scPion in the plot). We checked that the degeneracy holds for all non-Goldstone pion states. The lower left panel shows the infrared part of the directly calculated Dirac spectral density on the gauge configurations and its Chebyshev expansion based approximation. The lower right panel shows the pion decay constant F_π fitted with the mixed action for fixed sea mass as a function of valence masses.

Continued future work is needed for definitive results of BSM phenomenology.

4.4 The light 0^{++} scalar and the resonance spectrum

The most important goals of our lattice Higgs project are to establish the emergence of the light scalar state with 0^{++} quantum numbers and the resonance spectrum far separated from the light composite scalar.

4.4.1 The light scalar state

The $\mathrm{f_0}$ meson (in QCD terminology) has 0^{++} quantum numbers and acts as the scalar state in the sextet model (σ particle in QCD). Close to the conformal window, the $\mathrm{f_0}$ meson of the sextet model is not expected to be similar to its counterpart in QCD. If it turns out to be light, it can replace the elementary Higgs particle and pose as the Higgs impostor. Two types of different 0^{++} operators, the fermionic one and the gluonic one (0^{++} glueball), are expected to mix in the relevant correlation functions for mass determination. Such mixing was not included in the pilot study [94] but becomes an important goal of our ongoing effort. We will report our new results without including these mixing effects.

A particular flavor-singlet correlator is needed to capture the 0^{++} scalar state with vacuum quantum numbers. It requires connected and disconnected diagrams of fermion loop propagators on ensemble gauge configurations. The connected diagram corresponds to the non-singlet correlator $\mathrm{C_{non-singlet}(t)}$. The correlator of the disconnected diagram is $\mathrm{D(t)}$ at time separation t. The $\mathrm{f_0}$ correlator $\mathrm{C_{singlet}(t)}$ is defined as $\mathrm{C_{singlet}(t) \equiv C_{non-singlet}(t) + D(t)}$. The transfer matrix has the spectral decomposition of the $\mathrm{C_{singlet}(t)}$ correlator in terms of the sum of all energy levels $\mathrm{E_i(0^{++}), i = 0, 1, 2, ...}$ and their parity partners $\mathrm{E_j(0^{-+}), j = 0, 1, 2, ...}$ but at large time separation t the lowest states $\mathrm{E_0(0^{++})}$ and $\mathrm{E_0(0^{-+})}$ dominate. They correspond to $\mathrm{m_{f_0}}$ and $\mathrm{m}_{\eta_{sc}}$. The relevant non-singlet staggered correlator can be fitted well with non-oscillating a_0 contribution and oscillating π_{sc} contribution, with the non-Goldstone pion π_{sc} discussed in Section 3. One of the most important new developments in our analysis is to use correlators which project out non-zero momentum states of the scalar. This projection eliminates the vacuum contribution in the disconnected part and improves the mass extraction procedure.

We estimate the connected and disconnected diagrams with stochastic source vectors of fermion propagators. To evaluate the disconnected diagram, we need to calculate closed loops of quark propagators. We introduce Z_2 noise sources on the lattice where each source is defined on individual time-slice t_0 for color a. The scheme can be viewed as a “dilution” scheme which is fully diluted in time and color and even/odd diluted in space. Results from the original pilot study [94] on $32^3 \times 64$ lattice volumes at $\beta = 3.20$ could only extend down to the lowest fermion mass at $\mathrm{m} = 0.003$. From our new analysis some representative examples of 0^{++} effective mass fits are shown in Figure 4.4 probing the light scalar closer to the chiral limit than before at fermion mass $\mathrm{m} = 0.0015$. The upper left panel is at $\beta = 3.20$ with $48^3 \times 96$ lattice volume and the upper right panel is at $\beta = 3.20$ with $56^3 \times 96$ lattice volume to check against finite volume dependence in this low fermion mass range. The two lower panels of the plot show results at $\beta = 3.25$.

Although our original estimate $\mathrm{M_{0^{++}}/F} \sim 1 - 3$ for the chiral limit remains consistent with the ongoing new analysis, important further work is needed on the light

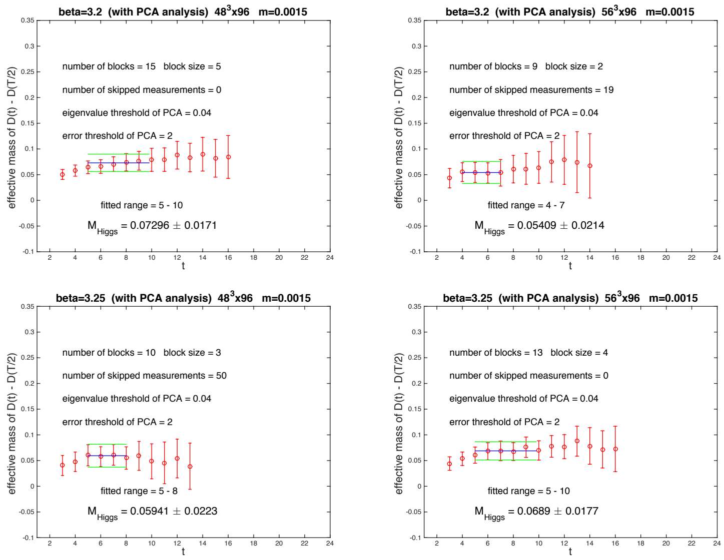

Figure 4.4: Representative fits of the low mass scalar from two ensembles using double Jackknife procedure on the covariance matrix with Principal Component Analysis (PCA).

f_0 scalar with 0^{++} quantum numbers. We want better control on the slowly changing topology of the RHMC algorithm and the related dependence of the extracted masses on the topological quantum numbers of the gauge configurations. We are also in the process of a closely related study of the η' problem which is particularly interesting and important in the staggered fermion formulation. Fermion mass deformations of the low-lying f_0 state and the Goldstone pion are expected to be entangled which requires extended χPT analysis. Our ongoing work will have to address these issues.

4.4.2 The emerging resonance spectroscopy

It is important to investigate the chiral limit of composite hadron states separated from the Goldstones and the light scalar by finite mass gaps. The baryon mass gap in the chiral limit, for example, provides further evidence for χSB. Resonance masses of parity partners provide important additional information with split parity masses in the chiral limit. This is particularly important for consistency with χSB and for a first estimate of the S parameter when probing the model via Electroweak precision tests [12].

A remarkable resonance spectrum is emerging in our new analysis which is sketched in Figure 4.5 for illustration only. The scale is set by F in TeV units at both lattice spacings with caveats from discussions in Section 3 of the report. Any conclusion about χSB or conformal behavior from eyeballed inspection of the data would be inappropriate and misleading. Although with more work needed for confirmation, the sextet model appears to be close to the conformal window and due to χSB exhibits the right Goldstone spectrum for the minimal realization of the composite Higgs mechanism with a light scalar separated from the associated resonance spectrum in the 2-3 TeV

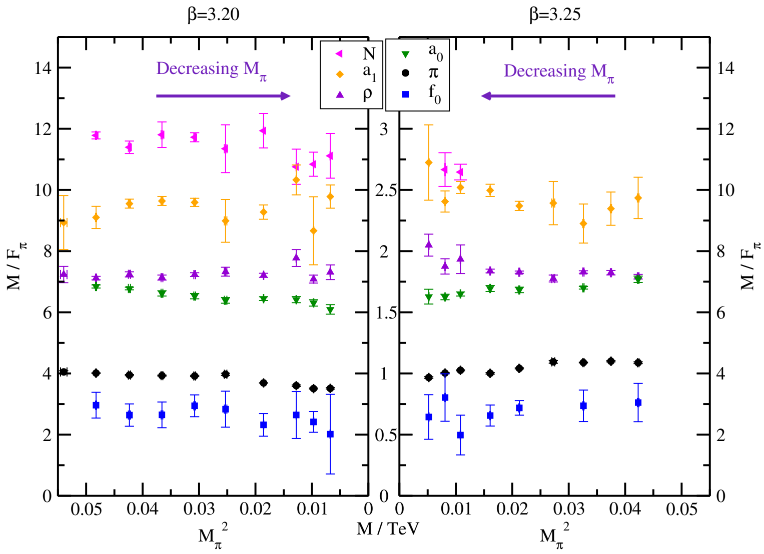

Figure 4.5: New resonance spectroscopy results are shown in the plot for illustration only. The scale is set by F=250 GeV at both lattice spacings with caveats from discussions in Section 3 of the report. Any conclusion about χSB or conformal behavior from eyeballed inspection of the data would be inappropriate and misleading.

region. Chiral symmetry breaking and a very small beta function are not sufficient to guarantee a light dilaton-like state as the natural interpretation for the emergence of the light scalar. Consistent with our observations, a light Higgs-like scalar is still expected to emerge near the conformal window as a composite state with 0^{++} quantum numbers, but not necessarily with a dilaton interpretation. This scalar state has to be light but is not required to match exactly the observed 125 GeV mass. The light scalar from composite strong dynamics gets lighter from electroweak loop corrections, dominated by the large negative mass shift from the top quark loop [97, 180, 181].

4.5 Running coupling

4.5.1 The gradient flow running coupling scheme

The gradient flow [154, 156, 182–186] is a particularly useful tool for studying the running coupling of a non-abelian gauge theory. There are various finite volume setups which mainly differ in the choice of boundary conditions for the gauge field [155, 187–193]. In the present work we follow [155, 187] where the gauge field is taken as periodic in all four directions. For the fermions on the other hand we impose anti-periodic boundary conditions again in all four directions. Other applications of the gradient flow can be found in [194–196].

More precisely, in our scheme a 1-parameter family of couplings is defined in finite 4-volume L^4 by

$$g_c^2 = \frac{128\pi^2 \langle t^2 E(t)\rangle}{3(N^2-1)(1+\delta(c))}\,, \qquad E(t) = -\frac{1}{2}\mathrm{Tr}\, F_{\mu\nu}F_{\mu\nu}(t) \tag{4.3}$$

where t is the flow parameter, N corresponds to the gauge group $SU(N)$, $c = \sqrt{8t}/L$ is a constant, $E(t)$ is the field strength squared at $t > 0$ and the numerical factor

$$\delta(c) = -\frac{c^4\pi^2}{3} + \vartheta^4\left(e^{-1/c^2}\right) - 1 \tag{4.4}$$

is chosen such that at leading order g_c^2 agrees with the coupling in $\overline{\text{MS}}$ for all c; ϑ is the 3rd Jacobi elliptic function. Hence the coupling $g_c(\mu)$ runs via the scale $\mu = 1/L$, for more details see [155, 187].

There is a peculiarity of our running coupling scheme related to the fact that we impose periodicity on the gauge fields, leading to zero modes [99, 197–204]. These gauge zero modes cause the perturbative expansion of g_c^2 in $g_{\overline{\text{MS}}}$ to contain both even and odd powers and potentially logarithms too. However for $N > 2$ logarithms do not appear in the first two non-trivial orders, only polynomials [187]. The first unusual odd power results in only the 1-loop β-function coefficient being the same as in $\overline{\text{MS}}$.

The constant $0 < c \leq 1/2$ specifying the scheme can in principle be chosen at will. However, as discussed in [155, 187], a small c leads to small statistical errors but large cut-off effects and a larger c results in larger statistical errors and smaller cut-off effects. In the present work we set $c = 7/20$, slightly higher than the value $c = 3/10$ in [155, 160], in order to reduce cut-off effects.

4.5.2 Rooted staggered formulation

The fermion doublet in the staggered fermion implementation requires the square root of the fermion determinant, also known as the rooting procedure. With the mass of the fermion doublet set to zero, the continuum step β-function as determined from a scale-dependent renormalized coupling $g_R^2(L)$ shows no sign of turning zero in the explored range, as we will see. Our results are consistent with chiral symmetry breaking when probed with finite fermion mass deformations in the p-regime [96].

Some preliminary work, with goals similar to ours but in the Wilson fermion formulation, reports consistency with a zero in the β-function in the renormalized running coupling in the same range where our β-function is positive and monotonically growing. If confirmed and further supported with conformal scaling laws, the new work in Wilson formulation might suggest a conformal infrared fixed point at vanishing fermion mass in the sextet model, inconsistent with our results and spontaneously broken chiral symmetry.

Motivated by this controversy, doubts were raised about our results questioning the application of the rooting procedure with the mass of the staggered fermion doublet set to zero in the simulations at finite lattice spacing. This lead to the speculation that in the staggered rooting procedure setting the fermion mass m to zero at fixed finite lattice spacing a might be incorrect because of the non-locality of the rooted staggered action we appear to deploy by interchanging the so-called required limit of $a \to 0$ first, while holding the fermion mass non-zero before taking the $m \to 0$ limit in the continuum theory as the last step, after the cutoff is removed. As a consequence of this issue of non-locality concerns were raised whether a rooted staggered theory is in the correct universality class of the continuum theory and whether rooting can identify a conformal theory.

To alleviate the concerns, we will show that the rooting procedure is correct when the fermion mass is set to zero at finite lattice spacing while the finite physical volume of the continuum limit is held fixed. Consequently, the conformality of a model would not be missed and the rooted staggered formulation in finite physical volume and in the infinite volume limit are expected to remain in the correct universality class.

4.5.3 Review of rooting in infinite volume

The method to address the rooting procedure properly has been developed in a series of papers by Bernard, Golterman, Shamir, and Sharpe [205–211] when the renormalized fermion mass is kept finite before the continuum limit is taken. We adapt their analysis to our model in finite physical volumes to demonstrate that the rooting procedure we apply at vanishing fermion mass and finite lattice spacing a should remain valid on the level of their reasoning.

The main results of the analysis at finite fermion mass and infinite volume are summarized first from two succinct exposures of the rooting issues [209, 211] that we closely follow here. Accordingly, the rooted staggered action is defined on a fine-grained lattice with lattice spacing a_f and connected with infrared physics using n renormalization group steps to a blocked physically equivalent lattice action on a coarse lattice with lattice spacing a_c which is held fixed on some physical scale [209, 211]. At fixed $a_c\Lambda_{IR}$, where Λ_{IR} designates some non-perturbative infrared scale, the continuum limit $a_f \to 0$ is investigated when $n \to \infty$.

In the technical implementation of the RG procedure, the blocked and unrooted staggered Dirac operator $D_{\rm stag,n}$ is split into the taste invariant part $D_{\rm inv,n} = D_n \otimes \mathbf{1_4}$ with exact taste symmetry of four degenerate fermions and the taste breaking part Δ_n after each blocking step,

$$D_{\rm stag,n} = D_{\rm inv,n} + \Delta_n, \qquad D_n = \frac{1}{4}\,{\rm Tr}\,\left(D_{\rm stag,n}\right), \tag{4.5}$$

where Tr denotes the trace in taste space. The trace of Δ_n vanishes in taste space, and $\mathbf{1_4}$ designates the taste identity matrix. The local taste invariant theory represented by $D_n \otimes \mathbf{1_4}$ has four degenerate fermions in taste space and the fourth root of the fermion determinant is trivially given by

$${\rm Det}^{1/4}(D_n \otimes \mathbf{1_4}) = {\rm Det}(D_n)\ . \tag{4.6}$$

After taking the fourth root of $D_{\rm stag,n}$, an estimate is needed to show the convergence of ${\rm Det}^{1/4}(D_{\rm stag,n})$ to the local single taste determinant ${\rm Det}(D_n)$ in the $n \to \infty$ limit. As shown in Eq. (4.9), the convergence of this expansion is controlled by $\|D^{-1}_{\rm inv,n}\Delta_n\|$. We need to estimate $\|a_c\Delta_n\|$ and $\|(a_cD_{\rm inv,n})^{-1}\|$ separately on the scale of the coarse lattice.

Following [209] we can safely assume the bound $\|a_c\Delta_n\| \lesssim a_f/a_c$ to hold on the coarse lattice and scaling with a_f. This is a basic feature of unrooted fermions simply stating that taste-breaking disappears in the continuum limit. By exploiting the proximity of the local re-weighted theory defined with $D_{\rm inv,n}$ after a large number n of blocking steps, it was argued that the bound $\|a_c\Delta_n\| \lesssim a_f/a_c$ and its scaling with a_f/a_c is also valid in rooted theories [209]. We will adapt this argument. The estimate for the upper bound on the inverse of the taste invariant operator is given by $\|(a_cD_{\rm inv,n})^{-1}\| \leq 1/(a_cm_R(a_c))$ with the renormalized fermion mass set at the physical scale a_c. The important combined estimate follows with

$$\|D^{-1}_{\rm inv,n}\Delta_n\| \leq a_f/(a_c^2m_R(a_c)) \tag{4.7}$$

and the small expansion parameter

$$\epsilon_n = \|a_c\Delta_n\| \cdot \|(a_c D_{\rm inv,n})^{-1}\| \le a_f/(a_c^2 m_R(a_c)) = \frac{1}{2^{n+1}a_c m_R(a_c)} \tag{4.8}$$

where in the first step the lattice spacing is doubled by the change from staggered fermion basis to Dirac basis followed by n blocking steps in the Dirac basis. This small expansion parameter implies the convergence of the rooted staggered theory to a local action of a single taste in the $n \to \infty$ limit,

$$\begin{aligned} {\rm Det}^{1/4}\left(D_n \otimes \mathbf{1}_4 + \Delta_n\right) &= {\rm Det}(D_n)\ \exp\left[\frac{1}{4}{\rm Tr}\ \log\left(\mathbf{1}_4 + D_{\rm inv,n}^{-1}\Delta_n\right)\right] \\ &= {\rm Det}(D_n)\left(1 + O\left(\frac{a_f}{a_c^2 m_R(a_c)}\right)\right). \end{aligned} \tag{4.9}$$

It is important to note that in estimating a lower bound on the norm of $(a_c D_{\rm inv,n})^{-1}$ the finite renormalized fermion mass $m_R(a_c)$ provides the infrared cutoff of the Dirac spectrum when the volume is infinite. Since renormalization is multiplicative in the staggered formulation, it is implemented on the physical scale a_c requiring the adjustment of the bare mass in the $n \to \infty$ limit which is equivalent to the $a_f \to 0$ continuum limit. The choice $m_R(a_c)$ is arbitrary once a physical scale a_c is set in the theory. This is expected because the RG invariant fermion mass related to $m_R(a_c)$ is arbitrary but as long as it is kept finite in the estimate of the expansion in Eq. (4.9) the convergence of the rooted theory to the local single taste action is assured.

This line of reasoning, based on [209, 211], explains why the sextet model of the rooted fermion doublet with finite renormalized mass is expected to be in the correct universality class when the continuum limit is taken. In our simulations of the volume dependent renormalized coupling g_R^2 the renormalized fermion mass $m_R(a_c)$ is set to zero on any physical scale a_c since the bare mass m itself is set to zero and the mass renormalization is multiplicative from the chiral symmetry of the staggered formulation. Since the estimate of the expansion for the convergence of the rooted determinant to the local single taste determinant as given in Eq. (4.9) is not applicable in the work presented here, the rooting procedure at $m_R(a_c) = 0$ requires separate discussion.

4.5.4 Rooting in finite physical volume at zero bare mass

It is important to precisely define our rooting procedure where the required limit suggested by Eq. (4.9) is not followed. In all of the simulations reported here the bare fermion mass is set to zero at finite lattice spacing a. This also sets the renormalized mass to zero on any choice of physical scale a_c on the coarse lattice. Although the estimate on the bound and its scaling with the RG steps in Eq. (4.8) is lost, there is no problem with the rooting procedure since anti-periodic boundary conditions are imposed on the fermions in all four directions.

As we will now show, the choice of anti-periodic boundary conditions for the fermions restores the validity of the rooting procedure. The simulations always target some chosen values of the scale-dependent renormalized coupling. Each choice selects the corresponding linear size L of the physical volume in the continuum. The renormalized coupling $g_R^2(a_c)$ in the finite volume L also depends on the ratio a_c/L from a 1-parameter family of schemes. As the number of RG steps keeps increasing toward the continuum limit, the coupling on the scale a_f (bare coupling on the cutoff scale) has to be adjusted while $g_R^2(a_c)$ is held fixed, and similarly the lattice size measured in a_f

units is adjusted to keep the physical size L fixed together with a_c/L. The scheme we introduced in section 4.5.1 defines a different but related finite volume scheme without affecting the reasoning. The former is built on the RG procedure and the other is defined on the gradient flow.

In the finite volume scheme a finite gap $\lambda_{\rm gap}(a_c)$ is created in the Dirac spectrum which depends on $g_R^2(a_c)$. Weak couplings correspond to small physical scales and the gap is approximately determined by the minimum momentum π/L in each direction with $\mathcal{O}(g_R^2(a_c))$ corrections. As the renormalized coupling become stronger with increasing volume and the interacting energy levels increasingly repel, they settle into a gradually decreasing but finite gap $\lambda_{\rm gap}(a_c)$ set by the physical scale of the volume. The estimate for the bound on the taste breaking operator remains unchanged with $\|a_c\Delta_n\| \lesssim a_f/a_c$. The new estimate for the upper bound on the inverse of the taste invariant operator is given by $\|(a_c D_{\rm inv,n})^{-1}\| \le 1/(a_c\lambda_{\rm gap}(a_c))$ with the gap of the spectrum set at the physical scale a_c. The important combined estimate follows with $\|D^{-1}_{\rm inv,n}\Delta_n\| \le a_f/(a_c^2\lambda_{\rm gap}(a_c))$ and the small expansion parameter is changed to

$$\epsilon_n = \|a_c\Delta_n\|\cdot\|(a_c D_{\rm inv,n})^{-1}\| \le a_f/(a_c^2\lambda_{\rm gap}(a_c)) = \frac{1}{2^{n+1}a_c\lambda_{\rm gap}(a_c)}. \tag{4.10}$$

The finite gap in the Dirac spectrum implies the convergence of the rooted staggered theory to a local action of a single taste in the $n\to\infty$ limit,

$$\begin{aligned}\mathrm{Det}^{1/4}\left(D_n\otimes\mathbf{1}_4+\Delta_n\right) &= \mathrm{Det}(D_n)\,\exp\left[\frac{1}{4}\mathrm{Tr}\,\log\left(\mathbf{1}_4+D^{-1}_{\rm inv,n}\Delta_n\right)\right]\\ &= \mathrm{Det}(D_n)\left(1+O\left(\frac{a_f}{a_c^2\lambda_{\rm gap}(a_c)}\right)\right).\end{aligned} \tag{4.11}$$

The conclusion from this simple analysis is that in the calculation of the volume dependent running coupling with a rooted and massless fermion doublet the role of the renormalized mass $m_R(a_c)$ on the physical scale is replaced by the $\lambda_{gap}(a_c)$ gap of the Dirac operator in the finite physical volume set by the targeted renormalized coupling $g_R^2(a_c)$ for fixed a_c/L. It is easy to see how this works at weak coupling and is sustained with growing volume if the gap does not collapse to zero at some critical volume size. At any targeted value of $g_R^2(L)$ while holding the physical size L fixed, the eigenvalues of the infrared Dirac spectrum will collapse into degenerate quartets in the $a_f\to 0$ limit, consistent with the locality of the rooted action in the continuum limit.

We know, however, that although the simulations become increasingly difficult with increasing volume, the ensemble-averaged gap cannot disappear in finite physical volumes not even after some rapid crossover into the phase which either has chiral symmetry breaking or is instead conformal. With chiral symmetry breaking, the low end of the spectrum is expected to scale as $\lambda\sim 1/V$ which protects the gap. In the conformal theory the spectral density is expected to scale as $\rho(\lambda)\sim\lambda^\alpha$ with some critical exponent α and $\lambda\sim(1/L)^{4/(1+\alpha)}$ for the low infrared part of the spectrum which also protects the gap from complete collapse. The finite gap cannot disappear in finite physical volumes even if the rooted model is conformal. In the conformal case the beta function is expected to turn zero at some critical coupling $g^2_{\rm crit}$ which can only be reached asymptotically at infinite volume. Our method with rooted staggered fermions can clearly distinguish a conformal model from one with chiral symmetry breaking.

The simulations, as reported here, reach a limited range in the renormalized coupling without any sign of the β function turning zero. Beyond our reach, the results do not rule out conformality in large volumes, although they remain consistent with chiral symmetry breaking. Although it is tempting to pursue further simulations in large volumes at vanishing fermion mass, it is not practical at very small values of the gap in the Dirac spectrum.

4.5.5 The bridge to large volume physics and simulations at finite cutoff $\mathbf{a_f}$

Studying small fermion mass deformations in large volumes at finite cutoff a_f can clearly differentiate between phases with chiral symmetry breaking, or conformality. Taste breaking at finite a_f is described by operators in the Symanzik effective theory (SET) as calculated in [177, 179]. As pointed out in [211], when the goal is to match the rooted theory to the Symanzik effective theory the $a_c m_R(a_c)$ term can be dropped from the denominator in Eq. (4.7) since matching to the taste breaking operators is done at some finite momentum $p \gg \Lambda_{IR}$ which serves in the matching loop diagrams as an IR cutoff.

The bound in Eq. (4.7) is much weaker than needed in the derivation of the SET, and it implies for infinite volume that the chiral $m \to 0$ limit can only be taken after the continuum ($a_f \to 0$) limit. In Eq. (4.7) the role of $m_R(a_c)$ was to establish the existence of the correct continuum limit of the full rooted theory on any scale including the far infrared when the volume is infinite [209]. It follows from [211] that the Symanzik effective theory is well-defined in the chiral limit, together with the chiral effective theory that can be derived from the SET. The requirement that the zero mass limit for staggered fermions should be taken only after the continuum limit is then reproduced by calculations within staggered ChPT [205] for certain operators.

To bridge the current work with inherently non-perturbative large volume analysis we follow the procedure just outlined with mass deformed analysis at finite cutoff. What we observe is consistent with chiral symmetry breaking of the non-perturbative phase in large volumes. To build the bridge to the results presented here we are interested in a scale-dependent and volume independent renormalized coupling in the symmetry breaking phase matching the scale dependent coupling $g_R^2(a_c)$ presented here. This would leave no room for the β function turning zero on any scale. This strategy is outlined in more detail in [96] with results of a preliminary implementation.

4.5.6 Numerical simulation

The details of the simulations are similar to [155, 160]. In particular we use the staggered fermion action with 4 steps of stout improvement [182] and stout parameter $\varrho = 0.12$. The bare fermion mass is set to zero, anti-periodic boundary conditions in all four directions are imposed on the fermions and the gauge field is periodic. The gauge action is the tree-level improved Symanzik action [212, 213]. For integration along the gradient flow we use both the Wilson plaquette and the tree-level improved Symanzik discretizations. The observable $E(t)$ is discretized as in [154]. Hence, in the terminology of [214], we consider the discretizations WSC and SSC for Wilson-flow and tree-level improved Symanzik-flow, respectively.

As detailed in section 4.5.2 a gap in the Dirac spectrum is needed for the validity of rooting hence the available physical volume is limited. This translates into the limitation that the renormalized coupling cannot be explored above a certain value

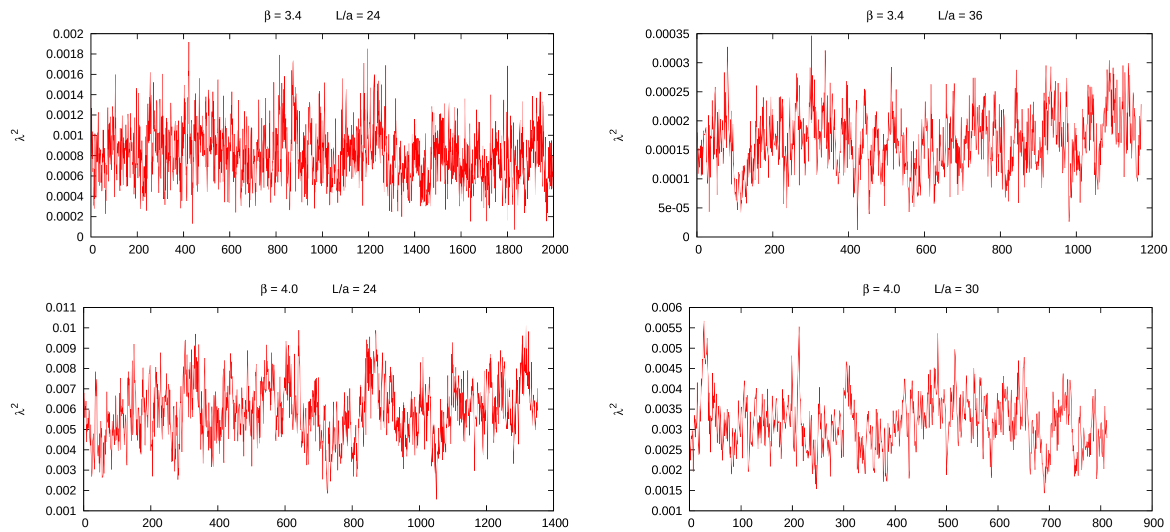

Figure 4.6: Monte-Carlo history of the lowest Dirac eigenvalue, measurements were done for every 10^{th} trajectory. The total number of trajectories are between 8000 and 20000.

with a given set of lattice volumes. This limitation is however not unique to our running coupling scheme and not even unique to staggered fermions. All running coupling studies that are directly at the massless limit (by either setting the mass to zero using staggered or chiral fermions, or tuning κ to the massless point κ_c using Wilson fermions) will be limited to a certain renormalized coupling range with a given set of lattice volumes. This is because on a given set of lattice volumes a quite large renormalized coupling can only be achieved by increasing the bare gauge coupling which in turn will produce small Dirac eigenvalues which in turn will cause the (R)HMC algorithm to break down because the condition number of the Dirac operator might be very large on some configurations.

We will see that in our scheme we are able to explore the range $0 < g_R^2 < 6.5$ which is however quite large and includes the location of the 3-loop and 4-loop fixed point in the $\overline{\mathrm{MS}}$ scheme [215, 216].

There is also a practical issue related to the rooting procedure. Rooting is implemented by the RHMC algorithm which relies on the Remez algorithm. The latter is used for the computation of the coefficients in the partial fraction expansion of the fourth root. A necessary input for the Remez algorithm is an upper and lower bound on the spectrum of the Dirac operator squared $D^\dagger D$. For $m > 0$ a strict lower bound with staggered fermions is m^2. However we set $m = 0$ and use the anti-periodic boundary conditions to produce a gap in the spectrum and no strict lower bound is available in this case. Hence we first need to measure the lowest and highest Dirac eigenvalues in all runs and then set the lower and upper bounds accordingly for the subsequent production runs. We found that this procedure is robust and a carefully chosen lower and upper bound on the spectrum is not violated in the production runs. Histories of the lowest eigenvalue for various parameters are shown for illustration in figure 4.6. As expected, increasing β leads to a larger lowest eigenvalue and similarly decreasing

$L/a \quad \beta$	3.2	3.4	3.6	4.0	5.0	7.0	11.0
8	6.90(1)	5.92(1)	5.011(8)	3.58(1)	1.982(5)	1.058(3)	0.547(1)
12	7.19(2)	6.33(1)	5.44(2)	4.02(1)	2.289(5)	1.220(4)	0.632(2)
16	7.34(2)	6.47(2)	5.66(2)	4.19(2)	2.410(9)	1.281(3)	0.666(3)
18	7.41(3)	6.57(2)	5.72(4)	4.31(1)	2.46(1)	1.311(4)	0.682(2)
20		6.65(3)	5.82(2)	4.34(1)	2.49(1)	1.337(5)	0.688(1)
24	7.69(4)	6.73(3)	5.906(9)	4.45(2)	2.56(1)	1.373(8)	0.702(3)
30		6.86(5)	6.07(7)	4.59(4)	2.66(2)	1.379(6)	0.713(4)
36		7.08(4)	6.24(3)	4.65(4)	2.64(3)	1.40(2)	0.714(7)

Table 4.1: Measured renormalized coupling values in the SSC setup for $c = 7/20$.

$L/a \quad \beta$	3.2	3.4	3.6	4.0	5.0	7.0	11.0
8	9.27(1)	7.76(1)	6.410(9)	4.43(1)	2.380(5)	1.247(3)	0.638(1)
12	8.38(2)	7.29(1)	6.21(2)	4.51(1)	2.520(6)	1.328(4)	0.684(2)
16	8.05(2)	7.04(2)	6.12(2)	4.49(2)	2.554(9)	1.349(3)	0.698(3)
18	7.97(3)	7.03(2)	6.09(4)	4.55(1)	2.58(1)	1.366(4)	0.708(2)
20		7.04(3)	6.13(2)	4.54(1)	2.59(1)	1.383(5)	0.709(1)
24	8.02(4)	7.01(3)	6.131(9)	4.60(2)	2.63(1)	1.406(8)	0.717(3)
30		7.04(5)	6.22(7)	4.70(4)	2.70(2)	1.401(6)	0.723(4)
36		7.22(4)	6.35(3)	4.72(4)	2.67(3)	1.41(2)	0.721(7)

Table 4.2: Measured renormalized coupling values in the WSC setup for $c = 7/20$.

the lattice volume also leads to larger lowest eigenvalues.

In a lattice setting a convenient and practical method of calculating the running coupling or its β-function is via step scaling [138,217]. In this context the finite volume L is increased by a factor s and the change of the coupling, $(g^2(sL) - g^2(L))/\log(s^2)$, is defined as the discrete β-function. Note that in this convention asymptotic freedom corresponds to a positive discrete β-function for small values of the renormalized coupling. If the ordinary infinitesimal β-function of the theory possesses a fixed point, the discrete β-function will have a zero as well. Note that as $s \to 1$ the discrete β-function turns into the infinitesimal variant. On the lattice the linear size L is easily increased to sL by simply increasing the volume in lattice units, $L/a \to sL/a$ at fixed bare gauge coupling. In the current work we set $s = 3/2$ and use volume pairs $8^4 \to 12^4$, $12^4 \to 18^4$, $16^4 \to 24^4$, $20^4 \to 30^4$ and $24^4 \to 36^4$. The continuum limit corresponds to $L/a \to \infty$. Hence our data set has 5 pairs of lattice volumes over a range of lattice spacings to cover a desired range of renormalized couplings.

The collected number of thermalized unit length trajectories at each bare coupling and volume was between 2000 and 20000 depending on the parameters and every 10^{th} was used for measurements. The acceptance rates were between 65% and 95%. The measured renormalized coupling values are listed in tables 4.1 and 4.2 and the resulting discrete β-functions are shown in figure 4.7 for the two discretizations we considered, SSC and WSC.

Clearly, at finite lattice spacing, or equivalently at finite lattice volume, the qualitative features of the two discretizations are quite different. While the discrete β-function is positive for the SSC setup it turns negative for the four roughest lattice spacings,

dc_1357_16

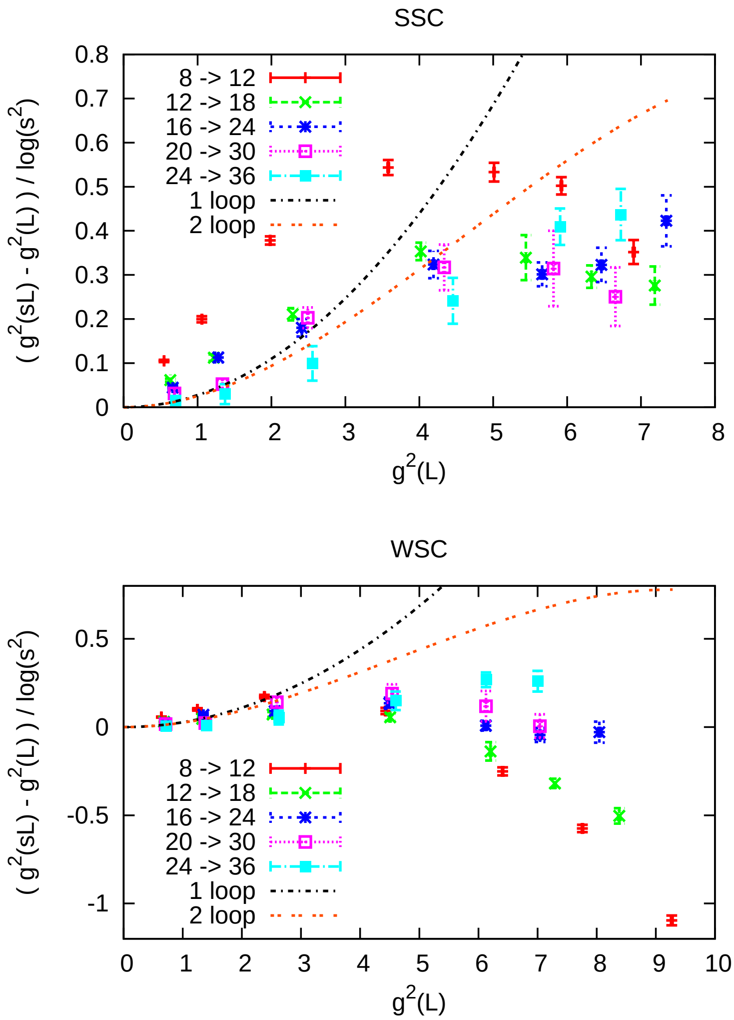

Figure 4.7: Measured discrete β-function in the SSC (top) and WSC (bottom) discretizations; the data correspond to five sets of matched lattice volumes $L \to sL$ with $s = 3/2$.

i.e. $8^4 \to 12^4$, $12^4 \to 18^4$, $16^4 \to 24^4$ and $20^4 \to 30^4$ for the WSC setup. On the finest lattice spacings, corresponding to $24^4 \to 36^4$, it does stay positive even in the WSC case, however. It is important to point out that the observed zeros of the discrete β-functions of the WSC setup for the roughest four lattice spacings are however such that as the lattice spacing *decreases*, the location of the zero *increases*.

Let us emphasize that the behavior of the discrete β-function *at finite lattice volume*, whether it crosses zero or not, is entirely irrelevant as far as the continuum model is concerned. The measured data at finite lattice volume need to be continuum extrapolated and zeros of the discrete β-function may or may not survive the continuum limit. It will turn out in the next section that in fact the zeros of the WSC setup do disappear in the continuum limit while there aren't any zeros to begin with in the SSC setup, and the continuum results for the WSC and SSC setups agree, as they should, and show no sign of a fixed point in the explored coupling range.

4.5.7 Continuum extrapolation

The simplest way to perform the continuum extrapolation of our data is to interpolate the renormalized coupling, $g^2(\beta)$, as a function of the bare coupling β at each lattice volume. We choose the interpolating functions as

$$\frac{\beta}{6} - \frac{1}{g^2(\beta)} = \sum_{m=0}^{n} c_m \left(\frac{6}{\beta}\right)^m , \tag{4.12}$$

similarly to [218]. The order of the above polynomial is allowed to be $n = 3, 4$ or 5 for the volumes $L/a = 8, 12, 16, 18, 24$ and $n = 3$ or 4 for the volumes $L/a = 20, 30, 36$. The corresponding degrees of freedom of the fits are $1, 2$ or 3 for the first set and 1 or 2 for the second set.

Once the parametrized curves $g^2(\beta)$ are obtained for all volumes the discrete β-function $(g^2(sL) - g^2(L))/\log(s^2)$ can be computed for arbitrary $g^2(L)$ for fixed L/a and $s = 3/2$. Then assuming that corrections are linear in a^2/L^2 the continuum extrapolation can be performed for each $g^2(L)$.

In [214, 219] we calculated the tree-level improvement of our observables in order to have smaller slopes in the continuum extrapolations. For the $SU(3)$ fundamental model with $N_f = 4$ tree-level improvement did indeed decrease the slopes over the full considered coupling range, however with $N_f = 8$ we observed in [160] that tree-level improvement only decreased the slopes for small couplings but in fact increased it for larger couplings. In the current work we observe the same. More precisely for approximately $g^2(L) < 3.0$ tree-level improvement decreased the absolute value of the slope of the continuum extrapolation but for $g^2(L) > 3.0$ it increased it. The reason most probably is the same as for $N_f = 8$, namely that the large fermion content enhances the fermion loops which are completely absent from the tree-level calculation and these fermion loops are bound to increase with increasing coupling. For this reason we do not include tree-level improvement in the current work because the phenomenologically interesting region is in the larger coupling range, $g^2(L) \sim 6$.

At small values of the renormalized coupling the continuum discrete β-function can be reliably calculated in continuum perturbation theory. For the $SU(3)$ sextet model with $N_f = 2$ we have,

$$\frac{g^2(sL) - g^2(L)}{\log(s^2)} = b_1 \frac{g^4(L)}{16\pi^2} + \left(b_1^2 \log(s^2) + b_2\right) \frac{g^6(L)}{(16\pi^2)^2} + \ldots \tag{4.13}$$

where $b_1 = 13/3$ and $b_2 = -194/3$. Due to the small volume gauge dynamics mentioned in section 4.5.1 only the first coefficient is the same in our finite volume scheme as above, but nevertheless for comparison we show both the 1-loop and 2-loop expressions. The numerical results, after continuum extrapolation, should agree with the perturbative result for small renormalized coupling and this test is an important cross-check of our procedures.

Following the above procedure with a fixed polynomial order for each volume for the interpolations one obtains a continuum result for both the SSC and WSC setups. The interpolations (4.12) are linear in the free parameters hence the statistical errors are easy to propagate to the final result. Of course one needs to make sure that the continuum extrapolations are acceptable from a statistical point of view, for example the χ^2/dof values are not very large, and one needs to test whether all 5, or perhaps only 4, or perhaps only 3 lattice spacings are in fact in the scaling region. The more lattice spacings that are useable in the continuum extrapolation, the more reliable the result is.

4.5.8 Systematic error estimate

Apart from the statistical errors we would like to estimate the systematic errors too as precisely as possible. The only source of systematic error is the continuum extrapolation. However two distinct types of systematic errors are present in our procedures. One, various polynomial orders can be used for the *interpolation* (4.12) for each lattice volume and two, one may perform the continuum *extrapolation* using 5 or 4 lattice spacings (assuming of course that all 5 lattice spacings are actually in the scaling region), i.e. dropping the roughest lattice spacing. As we discussed in section 4.5.6 the rooting trick of the staggered formulation itself does not introduce unwanted systematic effects.

We will apply the histogram method [7] in order to estimate the systematic uncertainties. The polynomial order n for the interpolation (4.12) is allowed to be $n = 3, 4, 5$ for $L/a = 8, 12, 16, 18, 24$ and $n = 3, 4$ for $L/a = 20, 30, 36$. All together this leads to $3^5 \cdot 2^3 = 1944$ interpolations and correspondingly to 1944 continuum results for a given discretization. Following [176] a Kolmogorov-Smirnov test is applied to the 1944 interpolations and only those are deemed acceptable to which the Kolmogorov-Smirnov test assigns at least a 30% probability. This requirement results in 240 and 306 acceptable interpolations for the SSC and WSC cases, respectively. These all correspond to continuum extrapolations using 5 lattice spacings.

In order to include the systematic effect coming from performing continuum extrapolations using 4 lattice spacings only, i.e. dropping the roughest, $8^4 \to 12^4$, we include such extrapolations too. Using the volumes $L/a = 12, 16, 18, 20, 24, 30, 36$ only with the polynomial orders as above, we have a total number of $3^4 \cdot 2^3 = 648$ interpolations. Out of these the Kolmogorov-Smirnov test allows 240 and 249 for the SSC and WSC cases, respectively[1].

Summarizing the above, we have $240 + 240 = 480$ continuum results for the SSC case and $306 + 249 = 555$ continuum results for the WSC case. In both cases these are binned into a weighted histogram where the weights are given by the Akaike Information Criterion (AIC). We take 68% of the full distribution around the average to estimate the systematic error. Further details are given in [160] where it is explained

[1]The fact that the number of allowed interpolations is the same, 240, for the SSC case for both the 5-point extrapolation and the 4-point extrapolations is purely accidental.

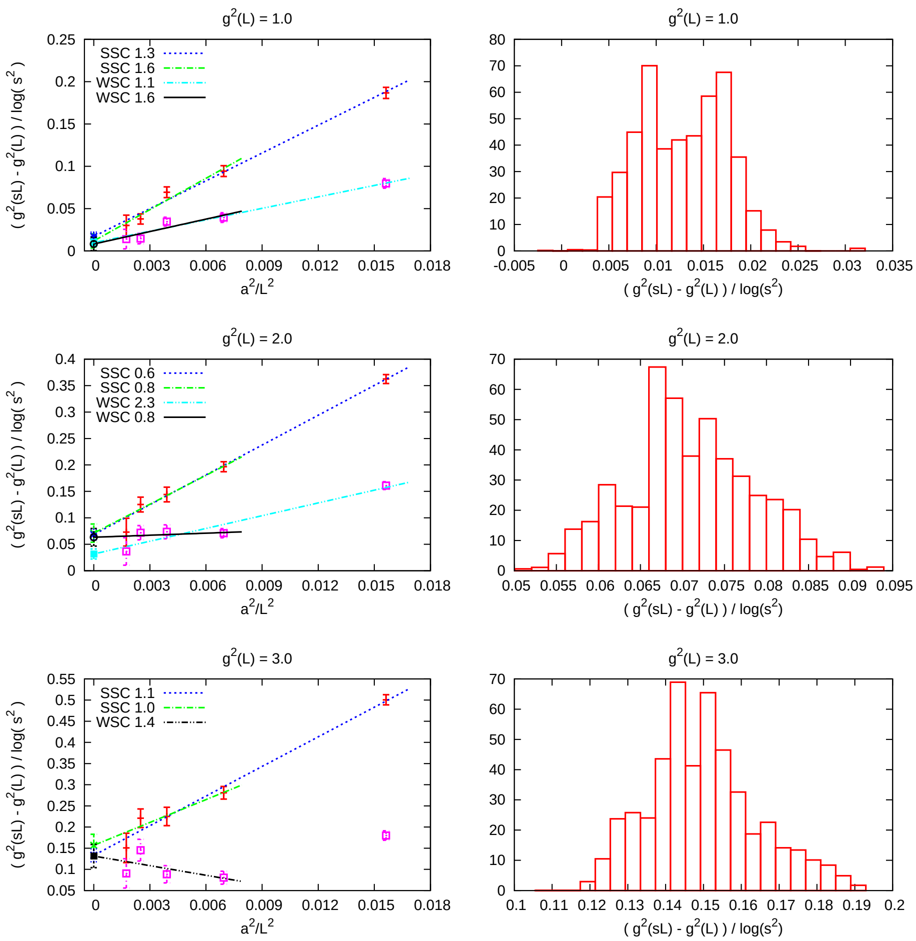

Figure 4.8: Right: the weighted histograms of all possible continuum extrapolations used for estimating the systematic uncertainty for the SSC setup. Left: a representative example of the continuum extrapolations for $g^2(L) = 1.0, 2.0, 3.0$. For comparison we also show a representative example continuum extrapolation in the WSC setup. In each case the χ^2/dof of the fit is shown in the legend. If both 5-point and 4-point continuum extrapolations can be found around the peak of the histogram, then we show examples from both, otherwise only a 4-point extrapolation. See text for more details.

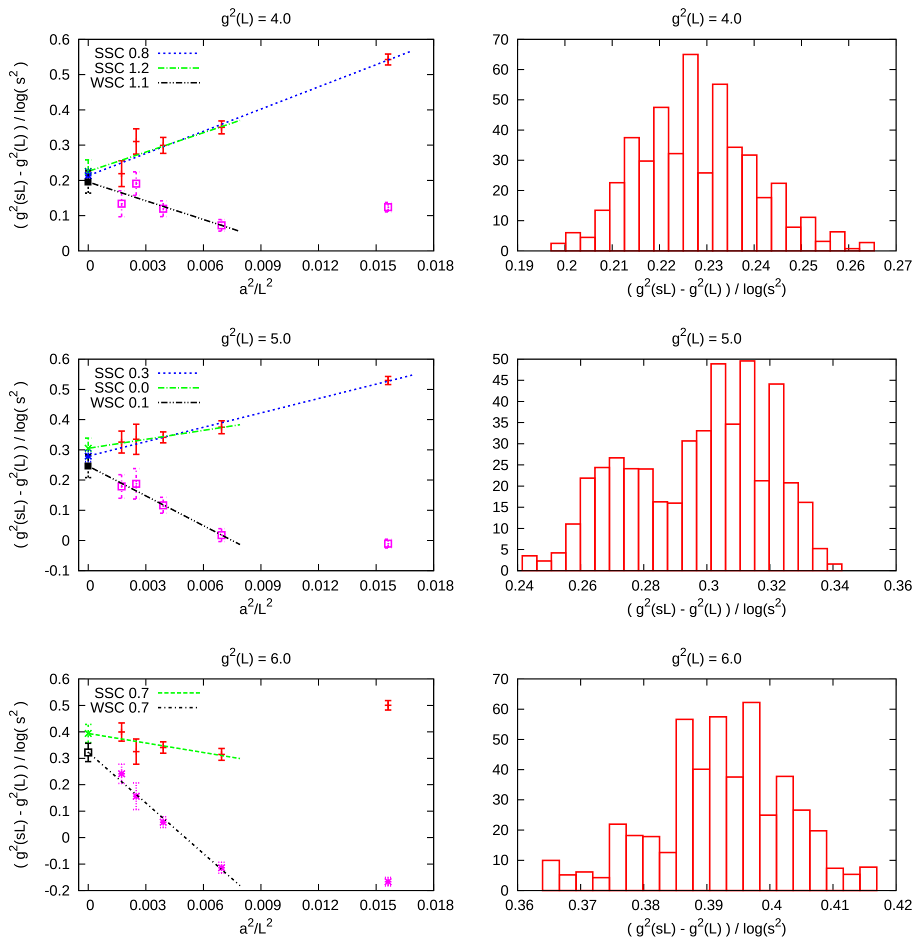

Figure 4.9: Right: the weighted histograms of all possible continuum extrapolations used for estimating the systematic uncertainty for the SSC setup. Left: a representative example of the continuum extrapolations for $g^2(L) = 4.0, 5.0, 6.0$. For comparison we also show a representative example continuum extrapolation in the WSC setup. In each case the χ^2/dof of the fit is shown in the legend. If both 5-point and 4-point continuum extrapolations can be found around the peak of the histogram, then we show examples from both, otherwise only a 4-point extrapolation. See text for more details.

how to perform the Kolmogorov-Smirnov test in a running coupling setup and also for the precise definition of the AIC weights.

4.5.9 Final results

In the final continuum result the statistical and systematic errors are added in quadrature. Examples of the weighted histograms for $g^2(L) = 1.0, \ldots, 6.0$ in the SSC setup are shown in the right panels of figures 4.8 and 4.9. For the same renormalized coupling values we show in the left panels some representative examples of continuum extrapolations for both the SSC and WSC setups and indicate the χ^2/dof values of the fits in the legend. If all 5 lattice spacings are in the scaling region we include an example with 5 lattice spacings and also one with 4 lattice spacings. From these plots the following can be inferred.

For approximately $g^2(L) < 2.5$ all 5 lattice spacings are in the scaling region and the 4-point and 5-point continuum extrapolations agree for the WSC setup, while the same is true for the SSC setup for $g^2(L) < 5.5$, i.e. on a much larger range. Hence for $g^2(L) > 2.5$ only the 4-point continuum extrapolations contribute for the WSC setup, as the 5-point extrapolations are completely suppressed by the AIC weights due to the large χ^2. On the other hand for the SSC setup over almost the entire range of renormalized couplings all 5 lattice spacings are in the scaling regime and the 4-point and 5-point extrapolations agree. For this reason in the final result we only use the SSC data. However the listed examples in figures 4.8 and 4.9 show that the final continuum result using the WSC data actually agrees within errors with the one obtained using the SSC data. This agreement between two different discretizations is a reassuring consistency check of our procedures, especially because we have seen in the WSC case in figure 4.7 that at the smaller lattice volumes the β-functions did cross zero. A remnant of the small lattice volume β-functions crossing zero is that for approximately $g^2(L) > 5.0$ some of the β-function values that are used in the extrapolation are negative. But it is clear from figure 4.9 that the continuum value is positive for both $g^2(L) = 5.0$ and 6.0 and in fact over the entire range. The zeros of the small volume β-functions hence did not survive the continuum limit and the WSC and SSC final results agree within errors.

It is worth emphasizing again: in a given discretization the finite (perhaps small) volume discrete β-functions can perfectly well cross zero while in another discretization the same thing may not happen. This in itself however is in no way indicative of the behavior in the continuum as these small volume zeros may disappear in the continuum. The present model, $SU(3)$ gauge theory with $N_f = 2$ flavors of sextet massless fermions using the WSC and SSC discretizations serves as an example.

Another cautionary note is in order regarding small volumes. It is clear from figures 4.8 and 4.9 that for approximately $g^2(L) < 5.5$ using only the 3 roughest lattice spacings, $8^4 \to 12^4$, $12^4 \to 18^4$ and $16^4 \to 24^4$ would in fact give a continuum result compatible with the one including all 5 lattice spacings in the SSC setup. Only at around $g^2(L) \sim 6.0$ the 3 roughest lattice spacings alone are not usable in a continuum extrapolation. The same, however, is not the case for the WSC discretization. Already for approximately $g^2(L) > 2.5$ the 3-point continuum extrapolations using only $8^4 \to 12^4$, $12^4 \to 18^4$ and $16^4 \to 24^4$ would result in very high χ^2/dof values. If one were to use $8^4 \to 12^4$ and $12^4 \to 18^4$ only as an estimate, this would lead to a continuum result which is much lower than the reliable 4-point or 5-point continuum extrapolations. Hence the larger volumes $L/a > 24$ are essential, without these one may obtain a much smaller β-function which actually would be totally unreliable. This is all the

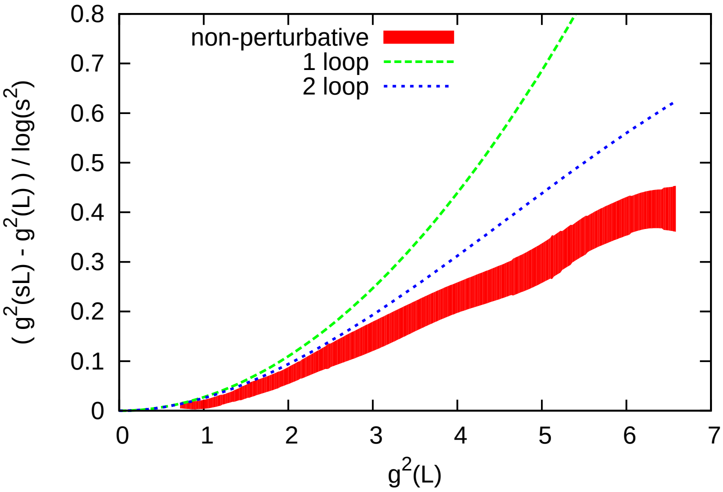

Figure 4.10: Continuum extrapolated discrete β-function for $s = 3/2$ and $c = 7/20$ using the SSC setup.

more important in the phenomenologically important larger coupling region $g^2(L) \sim 6$.

Preliminary results were reported by Anna Hasenfratz and collaborators on the sextet model favoring an infrared fixed point in the continuum. The scheme used is the same as ours except that the fermions were anti-periodic in one direction only. The lattice discretization was different, Wilson fermions were used, however the largest lattice volumes used in the step function were $16^4 \to 24^4$. We speculate the reported fixed point was a lattice artefact due to the large cut-off effects inherent in using small lattice volumes. This scenario would be analogous to some extent with our WSC setup and using only our roughest 3 lattice spacings. Similarly, the inconclusive findings in [149, 150] we speculate are also the result of using small lattice volumes without reaching the scaling regime.

If one were to work with a fixed discretization one of course would not know *a priori* how large volumes are needed for a reliable continuum extrapolation. That is why it is extremely important to consider several discretizations, check that the lattice spacings are in fact in the scaling region, estimate the systematic uncertainty coming from the continuum extrapolation reliably, and only trust results in the continuum if they agree for the considered discretizations. In our work we have performed this analysis in a fully controlled fashion.

We show the final continuum result in figure 4.10. Clearly the β-function stays positive over the entire range and is monotonically increasing, and agreement is found for $g^2(L) < 2.5$ between our result and the 2-loop perturbative result within 1.3σ.

Chapter 5

Many fundamental flavors

The lattice investigations of strong dynamics beyond the Standard Model initially started with fermions in the fundamental representation. The reason was of course simply that the fundamental representation is familiar from QCD. The $SU(3)$ gauge group is the most studied example again because of QCD. Asymptotic freedom for $SU(3)$ and the fundamental representation is lost at $N_f = 16.5$ and perturbative estimates for the lower end of the conformal window are around $N_f^* \sim 10 - 12$, hence the focus quickly became to study many massless flavor models.

It should be noted that the phenomenological relevance of the fundamental representation with gauge group $SU(3)$ is questionable. There are two main reasons. First, electro-weak precision measurements put stringent bounds on the S-parameter, in particular it can not be too large. Since the model needs to be close to the lower end of the conformal window the expectation is that flavor numbers $N_f \sim 8 - 12$ would be required. A perturbative calculation of the S-parameter results in it being proportional to N_f hence a many flavor model would automatically lead to a large S-parameter. There are however ways around this line of reasoning, namely non-perturbative effects may decrease the S-parameter close to the conformal window, but also one may envision only coupling some of the flavors to the electro-weak $SU(2)$. The second issue is that with many flavors chiral symmetry breaking leads to many massless Goldstone bosons, $N_f^2 - 1$. This large number of new massless particles needs to be accounted for. They may be promoted to dark matter particles for instance but it is far from clear that they can be made consistent with all electro-weak precision measurement results.

Both issues raised above are open problems for the phenomenology of the fundamental $SU(3)$ models. In any case as far as lattice investigations are concerned the fundamental model serves as a good testing ground. The models themselves are well-defined quantum field theories and so the non-perturbative results are interesting on their own right. The simulations are over more control than the virtually uncharted territory of higher dimensional representations simply because a vast literature exists for QCD.

We have also investigated the fundamental model motivated by the above observation and certainly much less by the phenomenological relevance of these models. The first task is to determine N_f^* by studying the model at various flavor numbers N_f and determining whether at that particular N_f chiral symmetry breaking takes place or not. Preferrably a variety of methods are employed and consistency in their conclusions is sought.

5.1 Chiral symmetry breaking below the conformal window

We will identify in lattice simulations the chirally broken phases with $N_f = 4, 8, 9$ flavors of staggered fermions in the fundamental SU(3) color representation using finite volume analysis. The staggered fermions are deployed with a special 6-step exponential (stout) smearing procedure [182] in the lattice action to reduce well-known cutoff effects with taste breaking in the Goldstone spectrum. The presence of taste breaking requires a brief explanation of how staggered chiral perturbation theory is applied in our analysis. The important work of Lee, Sharpe, Aubin and Bernard [177, 178, 220] is closely followed in the discussion.

5.1.1 Staggered chiral perturbation theory

Starting with the $N_f = 4$ example [177], the spontaneous breakdown of $SU(4)_L \times SU(4)_R$ to vector $SU(4)$ gives rise to 15 Goldstone modes, described by fields ϕ_i. These can be organized into an $SU(4)$ matrix

$$\Sigma(x) = \exp\Big(i\frac{\phi}{\sqrt{2}F}\Big), \quad \phi = \sum_{a=1}^{15} \phi_a T_a\,, \tag{5.1}$$

where F is the Goldstone decay constant in the chiral limit and the normalization $T_a = \{\xi_\mu, i\xi_{\mu 5}, i\xi_{\mu\nu}, \xi_5\}$ is used for the flavor generators. The leading order chiral Lagrangian is given by

$$\mathcal{L}_\chi^{(4)} = \frac{F^2}{4}\mathsf{Tr}(\partial_\mu\Sigma\partial_\mu\Sigma^\dagger) - \frac{1}{2}B\, m_q\, F^2\mathsf{Tr}(\Sigma + \Sigma^\dagger)\,, \tag{5.2}$$

with the fundamental parameters F and B measured on the technicolor scale $\Lambda_{\rm TC}$ which replaced $\Lambda_{\rm QCD}$ in the new theory. Expanding the chiral Lagrangian in powers of ϕ one finds 15 degenerate pions with masses given by

$$M_\pi^2 = 2Bm_q\left[1 + O(m_q/\Lambda_{\rm TC})\right]\,. \tag{5.3}$$

The leading order term is the tree-level result, while the corrections come from loop diagrams and from higher order terms in the chiral Lagrangian.

The addition of $a^2\mathcal{L}_\chi^{(6)}$ breaks chiral symmetry and lifts the degeneracy of the Goldstone pions. Correction terms are added to Eq. (5.3) which becomes

$$M_\pi^2 = C(T_a)\cdot a^2\Lambda_{\rm TC}^4 + 2Bm_q\left[1 + O(m_q/\Lambda_{\rm TC}) + O(a^2\Lambda_{\rm TC}^2)\right] \tag{5.4}$$

where the representation dependent $C(T_a)$ is a constant of order unity. Contributions proportional to a^2 are due to $\mathcal{L}_\chi^{(6)}$, and lead to massive Goldstone pions even in the $m_q \to 0$ chiral limit. The only exception is the pion with flavor ξ_5 which remains massless because the $U(1)_A$ symmetry is protected.

Lee and Sharpe observe that the part of $\mathcal{L}_\chi^{(6)}$ without derivatives, defining the potential $\mathcal{V}_\chi^{(6)}$, is invariant under flavor $SO(4)$ transformations and gives rise to the a^2 term in M_π^2. Terms in $\mathcal{L}_\chi^{(6)}$ involving derivatives break $SO(4)$ further down to the lattice symmetry group and give rise to non-leading terms proportional to a^2m and a^4.

The taste breaking potential is given by

$$
\begin{aligned}
-\mathcal{V}_\chi^{(6)} &= C_1 \mathrm{Tr}\,(\xi_5 \Sigma \xi_5 \Sigma^\dagger) \\
&+ C_2 \,\frac{1}{2}\left[\mathrm{Tr}\,(\Sigma^2) - \mathrm{Tr}\,(\xi_5 \Sigma \xi_5 \Sigma) + h.c.\right] \\
&+ C_3 \,\frac{1}{2} \sum_\nu \left[\mathrm{Tr}\,(\xi_\nu \Sigma \xi_\nu \Sigma) + h.c.\right] \\
&+ C_4 \,\frac{1}{2} \sum_\nu \left[\mathrm{Tr}\,(\xi_{\nu 5} \Sigma \xi_{5\nu} \Sigma) + h.c.\right] \\
&+ C_5 \,\frac{1}{2} \sum_\nu \left[\mathrm{Tr}\,(\xi_\nu \Sigma \xi_\nu \Sigma^\dagger) - \mathrm{Tr}\,(\xi_{\nu 5} \Sigma \xi_{5\nu} \Sigma^\dagger)\right] \\
&+ C_6 \sum_{\mu<\nu} \mathrm{Tr}\,(\xi_{\mu\nu} \Sigma \xi_{\nu\mu} \Sigma^\dagger)\,. \qquad (5.5)
\end{aligned}
$$

The six unknown coefficients C_i are all of size Λ^6_{TC}.

In the continuum, the pions form a 15-plet of flavor $SU(4)$, and are degenerate. On the lattice, states are classified by the symmetries of the transfer matrix and the Goldstone pions fall into 7 irreducible representations: four 3-dimensional representations with flavors ξ_i, ξ_{i5}, ξ_{ij} and ξ_{i4}, and three 1-dimensional representations with flavors ξ_4, ξ_{45} and ξ_5.

Close to both the chiral and continuum limits, the pion masses are given by

$$
M_\pi(T_a)^2 = 2Bm_q + a^2\Delta(T_a) + O(a^2 m_q) + O(a^4)\,, \qquad (5.6)
$$

with $\Delta(T_a) \sim \Lambda^4_{\mathrm{TC}}$ arising from $\mathcal{V}_\chi^{(6)}$. Since $\mathcal{V}_\chi^{(6)}$ respects flavor $SO(4)$, the 15 Goldstone pions fall into $SO(4)$ representations:

$$
\begin{aligned}
\Delta(\xi_5) &= 0\,, && (5.7)\\
\Delta(\xi_\mu) &= \frac{8}{F^2}(C_1 + C_2 + C_3 + 3C_4 + C_5 + 3C_6)\,, && (5.8)\\
\Delta(\xi_{\mu 5}) &= \frac{8}{F^2}(C_1 + C_2 + 3C_3 + C_4 - C_5 + 3C_6)\,, && (5.9)\\
\Delta(\xi_{\mu\nu}) &= \frac{8}{F^2}(2C_3 + 2C_4 + 4C_6)\,. && (5.10)
\end{aligned}
$$

In the chiral limit at finite lattice spacing the lattice irreducible representations with flavors ξ_i and ξ_4 are degenerate, those with flavors ξ_{i5} and ξ_{45}, and those with flavors ξ_{ij} and ξ_{i4} are degenerate as well. No predictions can be made for the ordering or splittings of the mass shifts. We also cannot predict the *sign* of the shifts, although our simulations indicate that they are all positive with the exponentially smeared staggered action we use. This makes the existence of an Aoki phase [177] unlikely.

The method of [177] has been generalized in a nontrivial way to the $N_f > 4$ case [178, 220] which we adopted in our calculations with help from Bernard and Sharpe. The procedure cannot be reviewed here but it will be used in the interpretation of our $N_f = 8$ simulations.

5.1.2 Finite volume analysis in the p-regime

Three different regimes can be selected in simulations to identify the chirally broken phase from finite volume spectra and correlators. For a lattice size $L_s^3 \times L_t$ in euclidean

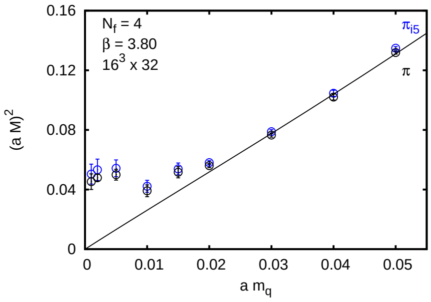

Figure 5.1: The crossover from the p-regime to the δ-regime is shown for the π and π_{i5} states at $N_f = 4$.

space and in the limit $L_t \gg L_s$, the conditions $F_\pi L_s > 1$ and $M_\pi L_s > 1$ select the the p-regime, in analogy with low momentum counting [221, 222].

For arbitrary N_f, in the continuum and in infinite volume, the one-loop chiral corrections to M_π and F_π of the degenerate Goldstone pions are given by

$$M_\pi^2 = M^2\left[1 - \frac{M^2}{8\pi^2 N_f F^2} ln\left(\frac{\Lambda_3}{M}\right)\right], \tag{5.11}$$

$$F_\pi = F\left[1 + \frac{N_f M^2}{16\pi^2 F^2} ln\left(\frac{\Lambda_4}{M}\right)\right], \tag{5.12}$$

where $M^2 = 2B \cdot m_q$ and $F, B, \Lambda_3, \Lambda_4$ are four fundamental parameters of the chiral Lagrangian, and the small quark mass m_q explicitly breaks the symmetry [104]. The chiral parameters F, B appear in the leading part of the Lagrangian in Eq. (5.2), while Λ_3, Λ_4 enter in next order. There is the well-known GMOR relation $\Sigma_{cond} = BF^2$ in the $m_q \to 0$ limit for the chiral condensate per unit flavor [223]. It is important to note that the one-loop correction to the pion coupling constant F_π is enhanced by a factor N_f^2 compared to M_π^2. The chiral expansion for large N_f will break down for F_π much faster for a given M_π/F_π ratio.

The finite volume corrections to M_π and F_π are given in the p-regime by

$$M_\pi(L_s, \eta) = M_\pi\left[1 + \frac{1}{2N_f}\frac{M^2}{16\pi^2 F^2} \cdot \tilde{g}_1(\lambda, \eta)\right], \tag{5.13}$$

$$F_\pi(L_s, \eta) = F_\pi\left[1 - \frac{N_f}{2}\frac{M^2}{16\pi^2 F^2} \cdot \tilde{g}_1(\lambda, \eta)\right], \tag{5.14}$$

where $\tilde{g}_1(\lambda, \eta)$ describes the finite volume corrections with $\lambda = M \cdot L_s$ and aspect ratio $\eta = L_t/L_s$. The form of $\tilde{g}_1(\lambda, \eta)$ is a complicated infinite sum which contains Bessel functions and requires numerical evaluation [222]. Eqs. (5.11-5.14) provide the foundation of the p-regime fits in our simulations.

5.1.3 δ-regime and ϵ-regime

At fixed L_s and in cylindrical geometry $L_t/L_s \gg 1$, a crossover occurs from the p-regime to the δ-regime when $m_q \to 0$. The dynamics is dominated by the rotator states of the chiral condensate in this limit [101] which is characterized by the conditions $FL_s > 1$ and $ML_s \ll 1$. The densely spaced rotator spectrum scales with gaps of the order $\sim 1/F^2L_s^3$, and at $m_q = 0$ the chiral symmetry is apparently restored. However, the rotator spectrum, even at $m_q = 0$ in the finite volume, will signal that the infinite system is in the chirally broken phase for the particular parameter set of the Lagrangian. This is often misunderstood in the interpretation of lattice simulations. Measuring finite energy levels with pion quantum numbers at fixed L_s in the $m_q \to 0$ limit is not a signal for chiral symmetry restoration of the infinite system [224].

If $L_t \sim L_s$ under the conditions $FL_s > 1$ and $ML_s \ll 1$, the system will be driven into the ϵ-regime which can be viewed as the high temperature limit of the δ-regime quantum rotator. Although the δ-regime and ϵ-regime have an overlapping region, there is an important difference in their dynamics. In the δ-regime of the quantum rotator, the zero spatial momentum of the pion field $U(x)$ dominates with time-dependent quantum dynamics. The ϵ-regime is dominated by the four-dimensional zero momentum mode of the chiral Lagrangian.

We report simulation results of all three regimes in the chirally broken phase of the technicolor models we investigate. The analysis of the three regimes complement each other and provide cross-checks for the correct identification of the phases. First, we will probe Eqs.(5.11-5.14) in the p-regime, and follow with the study of Dirac spectra and RMT eigenvalue distributions in the ϵ-regime. The spectrum in the δ-regime is used as a signal to monitor p-regime spectra as m_q decreases. Fig. 5.1 is an illustrative example for this crossover in our simulations.

5.2 Simulations results in the p-regime

The tree level improved Symanzik gauge action was used in our simulations. The link variables in the staggered fermion matrix were exponentially smeared with six stout steps at $N_f = 4, 8$ and four stout steps at $N_f = 9$. The RHMC algorithm was deployed in all runs but rooting of the fermion determinant only affected the $N_f = 9$ simulations. The results shown in Fig. 5.2 are from the p-regime of the chirally broken phase with the conditions $M_\pi \cdot L_s \gg 1$ and $F_\pi \cdot L \sim 1$ when the chiral condensate begins to follow the expected behavior of infinite volume chiral perturbation theory from Eqs. (5.11,5.12) with calculable finite volume corrections from Eqs. (5.13,5.14).

The $N_f = 4$ simulations work in the p-regime as expected. The pion spectrum is clearly separated from the technicolor scale of the ρ-meson whose quadratic fit is just to guide the eye. Moving towards the continuum limit with increasing $\beta = 6/g^2$, we see the split pion spectrum collapsing onto the true Goldstone pion. The true Goldstone pion and two additional split pion states are shown. Δ is the measure of the small quadratic pion mass splittings in lattice units. Their origin was discussed in Section 2 in Eqs. (5.7-5.10). The spectrum is parallel and the gaps appear to be equally spaced consistent with the earlier observation in QCD where the C_4 term seems to dominate taste breaking accounting for the equally spaced pion levels [177]. The simultaneous chiral fit of M_π^2/m_q and F_π based on Eqs. (5.11-5.14) works when the chiral loop term corrects the tree level value of $M_\pi^2/m_q = 2B$. This is a chirally broken phase and the picture holds in the $m_q \to 0$ limit. The fit to determine the $N_f = 4$ chiral condensate for $m_q = 0$ is shown in the second row on the right. It sets the scale of electroweak symmetry breaking in the Higgs mechanism.

As we move to the $N_f = 8$ p-regime simulations summarized in the third and forth rows of Fig. 5.2 we observe the weakening of the chiral condensate and increased diffi-

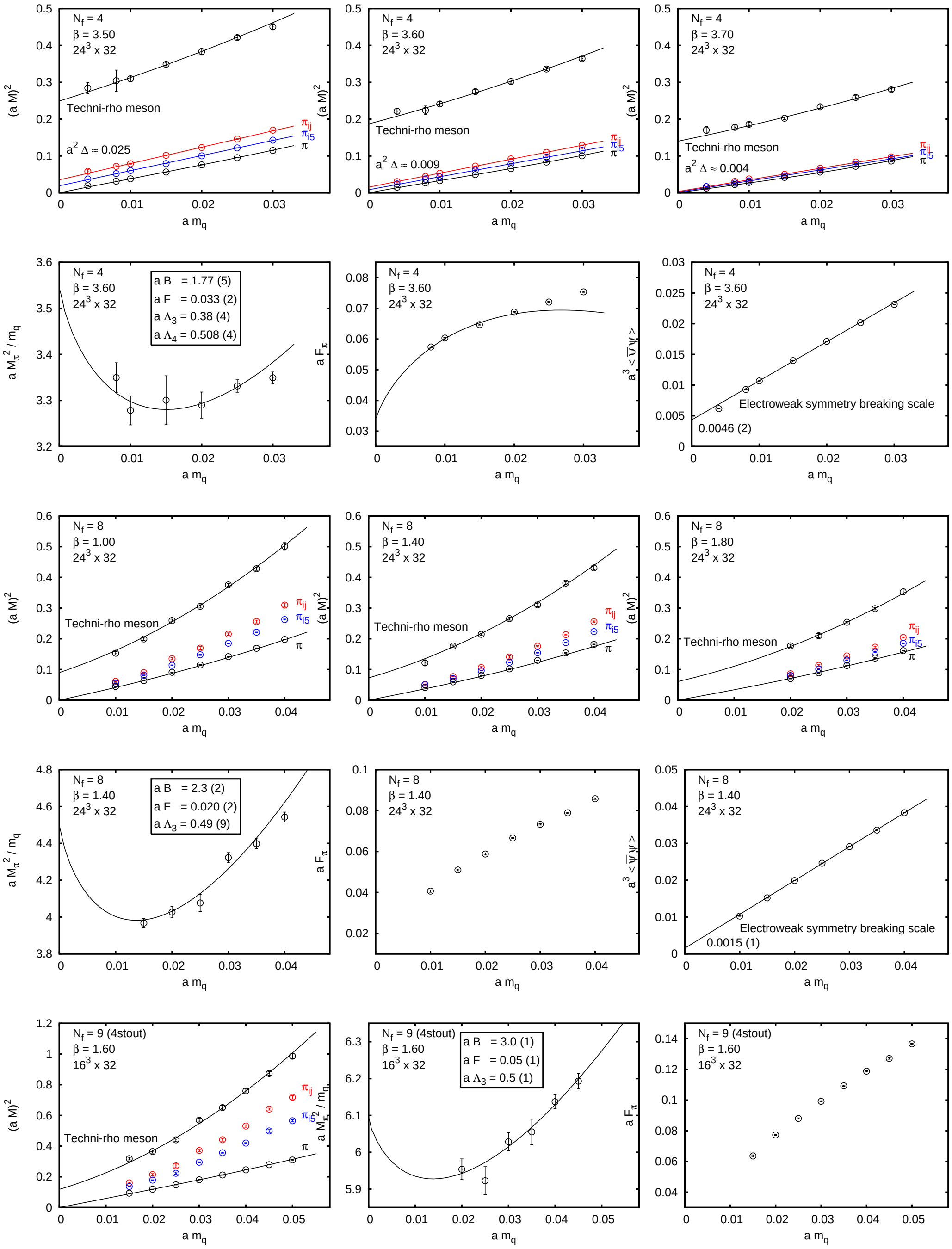

Figure 5.2: The first two rows of the composite figure show $N_f = 4$ simulation results in the p-regime. The first row depicts the collapsing pion spectrum and the techni-rho as the continuum limit is approached. The second row shows the chiral fits to M_π^2/m_q and F_π based on Eqs. (5.11-5.14). The third and fourth rows summarize the simulation results for $N_f = 8$. The third row shows the collapsing pion spectrum and the techni-rho as the continuum limit is approached. The chiral fit to M_π^2/m_q is shown based on Eq. (5.11). The fifth row illustrates our first simulation results for $N_f = 9$. It shows the split pion spectrum, chiral fit to M_π^2/m_q and the F_π data points are outside the convergence range of the chiral expansion.

culties in passing the chiral tests. The pion spectrum is still clearly separated from the technicolor scale of the ρ-meson. Moving towards the continuum limit with increasing $\beta = 6/g^2$, we see the split pion spectrum collapsing toward the true Goldstone pion with a new distinguished feature. The true Goldstone pion and two additional split pion states are shown with different slopes as m_q increases. Towards $m_q = 0$ the pion spectrum is collapsed at fixed gauge coupling, indicating that the effects of leading order taste breaking operators, the generalization of those from $N_f = 4$ to $N_f = 8$ as discussed in Section 2, are smaller than at $N_f = 4$ in the explored coupling constant range. This is somewhat unexpected and unexplained. Next to leading order taste breaking operators are responsible for the spread of the slopes and they seem to dominate. They were identified in Eq. (5.6) as the last two terms. It is reassuring to see that this structure is collapsing as we move toward the continuum limit. We analyzed this pattern within staggered perturbation theory in its generalized form beyond four flavors [178, 220]. The simultaneous chiral fit of M_π^2/m_q and F_π based on Eqs. (5.11-5.14) cannot be done at $N_f = 8$ within the reach of the largest lattice sizes we deploy since the value of aF is too small even at L=24 for coupling constants where taste breaking drops to an acceptable level. The chiral fit to M_π^2/m_q is shown based on Eq. (5.11) only since the F_π data points are outside the convergence range of the chiral expansion. We would need much bigger lattices to drop further down in the p-regime with m_q to the region where the simultaneous fit could be made. It is also important to note that the chiral condensate is very small in the $m_q \to 0$ limit in the region where taste breaking is not large. This is shown in row four of Fig. 5.2 on the right side.

The $N_f = 9$ p-regime simulations are summarized in the fifth row of Fig. 5.2 where we observe the continued weakening of the chiral condensate and the increased difficulties in passing the chiral tests. The pion spectrum is still clearly separated from the technicolor scale of the ρ-meson. Moving towards the continuum limit to see the split pion spectrum collapsing toward the true Goldstone pion is increasingly difficult. The true Goldstone pion and two additional split pion states are shown again with different slopes as m_q increases. Forcing the collapse of the split pion spectrum will require larger lattices with smaller gauge couplings. The trends and the underlying explanation is very similar to the $N_f = 8$ case. The chiral fit to M_π^2/m_q is shown based on Eq. (5.11) only since the F_π data points are outside the convergence range of the chiral expansion.

In summary, we have shown that according to p-regime tests the $N_f = 4, 8, 9$ systems are all in the chirally broken phase close to the continuum limit. Currently we are investigating $N_f = 9, 10, 11, 12$ on larger lattices to determine the lower edge of the conformal window. Lessons from the Dirac spectra and RMT to complement p-regime tests are discussed in the next section including comments about the controversial $N_f = 12$ case.

5.3 Epsilon regime, Dirac spectrum and RMT

If the bare parameters of a gauge theory are tuned to the ε-regime in the chirally broken phase, the low-lying Dirac spectrum follows the predictions of random matrix theory. The corresponding random matrix model is only sensitive to the pattern of chiral symmetry breaking, the topological charge and the rescaled fermion mass once the eigenvalues are also rescaled by the same factor $\Sigma_{cond}V$. This idea has been confirmed in various settings both in quenched and fully dynamical simulations. The

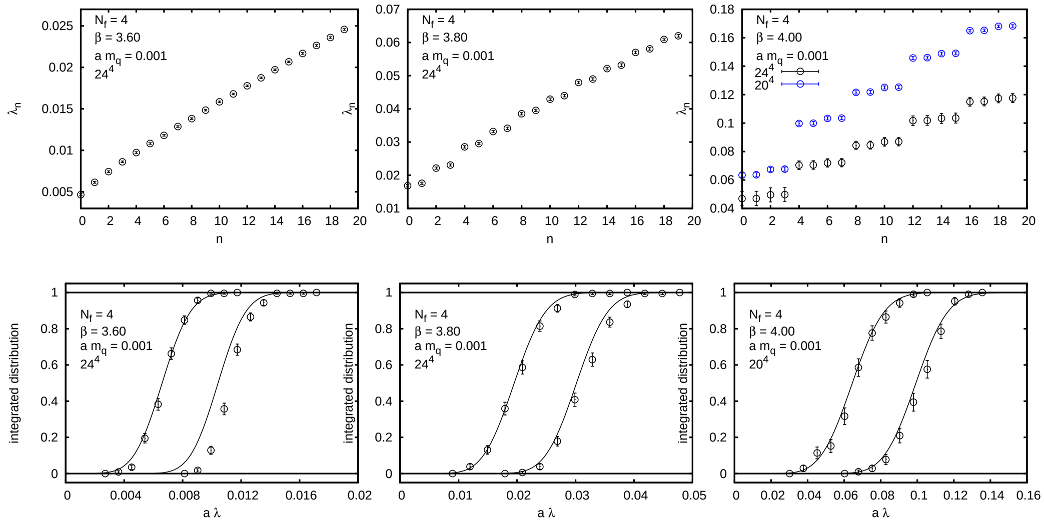

Figure 5.3: From simulations at $N_f = 4$ the first row shows the approach to quartet degeneracy of the spectrum as β increases. The second row shows the integrated distribution of the two lowest quartets averaged. The solid line compares this procedure to RMT with $N_f = 4$.

same method is applied here to nearly conformal gauge models.

The connection between the eigenvalues λ of the Dirac operator and chiral symmetry breaking is given in the Banks-Casher relation [225],

$$\Sigma_{cond} = -\langle\bar{\Psi}\Psi\rangle = \lim_{\lambda\to 0}\lim_{m\to 0}\lim_{V\to\infty}\frac{\pi\rho(\lambda)}{V},$$

where Σ_{cond} designates the quark condensate normalized to a single flavor. To generate a non-zero density $\rho(0)$, the smallest eigenvalues must become densely packed as the volume increases, with an eigenvalue spacing $\Delta\lambda \approx 1/\rho(0) = \pi/(\Sigma_{cond}V)$. This allows a crude estimate of the quark condensate Σ_{cond}. One can do better by exploring the ϵ-regime: If chiral symmetry is spontaneously broken, tune the volume and quark mass such that $\frac{1}{F_\pi} \ll L \ll \frac{1}{M_\pi}$, so that the pion is much lighter than the physical value, and finite-volume effects are dominant as we discussed in Section 2. The chiral Lagrangian of Eq. (5.2) is dominated by the zero-momentum mode from the mass term and all kinetic terms are suppressed. In this limit, the distributions of the lowest eigenvalues are identical to those of random matrix theory, a theory of large matrices obeying certain symmetries [226–228]. To connect with RMT, the eigenvalues and quark mass are rescaled as $z = \lambda\Sigma_{cond}V$ and $\mu = m_q\Sigma_{cond}V$, and the eigenvalue distributions also depend on the topological charge ν and the number of quark flavors N_f. RMT is a very useful tool to calculate analytically all of the eigenvalue distributions. The eigenvalue distributions in various topological sectors are measured via lattice simulations, and via comparison with RMT, the value of the condensate Σ_{cond} can be extracted.

After we generate large thermalized ensembles, we calculate the lowest twenty eigenvalues of the Dirac operator using the PRIMME package. In the continuum limit,

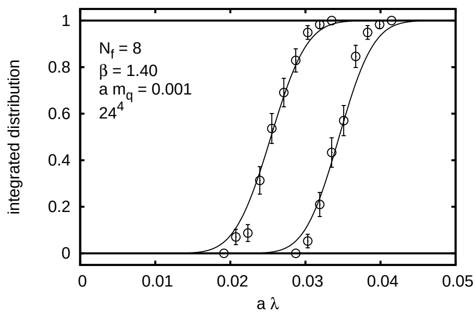

Figure 5.4: The solid lines compare the integrated distribution of the two lowest quartet averages to RMT predictions with $N_f = 8$.

the staggered eigenvalues form degenerate quartets, with restored taste symmetry. The first row of Fig. 5.3 shows the change in the eigenvalue structure for $N_f = 4$ as the coupling constant is varied. At $\beta = 3.6$ grouping into quartets is not seen, the pions are noticeably split, and staggered perturbation theory is just beginning to kick in. At $\beta = 3.8$ doublet pairing appears and at $\beta = 4.0$ the quartets are nearly degenerate. The Dirac spectrum is collapsed as required by the Banks-Casher relation. In the second row we show the integrated distributions of the two lowest eigenvalue quartet averages,

$$\int_0^\lambda p_k(\lambda')d\lambda', \qquad k = 1, 2 \tag{5.15}$$

which is only justified close to quartet degeneracy. All low eigenvalues are selected with zero topology. To compare with RMT, we vary $\mu = m_q \Sigma_{cond} V$ until we satisfy

$$\frac{\langle\lambda_1\rangle_{\rm sim}}{m} = \frac{\langle z_1\rangle_{\rm RMT}}{\mu}, \tag{5.16}$$

where $\langle\lambda_1\rangle_{\rm sim}$ is the lowest quartet average from simulations and the RMT average $\langle z\rangle_{\rm RMT}$ depends implicitly on μ and N_f. With this optimal value of μ, we can predict the shapes of $p_k(\lambda)$ and their integrated distributions, and compare to the simulations. The agreement with the two lowest integrated RMT eigenvalue shapes is excellent for the larger β values.

The main qualitative features of the RMT spectrum are very similar in our $N_f = 8$ simulations as shown in Fig. 5.4. One marked quantitative difference is a noticeable slowdown in response to change in the coupling constant. As β grows the recovery of the quartet degeneracy is considerably delayed in comparison with the onset of p-regime Goldstone dynamics. Overall, for the $N_f = 4, 8$ models we find consistency between the p-regime analysis and the RMT tests. Earlier, using Asqtad fermions at a particular β value, we found agreement with RMT even at $N_f = 12$ which indicated a chirally broken phase [229]. Strong taste breaking with Asqtad fermion leaves the quartet averaging in question and the bulk pronounced crossover of the Asqtad action as β grows is also an issue. Currently we are investigating the RMT picture for $N_f = 9, 10, 11, 12$ with our much improved action with four and six stout steps. This action shows no artifact transitions and handles taste breaking much more effectively. Firm conclusions on the $N_f = 12$ model will require continued investigations.

5.4 Inside the conformal window

We start our investigation and simulations of the conformal window at $N_f = 16$ which is the most accessible for analytic methods. We are particularly interested in the qualitative behavior of the finite volume spectrum of the model and the running coupling with its associated beta function which is expected to have a weak coupling fixed point around $g^{*2} \approx 0.5$, as estimated from the scheme independent two-loop beta function [230].

5.4.1 Conformal dynamics in finite volume

A distinguished feature of the $N_f = 16$ conformal model is how the renormalized coupling $g^2(L)$ runs with L, the linear size of the spatial volume in a Hamiltonian or Transfer Matrix description. On very small scales the running coupling $g^2(L)$ grows with L as in any other asymptotically free theory. However, $g^2(L)$ will not grow large, and in the $L \to \infty$ limit it will converge to the fixed point g^{*2} which is rather weak, within the reach of perturbation theory. There is nontrivial small volume dynamics which is illustrated first in the pure gauge sector.

At small g^2, without fermions, the zero momentum components of the gauge field are known to dominate the dynamics [99,100,164]. With $SU(3)$ gauge group, there are twenty seven degenerate vacuum states, separated by energy barriers which are generated by the integrated effects of the non-zero momentum components of the gauge field in the Born-Oppenheimer approximation. The lowest energy excitations of the gauge field Hamiltonian scale as $\sim g^{2/3}(L)/L$ evolving into glueball states and becoming independent of the volume as the coupling constant grows with L. Nontrivial dynamics evolves through three stages as L grows. In the first regime, in very small boxes, tunneling is suppressed between vacua which remain isolated. In the second regime, for larger L, tunneling sets in and electric flux states will not be exponentially suppressed. Both regimes represent small worlds with zero momentum spectra separated from higher momentum modes of the theory with energies on the scale of $2\pi/L$. At large enough L the gauge dynamics overcomes the energy barrier, and wave functions spread over the vacuum valley. This third regime is the crossover to confinement where the electric fluxes collapse into thin string states wrapping around the box.

It is likely that a conformal theory with a weak coupling fixed point at $N_f = 16$ will have only the first two regimes which are common with QCD. Now the calculations have to include fermion loops [199,231]. The vacuum structure in small enough volumes, for which the wave functional is sufficiently localized around the vacuum configuration, remains calculable by adding in one loop order the quantum effects of the fermion field fluctuations. The spatially constant abelian gauge fields parametrizing the vacuum valley are given by $A_i(x) = T^a C_i^a/L$ where T_a are the (N-1) generators for the Cartan subalgebra of $SU(N)$. For $SU(3)$, $T_1 = \lambda_3/2$ and $T_2 = \lambda_8/2$. With N_f flavors of massless fermion fields the effective potential of the constant mode is given by

$$V_{\text{eff}}^{\mathbf{k}}(\mathbf{C}^b) = \sum_{i>j} V(\mathbf{C}^b[\mu_b^{(i)} - \mu_b^{(j)}]) - N_f \sum_i V(\mathbf{C}^b \mu_b^{(i)} + \pi\mathbf{k}), \tag{5.17}$$

with $\mathbf{k} = \mathbf{0}$ for periodic, or $\mathbf{k} = (1,1,1)$, for anti-periodic boundary conditions on the fermion fields. The function $V(\mathbf{C})$ is the one-loop effective potential for $N_f = 0$ and the weight vectors $\mu^{(i)}$ are determined by the eigenvalues of the abelian generators. For SU(3) $\mu^{(1)} = (1,1,-2)/\sqrt{12}$ and $\mu^{(2)} = \frac{1}{2}(1,-1,0)$. The correct quantum vacuum

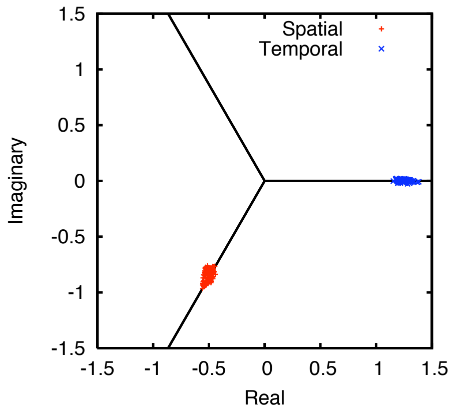

Figure 5.5: Polyakov loop distributions, blue in the time-like and red in the space-like directions, from our $N_f = 16$ simulation with 16^4 volume at $\beta = 18$ with tree level Symanzik improve gauge action and staggered fermions with six stout steps. The fermion boundary condition is anti-periodic in the time direction and periodic in the spatial directions.

is found at the minimum of this effective potential which is dramatically changed by the fermion loop contributions.

The Polyakov loop observables remain center elements at the new vacuum configurations with complex values

$$P_j = \frac{1}{N}\mathrm{Tr}\left(\exp(iC_j^b T_b)\right) = \frac{1}{N}\sum_n \exp(i\mu_b^{(n)} C_j^b) = \exp(2\pi i l_j/N), \tag{5.18}$$

for $SU(N)$. This implies that $\mu_b^{(n)}\mathbf{C}^b = 2\pi\mathbf{l}/N \pmod{2\pi}$, independent of n, and $V_{\mathrm{eff}}^{\mathbf{k}} = -N_f N V(2\pi\mathbf{l}/N + \pi\mathbf{k})$. In the case of anti-periodic boundary conditions, $\mathbf{k} = (1,1,1)$, this is minimal only when $\mathbf{l} = \mathbf{0} \pmod{2\pi}$. The quantum vacuum in this case is the naive one, $A = 0$ ($P_j = 1$). In the case of periodic boundary conditions, $\mathbf{k} = \mathbf{0}$, the vacua have $\mathbf{l} \neq \mathbf{0}$, so that P_j correspond to non-trivial center elements. For SU(3), there are now 8 degenerate vacua characterized by eight different Polyakov loops, $P_j = \exp(\pm 2\pi i/3)$. Since they are related by coordinate reflections, in a small volume parity (P) and charge conjugation (C) are spontaneously broken, although CP is still a good symmetry [199]. As shown in Fig. 5.5, our simulations in the $N_f = 16$ model near the fixed point g^{*2} confirm this picture. In the weak coupling phase of the conformal window the time-like Polyakov loop takes the real root, while the space-like Polyakov loops always take the two other complex values, as expected on the basis of the above picture. Next we will describe our method to probe the running coupling inside the conformal window. It is a pilot study for more comprehensive investigations of weak and strong coupling conformal dynamics.

5.4.2 Running coupling and beta function

Consider Wilson loops $W(R,T,L)$, where R and T are the space-like and time-like extents of the loop, and the lattice volume is L^4 (all dimensionful quantities are expressed in units of the lattice spacing a). A renormalized coupling can be defined by

$$g^2(R/L,L) = -\frac{R^2}{k(R/L)}\frac{\partial^2}{\partial R \partial T}\ln\langle W(R,T,L)\rangle\,|_{T=R}\,, \tag{5.19}$$

where for convenience the definition will be restricted to Wilson loops with $T = R$, and $\langle ...\rangle$ is the expectation value of some quantity over the full path integral. This definition can be motivated by perturbation theory, where the leading term is simply the bare coupling g_0^2. The renormalization scheme is defined by holding R/L to some fixed value. The quantity $k(R/L)$ is a geometric factor which can be determined by calculating the Wilson loop expectation values in lattice perturbation theory. The role of lattice simulations will be to measure non-perturbatively the expectation values. On the lattice, derivatives are replaced by finite differences, so the renormalized coupling is defined to be

$$g^2((R+1/2)/L,L) = \frac{1}{k(R/L)}(R+1/2)^2\chi(R+1/2,L)\,,$$
$$\chi(R+1/2,L) = -\ln\left[\frac{W(R+1,T+1,L)W(R,T,L)}{W(R+1,T,L)W(R,T+1,L)}\right]|_{T=R}\,,$$

where χ is the Creutz ratio [232], and the renormalization scheme is defined by holding the value of $r = (R + 1/2)/L$ fixed.

With this definition, the renormalized coupling g^2 is a function of the lattice size L and the fixed value of r. The coupling is non-perturbatively defined, as the expectation values are calculated via lattice simulations, which integrate over the full phase space of the theory. By measuring $g^2(r,L)$ non-perturbatively for fixed r and various L values, the running of the renormalized coupling is mapped out. In a QCD-like theory, g^2 increases with increasing L as we flow in the infrared direction. In a conformal theory, g^2 flows towards some non-trivial infrared fixed point as L increases, whereas in a trivial theory, g^2 decreases with L. The advantage of this method is that no other energy scale is required to find the renormalization group flow. The renormalized coupling g^2 is also a function of the bare coupling g_0^2, which is related to the lattice spacing a. Keeping the lattice spacing fixed, the running of $g^2(r,L)$ is affected by the lattice cut-off. The running has to be calculated in the continuum limit, extrapolating to zero lattice spacing. A similar method was developed independently in [233].

One way to measure the running of the renormalized coupling in the continuum limit is via step-scaling. The bare lattice coupling is defined in the usual way $\beta = 6/g_0^2$ as it appears in the lattice action. Some initial value of g^2 is picked from which the renormalization group flow is started. On a sequence of lattice sizes $L_1, L_2, ..., L_n$, the bare coupling is tuned on each lattice so that exactly the same value $g^2(r, L_i, \beta_i)$ is measured from simulations. Now a new set of simulations is performed, on a sequence of lattice sizes $2L_1, 2L_2, ..., 2L_n$, using the corresponding tuned couplings $\beta_1, \beta_2, ..., \beta_n$. From the simulations, one measures $g^2(r, 2L_i, \beta_i)$, which will vary with the bare coupling *viz.* the lattice spacing. These data can be extrapolated to the continuum as a function of $1/L_i$. This gives one blocking step $L \to 2L$ in the continuum renormalization group flow. The whole procedure is then iterated. The chain of measurements gives the flow $g^2(r,L) \to g^2(r,2L) \to g^2(r,4L) \to g^2(r,8L) \to ...$, as far as is feasible (Fig. 5.6). One is free to choose a different blocking factor, say $L \to (3/2)L$, in which case more blocking steps are required to cover the same energy range.

We applied the above procedure to the running coupling inside the conformal window with $N_f = 16$ flavors. The shortcut of this pilot study ignores the extrapolation

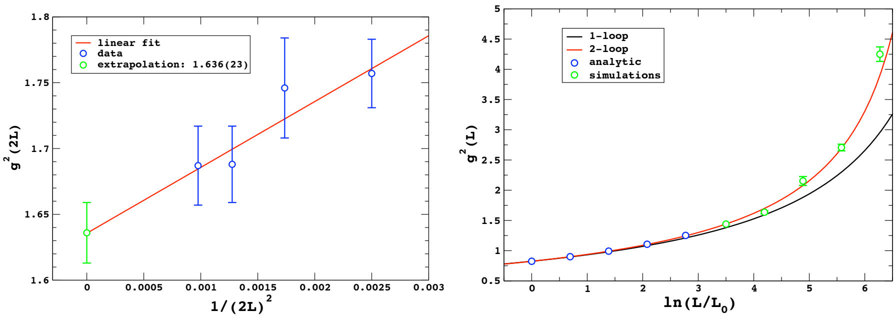

Figure 5.6: The method and the main test result for pure-gauge theory are shown in the figure. In the upper figure the extrapolation procedure picks up the leading a^2/L^2 cutoff correction term in the step function. It gives the fit to the continuum limit value of the step function. In the lower figure, the running coupling $g^2(L)$ is shown. The blue points are from results on Creutz ratios using analytic/numeric Wilson loop lattice calculations in finite volumes with fixed value of r. In this procedure we start from the one-loop expansion of Wilson loops in finite volumes based on the bare coupling [234]. The series is re-expanded in the boosted coupling constant at the relevant scale of the the Creutz ratio [235] to obtain realistic estimates of our running coupling without direct simulations. The rest of the procedure for the blue points follows what we described in the text. The green points are direct simulation results, following our procedure. The running starts at the point $g^2(L_0) = 0.825$. For almost all couplings there is excellent agreement with continuum 2-loop running. At the strongest coupling, the simulation results begin to break away from perturbation theory.

β	L	fermion mass	trajectories	$g^2(L)$
5	12	0.01	318	2.06(2)
	16	0.01	74	1.67(11)
7	12	0.01	317	1.207(5)
	12	0.001	116	1.207(12)
	16	0.01	198	1.13(1)
12	12	0.01	162	0.590(4)
	16	0.01	69	0.577(9)
15	12	0.01	144	0.447(3)
	12	0.001	91	0.460(5)
	16	0.01	62	0.444(7)
25	12	0.01	190	0.255(1)
	16	0.01	156	0.253(2)

Table 5.1: Running couplings bracketing the conformal fixed point of the $N_f = 16$ model in the conformal window.

to the continuum limit. The running coupling therefore is still contaminated with finite cutoff effects. If the linear lattice size L is large enough, the trend from the volume dependence of $g^2(L, a^2)$ should indicate the location of the fixed point. For $g^2(L, a^2) > g^{*2}$ we expect the decrease of the running coupling as L grows although the cutoff of the flow cannot be removed above the fixed point. Below the fixed point with $g^2(L, a^2) < g^{*2}$ we expect the running coupling to grow as L increases and the continuum limit of the flow could be determined. The first results are summarized in Table 1. They are consistent with the presented picture. For example, at bare couplings $\beta = 5, 7, 12$ the cutoff dependent renormalized coupling is larger than 0.5 and decreasing with growing L. At small bare couplings the renormalized coupling is flat within errors and the flow direction is not determined. The independence of the results from the small quark mass of the simulations is tested in two runs at $m_q = 0.001$. Precise determination of the conformal fixed point in the contiuum requires further studies.

5.5 Gradient flow running coupling $N_f = 4$

5.5.1 Introduction and summary

The Yang-Mills gradient flow − or Wilson flow − has proved to be a useful tool in lattice gauge theory. In the context of the Nicolai map it was studied in [184]; see also [183] for an earlier appearance. A systematic investigation, including suggestions for possible applications, has appeared relatively recently [154,156,185]. See also [186]. The first concrete very useful application of the flow for high precision setting of the physical scale in QCD simulations has been presented in [194]. The flow in QCD applications has so far been considered in infinite volume which is most appropriate for low energies.

In the present section the flow is calculated on the four dimensional torus, i.e. in a finite four dimensional box. The motivation for doing so is to obtain a new running coupling scheme in which the renormalized coupling runs with the linear size of the box. In principle the original infinite volume flow can also be used for defining a renormalized running coupling $g_R(q)$ with $q = 1/\sqrt{8t}$ where t is the flow time, but the control of finite volume corrections is an additional concern in this case. This issue is eliminated if the running $g_R(L)$ is with the linear size L. In particular, a step scaling analysis can be performed [138,217].

Due to asymptotic freedom perturbation theory is reliable for small volumes hence the appropriate framework is the small volume expansion or femto world [99,197–200]; see also [201–204]. The usual complication associated with calculations in the femto world is the presence of gauge zero modes which dominate the dynamics and are not Gaussian. They need to be treated exactly while the gauge non-zero modes can be integrated out in perturbation theory. As will be shown, the contribution of the non-zero modes renormalizes the bare coupling according to the 1-loop β-function and generates an effective action for the zero modes.

The quantity which turns out to be the most useful for our purposes is the one that has already been calculated in infinite volume in [154], namely the field strength squared at $t > 0$ flow time,

$$E(t) = -\frac{1}{2} \mathrm{Tr}\, F_{\mu\nu} F_{\mu\nu}(t) \; . \tag{5.20}$$

The expansion of its expectation value in finite volume is our main result and to leading order in the $\overline{\text{MS}}$ scheme it is given by

$$\langle t^2 E(t) \rangle = g_R^2(\mu) \frac{3(N^2-1)}{128\pi^2} (1+\delta) \tag{5.21}$$

where μ is the dimensional regularization scale, $g_R^2(\mu)$ is the renormalized coupling in the $\overline{\text{MS}}$ scheme. The correction factor $\delta = \delta_a + \delta_e$ is a sum of algebraic and exponential terms,

$$\begin{aligned} \delta_a &= -\frac{64 t^2 \pi^2}{3L^4} \\ \delta_e &= \vartheta^4 \left(\exp\left(-\frac{L^2}{8t} \right) \right) - 1 = 8 \exp\left(-\frac{L^2}{8t} \right) + 24 \exp\left(-\frac{L^2}{4t} \right) + \ldots \,, \end{aligned} \tag{5.22}$$

and where $\vartheta(q)$ is the standard Jacobi elliptic function (normally called $\vartheta_3(q)$) . Indeed, the infinite volume result in [154] is reproduced.

Equation (5.21) can be used to define a running coupling $g_R(L)$ which will run with the linear size once the dimensionless combination $c = \sqrt{8t}/L$ is held fixed and $\mu = 1/L$ is set. Different choices for c correspond to different schemes.

The organization of this section is as follows. In section 5.5.2 the small volume expansion is given on T^4 and the finite effective action for the gauge zero modes is calculated by integrating out the non-zero modes to 1-loop. In order for the presentation to be self-contained all details are spelled out although the methods are by no means new. In section 5.5.3 the gradient flow is considered and the expectation value of the quantity $E(t)$ is calculated by again treating the non-zero modes in 1-loop perturbation theory and using the previously obtained effective action for the zero modes. The result is then used in section 5.5.4 to define a renormalization scheme for the gauge coupling. As an illustration of the method, numerical simulations are used to compute the running coupling in $SU(3)$ gauge theory coupled to $N_f = 4$ massless quarks.

5.5.2 Small volume expansion

On the four dimensional Euclidean torus T^4 with periodic boundary conditions for the gauge field the zero momentum (constant) gauge mode is separated from the first non-zero momentum mode by the gap $2\pi/L$ and dominates the low energy small volume dynamics [99]; see also [197–204]. This dynamics is non-linear because of the quartic interaction and needs to be treated exactly while the dynamics of the non-zero modes can be treated perturbatively. Correspondingly the gauge field is split

$$A_\mu(x) = B_\mu + Q_\mu(x) \,, \qquad \int d^4x Q_\mu(x) = 0 \tag{5.23}$$

into the zero mode B_μ and non-zero modes $Q_\mu(x)$. The action for N_f flavors of massless Dirac fermions in representation R is

$$S = -\frac{1}{2g_0^2} \int d^4x \mathrm{Tr}\, F_{\mu\nu} F_{\mu\nu} + \sum_{f=1}^{N_f} \int d^4x \bar{\psi}_f \not{D} \psi_f \,. \tag{5.24}$$

where g_0 is the bare coupling constant. The boundary condition for the fermions is assumed to be anti-periodic in at least one direction. It is convenient to introduce

$\partial_\mu + B_\mu = D_\mu(B)$ acting in either the adjoint or representation R depending on whether it is applied to a gauge field or fermion.

Gauge fixing is only required for the gauge non-zero modes and a convenient gauge choice is the background gauge $\chi = D_\mu(B)Q_\mu = 0$. The constant gauge transformations do not need to be fixed as their volume is finite.

Neglecting interactions which are higher order in Q_μ and the ghost field one obtains the leading order Faddeev-Popov operator as $D_\mu(B)^2$ which is understood in the adjoint representation and acts on ghosts without zero-modes. The corresponding effective action for the zero mode B_μ is then

$$S_{gh}(B) = -\ln\det\left(D_\mu(B)^2\right) . \tag{5.25}$$

The quadratic term in Q_μ from the gauge action is

$$\frac{1}{2g_0^2}\int d^4x \mathrm{Tr}\, Q_\mu \left(D_\rho(B)^2\delta_{\mu\nu} - D_\mu(B)D_\nu(B) + 2[B_\mu, B_\nu]\right) Q_\nu . \tag{5.26}$$

A convenient way of implementing gauge fixing is by adding $\chi^2/2g_0^2$ to the action which allows integrating out the Q_μ field without the gauge constraint. The effective action from this bosonic integral is then,

$$S_Q(B) = \frac{1}{2}\ln\det\,\left(D_\rho(B)^2\delta_{\mu\nu} + 2[B_\mu, B_\nu]\right) . \tag{5.27}$$

In the fermionic action one may neglect the interaction between the Q_μ fields and the fermions. To leading order one obtains the effective action

$$S_F(B) = -\ln\det\left(\not{D}(B)\right)^{N_f} = -\ln\det\left(D_\mu(B)^2 + \frac{1}{2}\sigma_{\mu\nu}[B_\mu, B_\nu]\right)^{N_f/2} , \tag{5.28}$$

where $\sigma_{\mu\nu} = [\gamma_\mu, \gamma_\nu]/2$. Here the operators act on fermions with the appropriate boundary condition. The various determinants will be evaluated using dimensional regularization and all subsequent calculations are done in dimension $d = 4 - 2\varepsilon$.

The total effective action after integrating out the gauge non-zero modes, the ghosts and the fermions is then

$$S_{eff}(B) = -\frac{L^4}{2g_0^2(\mu L)^{2\varepsilon}}\mathrm{Tr}\,[B_\mu, B_\nu]^2 + S_Q(B) + S_{gh}(B) + S_F(B) , \tag{5.29}$$

where the first term is the tree level action for the constant mode and μ is the scale of dimensional regularization.

Now we will proceed to evaluating the various determinants. They will be Taylor-expanded in B_μ and we will see later that it is enough to expand them to fourth order for our purposes. Higher orders in B_μ will correspond to higher orders in the renormalized coupling. The expansion is around the free $B_\mu = 0$ determinants and these (infinite) constants are dropped as usual.

The derivatives in S_Q and S_{gh} are replaced by $2\pi i n_\mu/L$ where n_μ are integers and $n^2 \neq 0$. In S_F the derivatives are replaced by $2\pi i(n_\mu - k_\mu)/L$ where k_μ is $1/2$ in all anti-periodic fermion directions and the rest of its components are zero. We will assume $k^2 \neq 0$. It is furthermore convenient to introduce the hermitian matrices $C_\mu = LB_\mu/2\pi i$.

Straightforward calculation yields that up to fourth order in C_μ the following holds

$$S_Q(C) + S_{gh}(C) = \mathrm{Tr}_{\,ad}\log(D_\mu(C)^2) + \gamma\,\mathrm{Tr}_{\,ad}[C_\mu, C_\nu]^2 , \tag{5.30}$$

where the traces are in the adjoint representation and

$$\gamma = \sum_{n \neq 0} \frac{1}{n^4} \ . \tag{5.31}$$

Similarly, the fermionic contribution to the effective action up to fourth order in C_μ is

$$S_F(C) = -2N_f \left(\mathrm{Tr}_R \log(D_\mu(C)^2) + \frac{\gamma(k)}{4} \mathrm{Tr}_R [C_\mu, C_\nu]^2 \right) \ , \tag{5.32}$$

where all traces are in the representation R and

$$\gamma(k) = \sum_n \frac{1}{(n-k)^4} \ . \tag{5.33}$$

Equations (5.30) and (5.32) show that only the Laplacian is needed in the background of C_μ in arbitrary representation and with arbitrary boundary condition in order to evaluate the full effective action.

First, let us evaluate all determinants with periodic boundary condition and get back to the case of non-trivial boundary conditions for the fermions later. Explicit calculation yields up to fourth order in C_μ,

$$\begin{aligned} -\mathrm{Tr}_R \log(D_\mu(C)^2) &= \delta \frac{2-d}{d} \mathrm{Tr}_R C^2 + \gamma \frac{d-8}{2d} \mathrm{Tr}_R C^4 + \\ &\quad + 4 \sum_{n \neq 0} \frac{n_\mu n_\nu n_\rho n_\sigma}{n^8} \mathrm{Tr}_R C_\mu C_\nu C_\rho C_\sigma \ , \end{aligned} \tag{5.34}$$

where the new constant δ has been introduced and $C^2 = C_\mu C_\mu$ and $C^4 = (C_\mu C_\mu)^2$ are $SO(4)$ invariant combinations. It is useful to define two more constants α and β by

$$\delta = \sum_{n \neq 0} \frac{1}{n^2} \ , \qquad \alpha = \sum_{n \neq 0} \frac{n_1^4}{n^8} \ , \qquad \beta = \sum_{n \neq 0} \frac{n_1^2 n_2^2}{n^8} \ . \tag{5.35}$$

Using these the following is easy to show,

$$\sum_{n \neq 0} \frac{n_\mu n_\nu n_\rho n_\sigma}{n^8} \mathrm{Tr}_R C_\mu C_\nu C_\rho C_\sigma = (\alpha - 3\beta) \sum_\mu C_\mu^4 + \beta \left(3 \mathrm{Tr}_R C^4 + \frac{1}{2} \mathrm{Tr}_R [C_\mu, C_\nu]^2 \right) . \tag{5.36}$$

Since the torus breaks rotations the $SO(4)$-breaking first term on the right hand side is allowed. Combining equations (5.34) and (5.36) we obtain,

$$\begin{aligned} -\mathrm{Tr}_R \log(D_\mu(C)^2) &= \delta \frac{\varepsilon - 1}{2 - \varepsilon} \mathrm{Tr}_R C^2 + 4(\alpha - 3\beta) \sum_\mu C_\mu^4 + \\ &\quad + \left(12\beta - \gamma \frac{2 + \varepsilon}{4 - 2\varepsilon} \right) \mathrm{Tr}_R C^4 + 2\,\beta\, \mathrm{Tr}_R [C_\mu, C_\nu]^2 \ . \end{aligned} \tag{5.37}$$

Even though α, β and γ are all divergent the combinations appearing above for the terms that were not present at tree level, namely C^2, C^4 and $\sum_\mu C_\mu^4$, are all finite. Only the coefficient of $[C_\mu, C_\nu]^2$ is divergent.

Now the full effective action (5.29) is easily written down using (5.37) in the adjoint representation together with (5.30) and in representation R together with (5.32). The traces of the product of two Lie algebra elements in different representations can be all converted to the fundamental representation using the trace normalization factors $T(R)$ via $\mathrm{Tr}_R(\cdot\ \cdot) = 2T(R)\,\mathrm{Tr}(\cdot\ \cdot)$. Let us first collect the terms proportional to $\mathrm{Tr}\,[C_\mu, C_\nu]^2$ which is the only divergent term. Using $T(ad) = N$ and the poles of β and γ we obtain,

$$S_{eff}(C)|_{div} = -\frac{(2\pi)^4}{2}\left(\frac{1}{g_0^2(\mu L)^{2\varepsilon}} - \frac{\frac{11}{3}N - \frac{4}{3}T(R)N_f}{16\pi^2\varepsilon} + \text{finite}\right)\mathrm{Tr}\,[C_\mu, C_\nu]^2 \quad (5.38)$$

Clearly, by introducing the renormalized coupling $g_R(\mu)$ of the MS scheme,

$$\frac{1}{g_R^2(\mu)} = \frac{1}{g_0^2(\mu L)^{2\varepsilon}} - \frac{\frac{11}{3}N - \frac{4}{3}T(R)N_f}{16\pi^2\varepsilon}\ , \quad (5.39)$$

in place of the bare coupling g_0 a finite effective action is obtained. Going from MS to $\overline{\text{MS}}$ scheme only modifies the finite terms.

Up until this point the momentum sums corresponding to the fermions were computed with periodic boundary conditions, however we are interested in fermions that are anti-periodic in at least one direction. Instead of the coefficients α, β and γ we should have considered $\alpha_\mu(k), \beta_{\mu\nu}(k)$ and $\gamma(k)$,

$$\begin{aligned} \alpha_\mu(k) &= \sum_n \frac{(n_\mu - k_\mu)^4}{(n-k)^8} \\ \beta_{\mu\nu}(k) &= \sum_n \frac{(n_\mu - k_\mu)^2(n_\nu - k_\nu)^2}{(n-k)^8} \\ \gamma(k) &= \sum_n \frac{1}{(n-k)^4}\ , \end{aligned} \quad (5.40)$$

where $k_\mu \neq 0$ determines the boundary conditions. However, it is easy to see that the differences $\alpha_\mu(k)-\alpha$, $\beta_{\mu\nu}(k)-\beta$ and $\gamma(k)-\gamma$ are all finite. This is expected because UV divergences are insensitive to boundary conditions. Hence once the UV divergences are canceled only the finite terms can be effected by the change of boundary conditions.

Summarizing this section, a finite effective action is obtained for the gauge zero modes of the form,

$$\begin{aligned} S_{eff}(C) &= -\frac{(2\pi)^4}{2g_R^2(\mu)}\mathrm{Tr}\,[C_\mu, C_\nu]^2 + \\ &\quad + u_1\mathrm{Tr}\,C^2 + u_2\mathrm{Tr}_R C^4 + u_3\mathrm{Tr}_{ad}C^4 + \\ &\quad + u_4\sum_\mu \mathrm{Tr}_R C_\mu^4 + u_5\sum_\mu \mathrm{Tr}_{ad} C_\mu^4\ , \end{aligned} \quad (5.41)$$

where the finite expressions $u_1, \ldots, u_5$ depend on N, N_f, R and the boundary condition for the fermions. These are all known although in a bit cumbersome form. Their values will not be important for what follows, the only property we need is their finiteness. From now on we set $\mu = 1/L$.

5.5.3 Yang-Mills gradient flow on T^4

Now that a finite action is obtained for the gauge zero modes C_μ let us turn to our observable of interest, the field strength squared $E(t)$ at positive flow time (5.20). It will be evaluated by treating the gauge non-zero modes in perturbation theory and the zero mode C_μ exactly, similarly to the effective action. Let us first write down the Yang-Mills gradient flow,

$$\frac{dA_\mu}{dt} = D_\nu F_{\nu\mu} \,. \tag{5.42}$$

Using the decomposition (5.23) we obtain a coupled flow for the zero and non-zero modes. After taking into account gauge fixing and dropping terms higher order in Q_μ we arrive at,

$$\begin{aligned} \frac{dB_\mu}{dt} &= [B_\nu,[B_\nu,B_\mu]] \\ \frac{dQ_\mu}{dt} &= \left(D_\rho(B)^2\delta_{\mu\nu} + 2[B_\mu,B_\nu]\right) Q_\nu \,. \end{aligned} \tag{5.43}$$

Since we are interested in a perturbative expansion let us rescale $Q_\mu \to g_R Q_\mu$. The consistent rescaling of the zero mode is $B_\mu \to g_R^{1/2} B_\mu$. After the rescaling the gradient flow becomes

$$\begin{aligned} \frac{dB_\mu}{dt} &= g_R[B_\nu,[B_\nu,B_\mu]] \\ \frac{dQ_\mu}{dt} &= \Delta Q_\mu + O(g_R^{1/2}) \,. \end{aligned} \tag{5.44}$$

Clearly, to leading order in the coupling the zero mode is constant $B_\mu(t) = B_\mu$ and the solution for the non-zero mode is

$$Q_\mu(t) = e^{t\Delta} Q_\mu(0) \,. \tag{5.45}$$

In the path integral one integrates over the fields at $t = 0$, i.e. $Q_\mu(0)$ and B_μ.

The rescaling also effects the observable $E(t)$ and keeping the leading order term only we obtain,

$$E(t) = -\frac{g_R^2}{2}\mathrm{Tr}\,[B_\mu,B_\nu]^2 + \frac{g_R^2}{2}\mathrm{Tr}\; Q_\mu e^{2t\Delta}\left(\Delta\delta_{\mu\nu} - \partial_\mu\partial_\nu\right) Q_\nu \tag{5.46}$$

where Q_μ now stands for $Q_\mu(0)$ for the sake of brevity.

Let us evaluate $\langle E(t)\rangle$ by first integrating over Q_μ while B_μ is kept fixed. The first term in (5.46) is independent of Q_μ and the second term is quadratic, leading to

$$\langle E(t)\rangle_B = -\frac{g_R^2}{2}\mathrm{Tr}\,[B_\mu,B_\nu]^2 + \frac{g_R^2}{2L^4}\mathrm{Tr}\; e^{2t\Delta}\left(\Delta\delta_{\mu\nu} - \partial_\mu\partial_\nu\right)\frac{\delta_{\mu\nu}}{\Delta} \tag{5.47}$$

where only the leading order propagator is taken into account from the action. The integral and trace in the second term is given by,

$$\begin{aligned} & 3(N^2-1)\sum_{n\neq 0} e^{-\pi^2 n^2 8t/L^2} = \\ & = 3(N^2-1)\left(\vartheta^4(e^{-\pi^2c^2}) - 1\right) = 3(N^2-1)\left(\frac{1}{\pi^2c^4}\vartheta^4\left(e^{-1/c^2}\right) - 1\right) \,, \end{aligned} \tag{5.48}$$

where the ratio $c = \sqrt{8t}/L$ was introduced. The factor 3 comes from the trace over the Euclidean indices and the factor $N^2 - 1$ comes from the gauge trace.

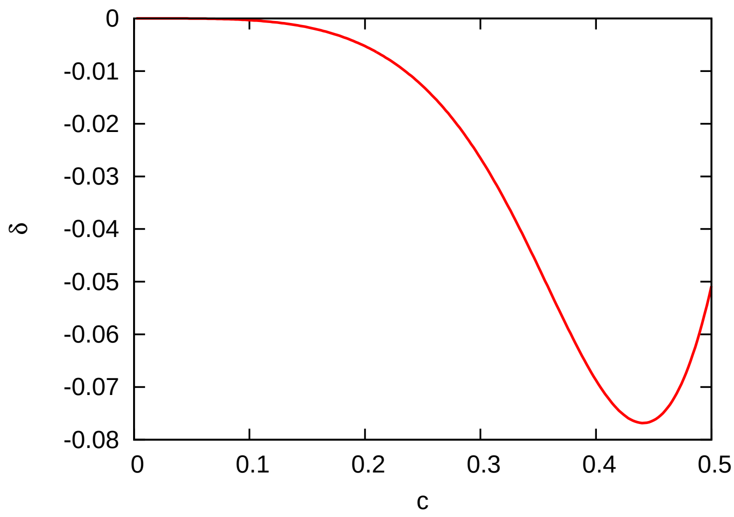

Figure 5.7: Finite volume correction factor $\delta(c)$.

Let us now integrate over B_μ using the effective action (5.41). One needs to keep the tree level part only, all further terms are higher order in g_R. The second term in (5.47) is independent of B_μ while for the first term we need the matrix integral

$$-\frac{\int dB \frac{1}{2}\mathrm{Tr}\,[B_\mu, B_\nu]^2 \exp\left(\frac{L^4}{2}\mathrm{Tr}\,[B_\mu, B_\nu]^2\right)}{\int dB \exp\left(\frac{L^4}{2}\mathrm{Tr}\,[B_\mu, B_\nu]^2\right)} = \frac{N^2-1}{L^4}\,. \tag{5.49}$$

Even though the integral is quartic it can easily be done with the result N^2-1 essentially determined by the dimensionality of the integral. Combining (5.47), (5.48) and (5.49) we obtain,

$$\langle t^2 E(t)\rangle = g_R^2 \frac{3(N^2-1)}{128\pi^2}\left(1+\vartheta^4\left(e^{-1/c^2}\right)-1-\frac{c^4\pi^2}{3}\right) \tag{5.50}$$

which is the advertised final result (5.21). The finite volume correction term $\delta(c)$ is plotted on figure 5.7 as a function of the ratio c. As can be seen the correction never reaches 10% for $0 \le c \le 1/2$.

5.5.4 Running coupling

The result (5.50) can be used to define a non-perturbative running coupling scheme in which the running scale is $\mu = 1/L$. As one changes the scale one keeps c fixed. Then the scheme is defined by the coupling constant

$$g_c^2(L) = \frac{128\pi^2\langle t^2 E(t)\rangle}{3(N^2-1)(1+\delta(c))} \tag{5.51}$$

where now the expectation value on the right hand side is understood non-perturbatively. The results from the preceding sections ensure that the above defined coupling for

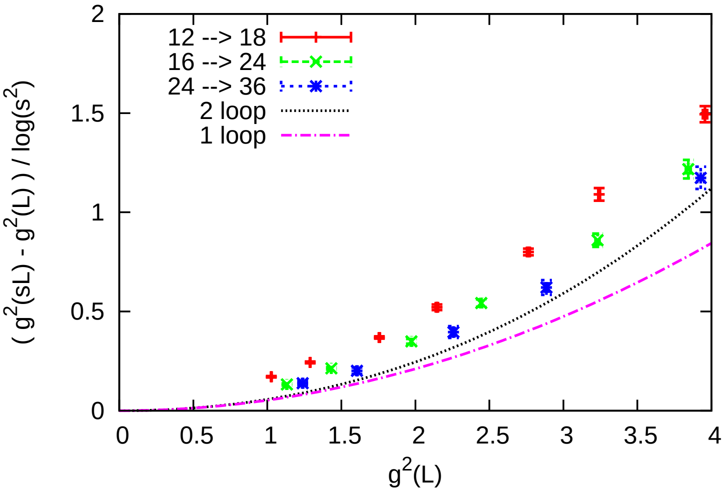

Figure 5.8: Discrete β-function of $SU(3)$ gauge theory coupled to $N_f = 4$ flavors of massless fundamental fermions for a scale change of $s = 3/2$. The results at 3 lattice spacings are shown together with the continuum 1 and 2-loop result from (5.54) for comparison.

small L will run according to the universal 1-loop β-function. Different choices for c correspond to different schemes.

A note is in order about the 2-loop β-function. As is well known both the 1 and 2 loop coefficients are universal under a scheme change of the type $\tilde{g} = g(1 + O(g^2))$ where the expansion on the right hand side only contains even powers of the coupling. However if one allows scheme changes of the type $\tilde{g} = g(1+O(g))$ where the expansion contains both even and odd powers then only the 1-loop coefficient remains scheme independent. Our scheme is related to the $\overline{\mathrm{MS}}$ scheme by such an expansion since it is easy to see that both even and odd powers of the coupling will appear as subleading terms to the leading result (5.21) but fractional powers will not. Our scheme is nevertheless well-defined and has for instance the property that if a theory has an infrared fixed point in one scheme it will have a fixed point in our scheme as well.

In order for the system to be controlled by a single scale L the bare fermion mass was set to zero in the preceding sections. The spectrum of the Dirac operator nevertheless has a gap $\sim 1/L$ due to the non-trivial boundary conditions for the fermions.

5.5.5 Numerical results

We have tested the new running coupling scheme in $SU(3)$ gauge theory coupled to $N_f = 4$ massless fundamental fermions. The Schrödinger functional analysis of the same model can be found in [218, 236]. The fermion action was the 4-step stout improved [182] staggered action with smearing parameter $\varrho = 0.12$. Since the number of flavors is a multiple of four no rooting was necessary. For the gauge sector tree level improved Symanzik action [212,213] was used. The hybrid Monte Carlo algorithm [237] was used together with multiple time scales [238] and Omelyan integrator [239].

L/a β	4.25	4.50	4.75	5.00	5.50	6.00	7.00	8.00
12	5.08(1)	3.96(1)	3.241(6)	2.764(9)	2.146(8)	1.757(3)	1.289(2)	1.027(2)
16	6.41(3)	4.79(2)	3.84(2)	3.23(1)	2.446(6)	1.974(5)	1.432(2)	1.132(3)
18	7.05(3)	5.17(3)	4.13(3)	3.41(1)	2.569(9)	2.056(3)	1.486(3)	1.166(2)
24		6.34(4)	4.83(3)	3.93(2)	2.89(1)	2.257(9)	1.605(5)	1.239(4)
36			6.19(5)	4.88(4)	3.39(3)	2.58(2)	1.77(1)	1.352(8)

Table 5.2: Measured renormalized couplings $g_c^2(L)$ from (5.51) at $c = 0.3$ and given bare couplings β and lattice volumes L/a.

The observable $E(t)$ and the flow itself can be discretized in a number of ways. Both the discretization in [154] and also the tree level improved Symanzik discretization of [194] was measured. We have found that the latter displays better scaling as expected hence in the following only the results from the Symanzik discretization will be presented. The bare quark mass was set to zero and anti-periodic boundary conditions were used for the fermions in all four directions. As mentioned in the previous section this leads to a gap $\sim 1/L$ in the spectrum of the Dirac operator. The gauge field was periodic in all directions.

The choice of $0 \leq c \leq 1/2$ is limited by the observations that a small c leads to large cut-off effects while large c leads to large statistical errors. We found that $c = 0.3$ is a convenient choice and from here on will drop the index c or R on the renormalized coupling g^2.

The discrete version of the β-function, or step scaling function, was computed for a scale change of $s = 3/2$. Three lattice spacings are used corresponding to $12^4 \to 18^4$, $16^4 \to 24^4$ and $24^4 \to 36^4$. Then the discrete β-function

$$\frac{g^2(sL) - g^2(L)}{\log(s^2)} \tag{5.52}$$

can be calculated as a function of $g^2(L)$. Holding L fixed in physical units the continuum limit corresponds to $L/a \to \infty$.

The numerical results can be compared with the perturbative β-function for small renormalized couplings. The 2-loop β-function is given by

$$L^2 \frac{dg^2}{dL^2} = b_1 \frac{g^4}{16\pi^2} + b_2 \frac{g^6}{(16\pi^2)^2}\,, \qquad b_1 = \frac{25}{3}\,, \qquad b_2 = \frac{154}{3}\,. \tag{5.53}$$

The discrete β-function up to 2 loops for a finite scale change s is then

$$\frac{g^2(sL) - g^2(L)}{\log(s^2)} = b_1 \frac{g^4(L)}{16\pi^2} + \left(b_1^2 \log(s^2) + b_2\right) \frac{g^6(L)}{(16\pi^2)^2}\,, \tag{5.54}$$

which will be used for comparison although the zero mode of our finite volume scheme will introduce modifications which have not yet been calculated.

The measured results for the renormalized coupling at each bare coupling and lattice volume are tabulated in table 5.2. At the volumes 12^4, 16^4, 18^4, 24^4 and 36^4 the number of equilibrium trajectories were 10000, 10000, 10000, 8000 and 4000, respectively and every 10^{th} configuration was used for measurements. Auto correlation times were also measured and are around $10-30$, $10-40$, $10-70$, $30-100$, $30-100$

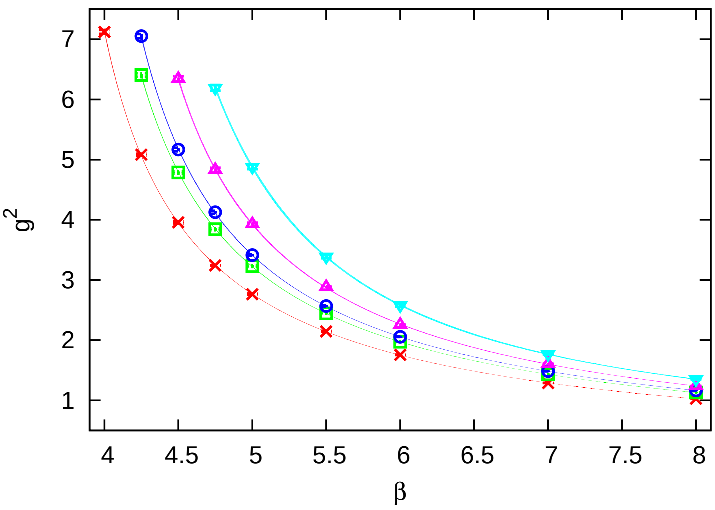

Figure 5.9: Parametrization of the curves $g^2(\beta)$ at fixed lattice volumes using the expression (5.55). Red: 12^4, green: 16^4, dark blue: 18^4, magenta: 24^4, light blue: 36^4.

for the five volumes, respectively. The lower auto correlation times in the indicated intervals correspond to larger β and the higher ones to smaller β.

The discrete β-function obtained from the data is shown on figure 5.8. The continuum extrapolation can be performed in (at least) two different ways. In the first method a cubic spline interpolation is done at fixed $L/a \to sL/a$ for $(g^2(sL) - g^2(L))/\log(s^2)$ as a function of $g^2(L)$. Then the resulting three curves together with their errors are used for the continuum limit at each fixed $g^2(L)$. The continuum extrapolation is linear in a^2/L^2 since both the action and the observable only contain $O(a^2)$ corrections. This latter step is repeated for each value of $g^2(L)$.

In the second method, similarly to [218], the dependence of $g^2(\beta)$ on β at fixed L/a is parametrized by the expression

$$\frac{\beta}{6} - \frac{1}{g^2(\beta)} = \sum_{m=0}^{3} c_m \left(\frac{6}{\beta}\right)^m , \tag{5.55}$$

and the coefficients c_m are fixed by fitting to the measured values. The χ^2/dof values from the fits for the five volumes are 1.59, 0.39, 0.45, 1.11 and 0.08, respectively from 12^4 to 36^4. The fitted curves together with the data are shown on figure 5.9. Since the parametrization is linear in the coefficients c_m the error on the fitted curve can be computed in a straightforward manner. Then $g^2(L)$ together with the discrete β-function $(g^2(sL) - g^2(L))/\log(s^2)$ and its error can be obtained for any β for all three lattice spacings corresponding to $12^4 \to 18^4$, $16^4 \to 24^4$ and $24^4 \to 36^4$. From here the procedure is identical to the previous method; at fixed $g^2(L)$ the three discrete β-function values are extrapolated to the continuum assuming $O(a^2/L^2)$ corrections.

The continuum extrapolation is shown on figure 5.10 for both methods and for four representative values of $g^2(L)$, 1.4, 2.2, 3.0 and 3.8 together with the χ^2/dof values of the fits. The continuum results agree nicely between the two methods.

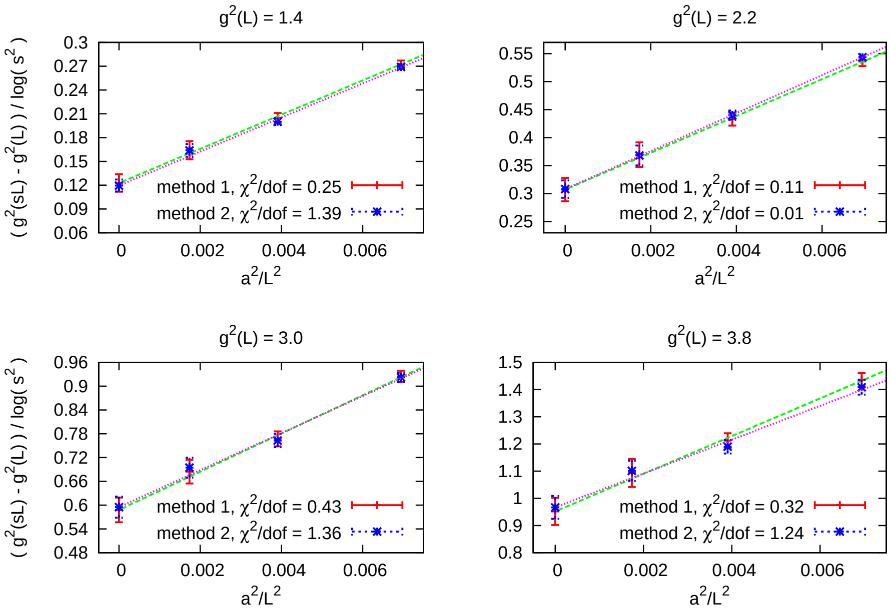

Figure 5.10: Continuum extrapolations of the discrete β-function for four selected $g^2(L)$ values 1.4, 2.2, 3.0 and 3.8. Both methods are shown together with the χ^2/dof values of the fits.

It is reassuring to note that the continuum extrapolations from the two methods yield continuum results that agree with each other within error showing the robustness of the procedures. Also the continuum result is quite insensitive to the order of the polynomial used in (5.55) or other details of the fitting procedures.

The final continuum extrapolated result agrees approximately with the 2-loop perturbative expression (5.54) as shown on figure 5.11 (only the final result from the first method is shown, but the second one gives a result which agrees with it within errors in the entire $g^2(L)$ range). As noted in section 5.5.4 our scheme is related to the $\overline{\mathrm{MS}}$ scheme via $g_c^2 = g_{\overline{\mathrm{MS}}}^2(1 + a_1(c)g_{\overline{\mathrm{MS}}} + \ldots)$ where $a_1(c)$ is non-zero leaving only the first β-function coefficient scheme independent. It can be shown from the measured gradient flow at $c = 0.2$ that the discrete β-function in figure 5.11 is not sensitive to the volume beyond the leading $\delta(c)$ correction factor. This explains the approximate agreement with the 2-loop universal β-function keeping contributions from $a_1(c)$ undetectable within errors.

5.6 Gradient flow running coupling $N_f = 8$

In this section the same technique is applied as for $N_f = 4$ to obtain the discrete β-function of the $N_f = 8$ model. This flavor number is expected to be close to the conformal window hence a slower running is expected.

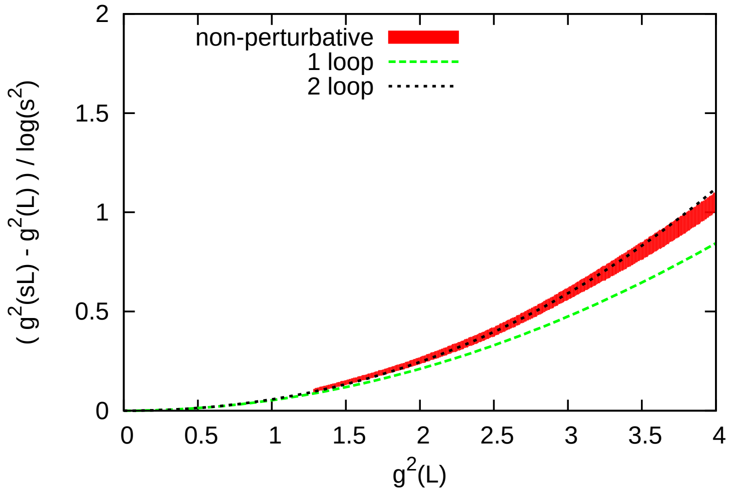

Figure 5.11: Discrete β-function of $SU(3)$ gauge theory coupled to $N_f = 4$ flavors of massless fundamental fermions for a scale change of $s = 3/2$. The continuum extrapolated result from method 1 (see text for details) is shown together with the 1 and 2-loop results from (5.54) for comparison.

5.6.1 Numerical simulation

The technical details of the simulations closely follow our work on $N_f = 4$ in [155,187]. In particular we use the staggered fermion action with 4 steps of stout improvement with $\varrho = 0.12$ [182]. The bare fermion mass is set to zero and anti-periodic boundary conditions in all four directions are imposed on the fermions and the gauge field is periodic. The gauge action is the tree-level improved Symanzik action [212, 213]. The observable $E(t)$ is discretized by the clover-type construction as in [154].

Along the gradient flow we use two discretizations, the Wilson plaquette action and the tree-level improved Symanzik gauge action. These setups correspond to the WSC and SSC cases in the terminology of [214]: the notation is Flow-Action-Observable and W stands for Wilson plaquette action, S for tree-level improved Symanzik action and C for the clover discretization. Both setups lead to the same continuum limit, only the size of cut-off effects is different. This fact allows for the introduction of yet another coupling definition at finite lattice spacing, which however again leads to the same continuum limit,

$$g_X^2 = X g_{SSC}^2 + (1 - X) g_{WSC}^2 \; . \tag{5.56}$$

Here the parameter X is arbitrary, the choice of the two coefficients, X and $1 - X$, guarantees that the continuum limit of g_X^2 is the same as that of g_{SSC}^2 or g_{WSC}^2, i.e. the correct one. It is important to note that X is a constant and does not depend on the bare gauge coupling β or the lattice volume L/a. In practice we have found that the choice $X = 1.75$ is most useful. Note that in principle X could depend on the renormalized coupling but in the present work we do not explore this possibility.

Just as in [155, 187] where $N_f = 4$ was considered we do not need to take the root of the fermion determinant. Hence the results do not depend on the validity of

$L/a \quad \beta$	3.5	3.6	3.7	4.0	4.5	5.0
12	6.42(4)	5.85(4)	5.29(2)	4.00(2)	2.775(7)	2.12(1)
16	7.66(6)	6.94(4)	6.28(2)	4.67(4)	3.19(1)	2.43(2)
18	8.17(7)		6.6(1)	4.95(3)	3.36(2)	2.52(1)
20	8.55(5)	7.77(4)	6.98(3)	5.17(3)	3.51(2)	2.63(1)
24	9.33(8)	8.51(5)		5.50(7)	3.68(2)	2.76(2)
30	10.4(1)		8.3(1)	6.03(9)	4.02(4)	2.93(3)
36		10.2(1)		6.52(8)	4.19(4)	3.07(4)
$L/a \quad \beta$	6.0	7.0	8.0	9.5	15.0	
12	1.444(6)	1.098(4)	0.890(2)	0.696(2)	0.383(2)	
16	1.64(1)	1.242(6)	1.000(6)	0.774(3)	0.426(1)	
18	1.704(6)	1.288(4)	1.035(7)	0.799(4)	0.437(1)	
20	1.757(8)	1.322(5)	1.062(5)	0.820(1)	0.449(2)	
24	1.84(1)	1.376(7)	1.099(6)	0.847(4)	0.463(2)	
30	1.93(2)	1.43(1)	1.141(4)	0.880(4)	0.481(3)	
36	2.00(2)	1.48(2)	1.17(1)	0.90(1)		

Table 5.3: Measured renormalized couplings $g^2(L)$ for given bare couplings β and lattice sizes L/a using the linear combination method with $X = 1.75$ at $c = 3/10$.

the fourth-root-trick commonly used for QCD. The evolution along a trajectory of the hybrid Monte Carlo algorithm [237] is implemented with multiple time scales [238] and Omelyan integrator [239].

In a lattice setting the most practical method of calculating the running coupling or its β-function is via step scaling [138,217]. In this context the linear size L is increased by a factor s and the difference of couplings

$$\frac{g^2(sL) - g^2(L)}{\log(s^2)} \;, \tag{5.57}$$

is defined as the discrete β-function. If the ordinary infinitesimal β-function of the theory possesses an infrared fixed point, the discrete β-function will have a zero as well. On the lattice the linear size L is easily increased to sL by simply increasing the volume in lattice units, $L/a \to sL/a$ at fixed bare gauge coupling. In the current work we set $s = 3/2$ and use volumes $12^4 \to 18^4$, $16^4 \to 24^4$, $20^4 \to 30^4$ and $24^4 \to 36^4$. The continuum limit corresponds to $L/a \to \infty$. These lattice volumes determine the β-function at 4 lattice spacings, allowing for a fully controlled continuum extrapolation. Leading cut-off effects are known to be $O(a^2/L^2)$.

The collected number of thermalized trajectories at each bare coupling and volume was in the range between 5000 and 10000 and every 10^{th} was used for measurement. The measured renormalized couplings at each β and lattice volume are shown in table 5.3 for the definition (5.56) using $X = 1.75$. By taking the difference of renormalized couplings for lattice volumes scaled by a factor $s = 3/2$ and at the same bare β one obtains the discrete β-function at finite lattice spacings; see figure 5.12. Clearly, there is no sign of a fixed point, the running is monotonically increasing, at least at finite lattice spacing, i.e. finite lattice volumes. However we are of course interested in the behavior of the continuum model and the behavior of the discrete β-function on finite lattice volumes is irrelevant. It is a priori possible that the discrete β-functions on

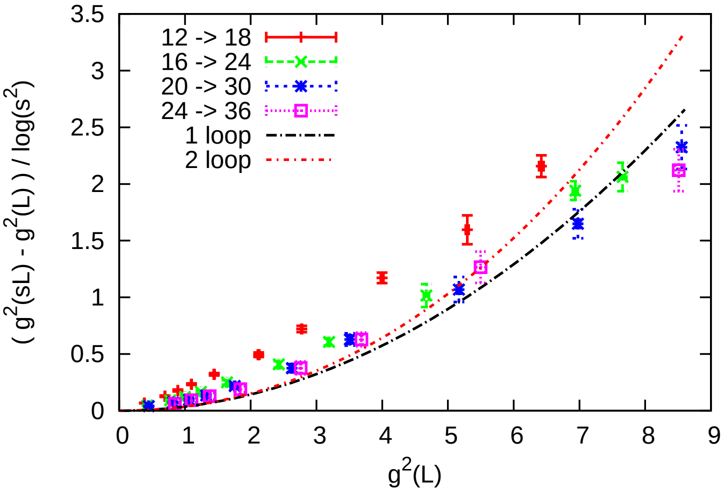

Figure 5.12: Measured discrete β-function for the linear combination setup with $X = 1.75$ and $c = 3/10$; data corresponding to four lattice spacings.

several finite lattice volumes, corresponding to a fixed set of $L/a \to sL/a$ steps, cross zero but the continuum extrapolated result does not have a zero and conversely it is possible that none of the finite lattice volume β-functions cross zero yet the continuum extrapolated result does have a zero. Hence we turn to the continuum extrapolation next.

5.6.2 Continuum extrapolation

In order to perform a continuum extrapolation we parametrize the renormalized coupling as a function of the bare coupling, $g^2(\beta)$ at each fixed lattice volume L/a by

$$\frac{1}{g^2(\beta)} = \frac{\beta}{6} \sum_{m=0}^{n} C_m \left(\frac{6}{\beta}\right)^m , \tag{5.58}$$

similarly as in [218]. The order n of the polynomial may be chosen such that acceptable fits are obtained, however in this work we would like to estimate the systematic errors that come from various choices for n; see section 5.6.3.

Using the parametrized curves the discrete β-function (5.57) can be obtained for arbitrary $g^2(L)$ for fixed L/a and $s = 3/2$. Estimating the error on the interpolated values is straightforward because the interpolation is linear in the fit parameters C_m. Then assuming that corrections are linear in a^2/L^2 the continuum extrapolation can be performed.

5.6.3 Systematic error

In our previous work [155, 187] the polynomial order for the interpolation (5.58) was fixed at each lattice volume. However different choices lead to similarly acceptable interpolating fits and these in turn lead to slightly different continuum results. Even

dc_1357_16

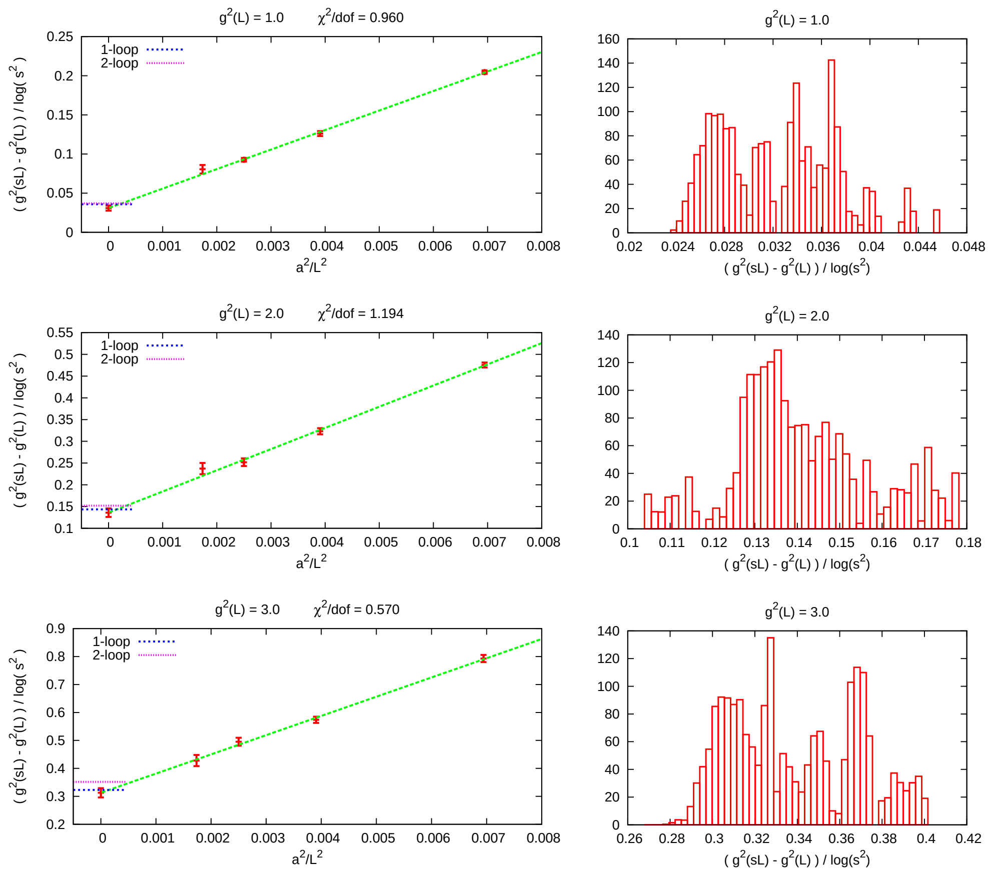

Figure 5.13: Right: the weighted histograms of all possible continuum extrapolations used for estimating the systematic uncertainty. Left: a representative example of the continuum extrapolations for $g^2(L) = 1.0, 2.0, 3.0$; the 1-loop and 2-loop results are also shown for comparison. All data is with $c = 3/10$ and using the linear combination method with $X = 1.75$.

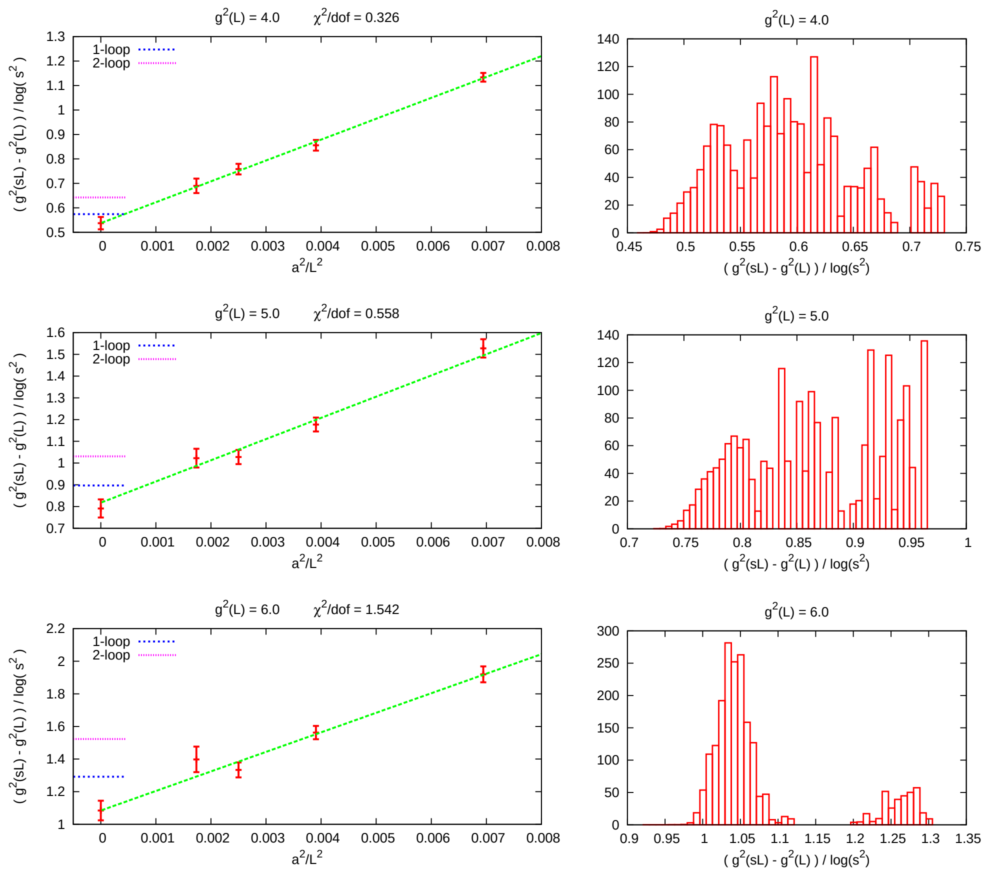

Figure 5.14: Right: the weighted histograms of all possible continuum extrapolations used for estimating the systematic uncertainty. Left: a representative example of the continuum extrapolations for $g^2(L) = 4.0, 5.0, 6.0$; the 1-loop and 2-loop results are also shown for comparison. All data is with $c = 3/10$ and using the linear combination method with $X = 1.75$.

though the final continuum result varies only a bit and generally within 1-σ of the statistical error in the current work we would like to estimate the systematic error as precisely as possible. In order to achieve this the histogram method introduced in [7] is used. There are two sources of systematic uncertainties. First, it is a priori unknown what interpolation function to use for the renormalized coupling as a function of β at fixed lattice volumes, and second, one may perform continuum extrapolations using 3 or 4 lattice spacings.

We interpolate using (5.58) for each lattice volume, 12^4, 16^4, 18^4, 20^4, 24^4, 30^4, 36^4, with three choices of polynomial orders, $n = 4, 5$ and 6. All together these produce $3^7 = 2187$ combination of interpolations and correspondingly lead to 2187 different continuum results. Since the data on different volumes at different β are all independent we perform a Kolmogorov-Smirnov test on the 2187 interpolations and demand that only those assignments of polynomial orders are allowed to which the Kolmogorov-Smirnov test assigns at least a 30% probability, similarly to [176].

The Kolmogorov-Smirnov test is applied as follows [176]. The χ^2 values of independent fits are distributed according to the χ^2-distribution. The goodness of fits, or q-values, are on the other hand distributed uniformly. The Kolmogorov-Smirnov test is an estimate of the probability that the actual measured q-values were indeed distributed uniformly. The cumulative distribution function of the uniform distribution is a straight line and the Kolmogorov-Smirnov test takes as input the largest distance between the actual measured cumulative distribution function and the expected cumulative distribution function (straight line). Call this largest distance D. Then the Kolmogorov-Smirnov probability is defined by

$$P = Q\left(D\left(\sqrt{N} + 0.12 + \frac{0.11}{\sqrt{N}}\right)\right), \qquad Q(x) = 1 - \vartheta_4\left(e^{-2x^2}\right) \tag{5.59}$$

where ϑ_4 is the 4^{th} Jacobi elliptic function and N is the sample size.

The Kolmogorov-Smirnov test with $P > 0.3$ reduced the total number of allowed interpolations from 2187 to 1233 as far as 4 lattice spacings are concerned corresponding to $12^4 \to 18^4$, $16^4 \to 24^4$, $20^4 \to 30^4$ and $24^4 \to 36^4$.

In order to include the systematic uncertainty from the continuum *extrapolation* itself, as opposed to the *interpolation* at fixed lattice volume, we consider dropping the roughest lattice spacing corresponding to $12^4 \to 18^4$ and use only $16^4 \to 24^4$, $20^4 \to 30^4$ and $24^4 \to 36^4$. From the 1233 continuum extrapolations using 4 lattice spacings only those extrapolations using 3 lattice spacings are kept to which again the Kolmogorov-Smirnov test assigns a probability larger than 30%, in terms of the 5 independent volumes, $16^4, 20^4, 24^4, 30^4, 36^4$. This test leads to 813 continuum extrapolations using 3 lattice spacings. Some of these are of course the same, but needs to be counted in order to have the proper weight in the final histogram.

The $1233 + 813 = 2046$ continuum results at each $g^2(L)$ can be binned in a weighted histogram and the weight can be the goodness of the fit, a weight provided by the Akaike information criterion (AIC) or no weight at all. If a fit has p free parameters its associated AIC weight is $\sim \exp(-\chi^2/2 - p)$. Examples of AIC-weighted histograms are shown in figures 5.13-5.14.

Our continuum central values at each $g^2(L)$ are the medians of the histograms and the systematic uncertainty can then be determined by counting 68% of the total starting symmetrically from the central value. The three types of weights lead to compatible results and for our final results we use the AIC-weighted histograms.

The systematic and statistical errors are of the same order, there is never a larger factor between them than two.

5.6.4 Final results

At 6 chosen values of $g^2(L)$ the histograms of the discrete β-function for all continuum extrapolations are shown in the right panels of figures 5.13-5.14. On the left we show typical continuum extrapolations from within a $1-\sigma$ systematic uncertainty around the median of the histograms. Clearly, all 4 lattice spacings are in the scaling region and nicely fit on a straight line with good χ^2/dof. In fact, the choice $X = 1.75$ was motivated by exactly the requirement that all 4 lattice spacings should be in the scaling region. This is not a sharp requirement, one may choose any value in the approximate range $1.6 < X < 1.9$.

It is quite instructive to look at the details of these figures and discuss the source of the most important systematic error, the continuum extrapolation. Our theory is a confining one in which large bare couplings (small βs) correspond to large lattice spacings. As table 5.3 shows large renormalized couplings are obtained with large lattice volumes and small β values. Thus, for a given renormalized coupling one reaches the continuum limit by increasing both β and the lattice volume. Since the largest volume, independently of β, was 36^4, large renormalized couplings correspond within our parameter set to large lattice spacings and obviously large cutoff effects.

It is of obvious interest to turn this qualitative statement to a quantitative one and to determine the size of the systematic uncertainty related to this question. Most importantly, we want to know where to stop with the present lattice sizes because no controlled continuum extrapolation can be carried out any further. As our $g^2 = 6$ case illustrates for this large value of the renormalized coupling one has a two peak structure for the histogram. The two peaks are the result of the significant difference between using only the finer lattices with 3 points or taking 4 points (including also the coarsest lattices) for the continuum extrapolations. This phenomenon clearly indicates that the results from the coarsest lattices are starting to deviate from the a^2 scaling showed by the finer lattices. The difference between the peaks still quantifies the systematic uncertainty for $g^2 = 6$ and tells us that for even larger g^2 values the control over this systematic effect could be lost and finer lattices with larger lattice volumes are needed.

The discrete β-function may reliably be calculated in (continuum) perturbation theory for small values of the renormalized coupling. In terms of the well-known infinitesimal 1 and 2 loop β-function coefficients, b_1 and b_2 the discrete variant is given by

$$\frac{g^2(sL) - g^2(L)}{\log(s^2)} = b_1 \frac{g^4(L)}{16\pi^2} + \left(b_1^2 \log(s^2) + b_2\right) \frac{g^6(L)}{(16\pi^2)^2} + \dots \tag{5.60}$$

As noted already in our finite volume gradient flow scheme only b_1 is the same as in every other well-defined scheme. The reason is a well-understood feature of the finite 4-volume or femtoworld [155, 187]. Nevertheless we include not only the 1-loop continuum β-function but also the 2-loop approximation in our comparisons, even though strictly speaking agreement is only expected with the 1-loop result.

Had we not used the linear combination (5.56) only 3 lattice spacings would have been in the scaling region, $16^4 \to 24^4$, $20^4 \to 30^4$ and $24^4 \to 36^4$ assuming a fit linear in $O(a^2/L^2)$. As mentioned in section 5.6.1 tree-level improvement [214] did not reduce the slope of the continuum extrapolations as dramatically as for $N_f = 4$ in our previous study. The reason is presumably that the larger fermion content results in larger fermionic contributions which are, of course, completely absent from the tree-level expressions. We illustrate both points, the smaller scaling region without employing the linear combination (5.56) and the less effective tree-level improvement

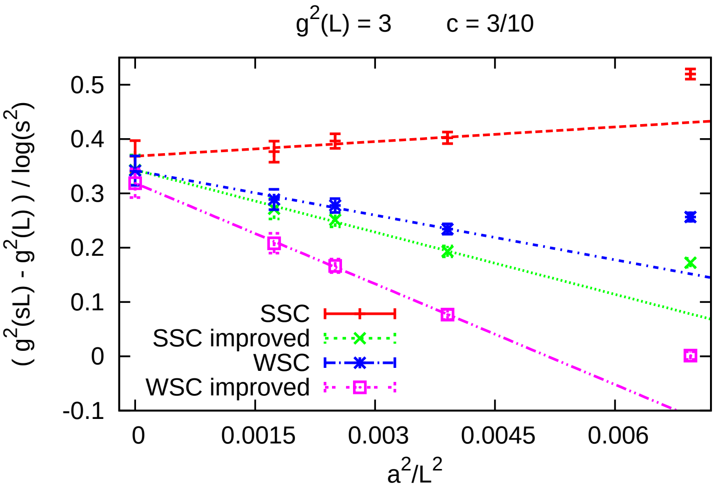

Figure 5.15: Comparison of the tree-level improved and unimproved continuum extrapolations for the SSC and WSC cases at $c = 3/10$. Clearly the roughest lattice spacing corresponding to $12^4 \to 18^4$ is not in the scaling region. The choice $X = 1.75$ does bring this point also into the scaling region however; see text for details.

in figure 5.15. Clearly, the continuum results are always consistent, as they should be, the various choices (improvement vs. non-improvement, linear combination vs. no linear combination) only affect the slopes of the extrapolations and the size of the scaling region.

In figure 5.16 we illustrate another aspect mentioned in section 5.6.1, namely c-dependence. Different choices of c define different schemes, i.e. the β-function will be c-dependent. For small coupling the difference should be very small since regardless of what c is, agreement is expected with the perturbative 1-loop result. Furthermore, the expectation is that a smaller c leads to smaller statistical errors because of smaller autocorrelations and also to larger cut-off effects because of the smaller flow time t. This is illustrated in figure 5.16 where the continuum extrapolation is shown for $g^2 = 3$ and both for $c = 3/10$ and $c = 1/5$.

Finally, in figure 5.17 we show the continuum extrapolated β-function over the entire $0.9 < g^2 < 6.3$ range accessible to our simulations together with the 1-loop and 2-loop results. The linear combination method (5.56) was used with $X = 1.75$ and $c = 3/10$ was chosen. Our non-perturbative continuum result is in nice agreement with the perturbative results for small renormalized coupling and deviates from it for larger values. Most importantly, the deviation from the perturbative 1-loop result is downward. This could have been expected because at some higher N_f value we do expect a fixed point and by continuity one might argue that this is only possible if the running is slower than the monotonically increasing 1-loop result, at least for some N_f value which is not far below the conformal window. At $N_f = 8$ we do not see a sign of a fixed point in any case, at least in the explored range $0.9 < g^2 < 6.3$.

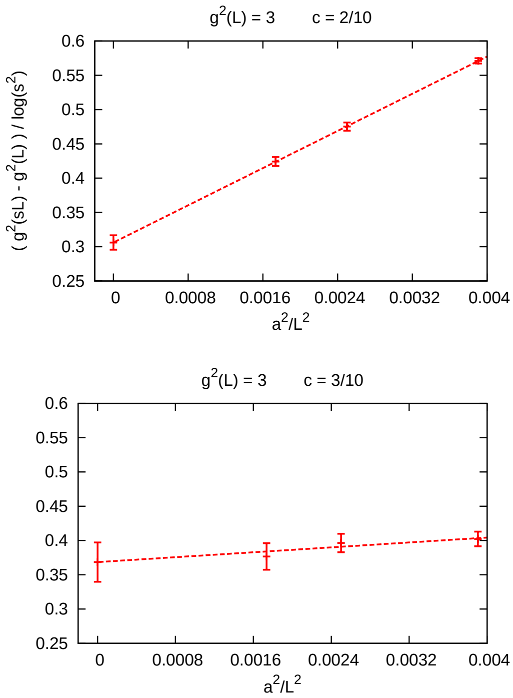

Figure 5.16: Continuum limit of the (unimproved) SSC setup at $g^2(L) = 3.0$; comparing $c = 2/10$ (left) and $c = 3/10$ (right). Clearly, as c increases the cut-off effects become smaller but the statistical errors grow. The continuum extrapolations do not have to agree since different c values correspond to different schemes.

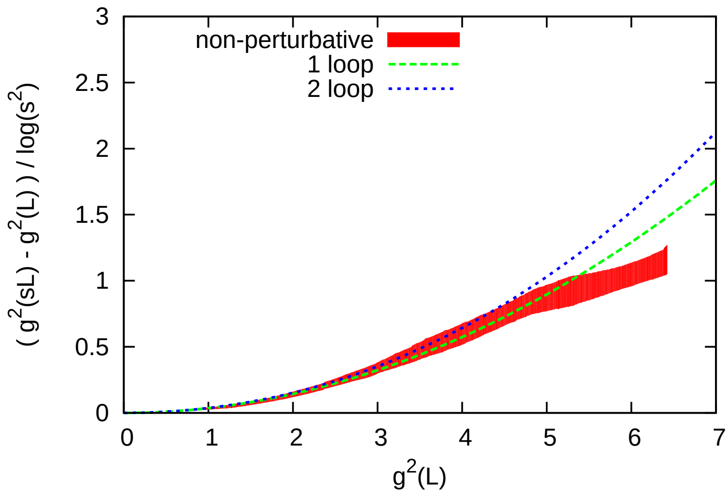

Figure 5.17: Our final result for the continuum extrapolated discrete β-function for $N_f = 8$.

5.7 Gradient flow running coupling $N_f = 12$

5.7.1 Introduction and motivation

Investigations of strongly coupled gauge theories with massless fermions in the fundamental or two-index symmetric (sextet) representation of the SU(3) color gauge group serve considerable theoretical interest with added relevance as important building blocks of composite Higgs theories beyond the Standard Model (BSM). Two complementary aspects of the composite Higgs paradigm are investigated in this large class of theories: (1) a near-conformal and unexpectedly light scalar particle, perhaps dilaton-like with mass at the Electroweak scale or (2) a parametrically light pseudo Nambu-Goldstone boson (PNGB) combined with partial compositeness for fermion mass generation to avoid the flavor problem. Both paradigms are based on strongly coupled gauge dynamics to address important aspects of conformal and chiral symmetries and their symmetry breaking patterns in BSM theories. The precise determination of near-conformal or conformal behavior of SU(3) gauge theory with twelve flavors is relevant for both paradigms.

(1) Light scalar, perhaps dilaton-like?

Near-conformal strong dynamics with spontaneous chiral symmetry breaking (χSB) is focused on its emergent light scalar with 0^{++} quantum numbers of the σ-meson, perhaps with dilaton-like properties. With early results reviewed in [240], this paradigm is very different from scaled up Quantum Chromodynamics (QCD) which was the prototype of old Higgs-less Technicolor. Comparing near-conformal models, with details explained in Figure 5.21, a light composite scalar of the massless SU(2) flavor doublet in the sextet fermion representation of SU(3) color was reported in [94, 240] whereas the $N_f = 8$ light scalar with fermions in the fundamental representation was discovered in [91] and confirmed recently [93]. The sextet model β-function, with the minimal flavor doublet required for the composite Higgs mechanism, indicates the closest position to the lower edge of the conformal window (CW) among recently investigated SU(3) gauge theories, exhibiting the lightest scalar accordingly. The β-function of the sextet theory with three massless flavors has a weakly coupled conformal fixed point close to the upper end of the CW [241] with apparent crossing into the CW between two and three flavors. In contrast, uncertainties in crossing into the CW with fermions in the fundamental representation appear to extend into the wider $N_f = 8$–12 flavor range. For example, it is not known if for more than eight flavors the theory gets very close to the CW with a much lighter scalar mass than at $N_f = 8$. Based on the findings of [158] and a similar zero in the β-function reported earlier [148], the $N_f = 12$ model has been investigated as a composite Higgs model built on a conformal fixed point inside the CW [52]. The importance of the question warrants independent determination [53].

(2) PNGB with partial compositeness? Challenges for the near-conformal light scalar paradigm to generate fermion masses and Yukawa couplings motivates the alternate PNGB scenario with a massless scalar boson emerging from vacuum misalignment of χSB as reviewed recently [242]. Model studies with a parametrically light Higgs based on $N_f = n_f + \nu_f$ fermion flavors in the fundamental representation of the SU(3) color gauge group could address the hierarchy problem and fermion mass generation with partial compositeness, if N_f is large enough to bring the theory inside the CW before mass deformations of conformal symmetries are turned on [242–244]. For the simple choice $n_f = 4$, the global flavor symmetry SU(4)×SU(4) is broken to the diagonal SU(4) flavor group and a Higgs-like scalar state is identified in the PNGB set via χSB. The custodial SO(4) symmetry of the Standard Model remains

protected [243, 244] while a large enough ν_f is required to bring the theory close to a strongly coupled IRFP with expectations of large baryon anomalous dimensions as the key ingredients of partial compositeness. The $N_f = 12$ choice with $n_f = 4$ and $\nu_f = 8$ for this PNGB paradigm is discussed in [52] building on the conformal fixed point of twelve flavors, warranting again independent confirmation.

5.7.2 Lattice implementation of the step β-function

The gradient flow based diffusion of the gauge fields of lattice configurations from Hybrid Monte Carlo (HMC) simulations became the method of choice for studying renormalization effects with great accuracy [154, 156, 182–186]. In particular, we adapted the method and introduced the scale-dependent renormalized gauge coupling $g^2(L)$ where the scale is set by the linear size L of the finite volume [155, 187]. This implementation is based on the gauge invariant trace of the non-Abelian quadratic field strength, $E(t) = -\frac{1}{2}\mathrm{Tr}F_{\mu\nu}F_{\mu\nu}(t)$, renormalized as a composite operator at gradient flow time t on the gauge configurations and measured from the discretized lattice implementation, as in [154] . Following [155, 187], we define the one-parameter family of renormalized non-perturbative gauge couplings for strongly coupled gauge theories built on the SU(N) color group with N_f massless dynamical fermions,

$$g_c^2(t(L)) = \frac{128\pi^2\langle t^2E(t)\rangle}{3(N^2-1)(1+\delta(c))}\ , \tag{5.61}$$

where the volume-dependent gradient flow time $t(L)$ is set by the constant $c = \sqrt{8t}/L$ from the one-parameter family of renormalization schemes, with $c = 0.2$ chosen in this work. The factor $\delta(c)$ is given by equation (4.4) and is chosen to match $g_c^2(t(L))$ to the conventional coupling $g^2_{\overline{\mathrm{MS}}}(t(L))$ in leading order of perturbation theory for any choice of c and with periodic boundary conditions for the gauge fields in all four directions. The origin of the 3rd Jacobi elliptic function ϑ in Eq. (4.4) was explained in [155] including the treatment of zero modes from periodic gauge fields in finite volumes [99, 199, 202, 203, 245].

A scale-dependent renormalized gauge coupling $g^2(L)$ was introduced earlier to probe the step β-function, defined as $(g^2(sL) - g^2(L))/\log(s^2)$ for some preset finite scale change s in the linear physical size L of the four-dimensional volume in the continuum limit of lattice discretization [138, 217]. The gauge coupling $g^2(L)$ for the determination of the step β-function is identified in our case with the definition in Eq. (5.61) as we drop the preset label c in the notation and $t(L)$ is simply replaced by L. The renormalization scheme with the preset choice $c = 0.2$ and the preset scale factor $s = 2$ in our work is identical to the one of the previous study [158] including the boundary conditions on gauge fields and fermion fields. In the continuum limit, the monotonic function $g^2(L)$ implies in any of the volume-dependent schemes that a selected value of the renormalized gauge coupling sets the physical size L measured in some particular dimensionful physical unit. Fixed physical size L on the lattice is equivalent to holding $g^2(L)$ fixed at some selected value as the lattice spacing a is varied and the fixed physical length L is held by the variation of the dimensionless linear scale L/a as the bare lattice coupling is tuned without changing the selected fixed value of the renormalized gauge coupling. The continuum limit at fixed $g^2(L)$ is obtained by $a^2/L^2 \to 0$ extrapolation of the residual cut-off dependence in the step β-function at the target gauge coupling.

In the convention we use, asymptotic freedom in the UV regime corresponds to a positive step β-function given by the perturbative loop expansion for small values of the renormalized coupling. In the infinitesimal derivative limit $s \to 1$ the step β-function turns into the conventional one. If the conventional β-function of the theory possesses a fixed point, the step β-function will have a zero at the same critical gauge coupling g_*^2 as well. The scale-dependence of the gauge coupling $g^2(L)$ can be determined from repeated application of the step β-function starting at some scale L_0 set by the initial gauge coupling $g^2(L_0)$ we choose.

5.7.3 Simulation setup

The algorithmic details of our new $N_f = 12$ simulations are similar to [155, 160]. Periodic boundary conditions already defined on the gauge fields, the fermion fields are chosen to be anti-periodic in all four directions. We utilize the staggered fermion action with massless fermions and 4 steps of stout smearing with stout parameter $\varrho = 0.12$ on the gauge links [182]. The gauge action is the tree-level improved Symanzik action [212, 213]. The evolution along a trajectory of the Hybrid Monte Carlo algorithm [237] is implemented with multiple time scales [238] and Omelyan integrator [239]. For integration along the gradient flow we use the tree-level improved Symanzik action based discretization scheme. The observable $E(t)$ is discretized as in [154].

The final 28 runs of Table 5.4 ranged in length between 5,000 and 20,000 time units of molecular dynamics. The statistical analysis of the renormalized gauge coupling of each run followed [246] and used similar software. Autocorrelation times were measured for each run in two independent ways, using estimates from the autocorrelation function of each run, and from Jackknifed blocking procedure. Errors on the renormalized couplings were consistent from the two procedures and the one from autocorrelation functions is listed in Table 5.4. Each run went through thermalization and these segments were not included in the analysis. For detection of residual thermalization effects the replica method of [246] was used in the analysis. All 28 runs passed Q value tests when mean values and statistical errors of the replica segments were compared for thermal and other variations.

	Target A		Target B		Target C	
L/a	$6/g_0^2$	g^2	$6/g_0^2$	g^2	$6/g_0^2$	g^2
16	3.1519	5.9801(29)	3.0830	6.1786(39)	3.0110	6.3930(30)
32	3.1519	5.9952(79)	3.0830	6.1597(64)	3.0110	6.3233(74)
18	3.1510	5.9767(40)	3.0785	6.1871(37)	3.0055	6.3909(51)
36	3.1510	6.0101(71)	3.0785	6.1840(81)	3.0055	6.3446(64)
20	3.1499	5.9828(64)	3.0704	6.1922(64)	2.9896	6.3942(59)
40	3.1499	6.0419(73)	3.0704	6.2137(67)	2.9896	6.4000(67)
24	3.1480	5.9784(68)	3.0680	6.1861(55)	2.9800	6.3976(60)
48	3.1480	6.0758(84)	3.0680	6.2497(109)	2.9800	6.4404(122)
28			3.0698	6.1839(58)	2.9819	6.3900(37)
56			3.0698	6.2792(142)	2.9819	6.4610(124)

Table 5.4: The final 28 runs are tabulated with 14 tuned runs and 14 paired steps.

We targeted the step β-function at three preselected values of the renormalized gauge coupling to cover the interval where the IRFP was reported [158]. In Table 5.4 results are shown for gauge ensembles from the three target groups A, B, C of the

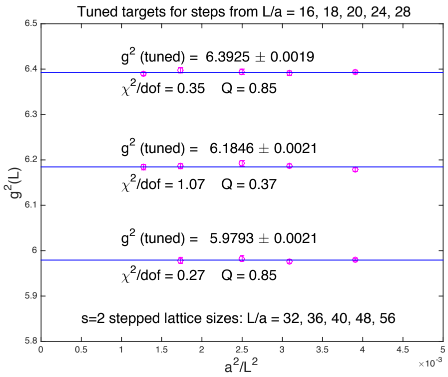

Figure 5.18: The statistical significance of precise tuning to three targeted gauge couplings is shown by fitting a constant to each g^2 at the lower L/a values of the steps.

final run sets. The 28 runs were grouped into 14 steps of pairs where the lower L/a value was precisely tuned to the target value of the renormalized gauge coupling. The higher L/a volume at the doubled physical size determined the step β-function at finite lattice spacing. The first group with 4 steps is target A at $g^2(L) = 5.979(2)$ with $L/a = 16 \to 32, 18 \to 36, 20 \to 40, 24 \to 48$. Both target B at $g^2(L) = 6.185(2)$ and target C at $g^2(L) = 6.393(2)$ have an added fifth step of $L/a = 28 \to 56$ for more robust continuum extrapolation. Precise tuning for g_0^2 of the 14 steps of the three targets eliminated the largest systematic uncertainty in the step β-function from model-dependent interpolation in the bare gauge coupling. Figure 5.18 shows the remarkable accuracy of tuning for the three targets at better than per mille accuracy level, like for the entries of Table 5.4.

5.7.4 Continuum extrapolation

Cut-off effects have to be removed from the step β-functions at finite lattice spacing.

The leading cut-off effects are a^2/L^2 corrections in each $L/a \to 2L/a$ pair for the step β-function at the targeted renormalized couplings. Linear fits to the lattice step functions in a^2/L^2 allows continuum extrapolation to the $a^2/L^2 \to 0$ limit, as shown in Figure 5.19. For all three targets linear four-point fits of the step functions were used with consistently good χ^2 results.

The final results of our continuum step β-function are shown in Figure 5.20 with overwhelming statistical evidence against the IRFP of [158] in the targeted interval. Leaving open the existence of the IRFP in [158], a new study of the β-function appeared recently in a different renormalization scheme of the model and without our targeted goal [48].

5.7.5 Conclusions

Curiously, a conjectured inequality $f_{IR} \leq f_{UV}$ of the free energy comparing the infrared and ultraviolet limits in models with SU(N) color would predict an upper limit $N_f^{crit} \leq 4\sqrt{N^2 - 16/81}$ before the theory becomes conformal, numerically

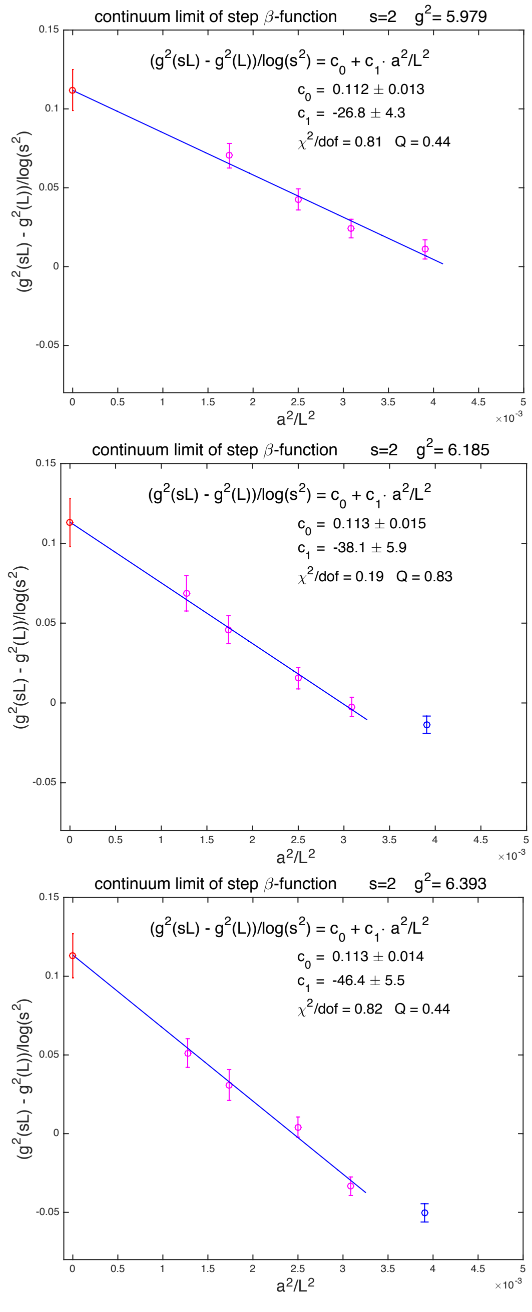

Figure 5.19: Linear fits in a^2/L^2 are shown as explained in the text. The $16 \to 32$ steps of target B and target C are not included in the 4-point fits without any influence on the overwhelming statistical significance of the results. When they are included, the continuum step β-function drops lower by approximately one standard deviation with comparable errors and increased $\chi 2/\mathrm{dof} \sim 1.5$, perhaps hinting at sub-leading small a^4/L^4 cutoff corrections at low L/a when the renormalized gauge coupling gets stronger.

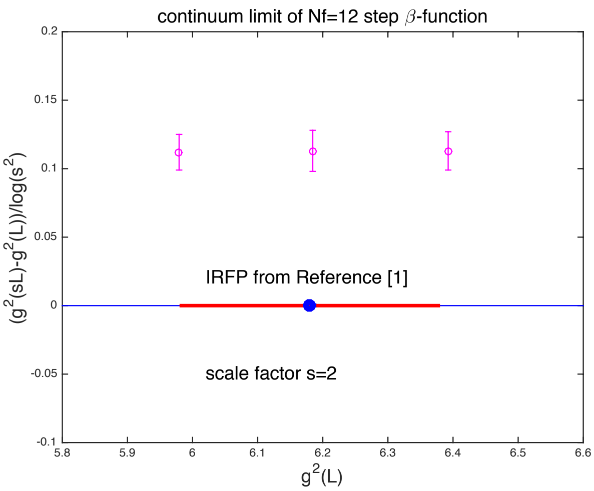

Figure 5.20: Our step β-function demonstrates that the conformal fixed point of [158] is eliminated in the targeted interval with overwhelming statistical evidence.

$N_f^{crit} \leq 11.87$ for the crossing point for $N = 3$ colors [247]. Avoiding the violation of the conjecture for the inequality of the free energy in the model would require a credible fixed point identified at strong coupling above the [6.0-6.4] interval.

Credible proof of conformal behavior based on the β-function requires two necessary steps in strongly coupled gauge theories. First, the critical gauge coupling g_*^2 has to be determined where the scheme-dependent β-function vanishes and signals the location of the conformal IRFP. The slope of the β-function at the fixed point is a scheme-independent scaling exponent ω which controls the leading conformal scaling corrections to fermion mass deformations close to the IRFP [44, 102, 240, 248]. The choice in scheme dependence can move the position of the conformal IRFP but cannot destroy its existence, or change the universal scaling exponent ω. We were unable to find in the published literature of the model any IRFP which would satisfy these demanding criteria.

Other lattice efforts to determine the precise position of the $N_f = 12$ model with respect to the conformal window were discussed in a recent review [35] surveying with extensive references the scaling analysis of the mass-deformed composite spectrum, the finite temperature phase transition, the study of the fermion mass anomalous dimension, and hunt for fixed point zeros in the β-function featuring the conformal IRFP discussed here. Contrary to [35], we do not find compelling evidence in the survey for conformal behavior in the model. Close to the CW, scaling analysis of the mass-deformed composite spectrum cannot be conclusive before the massless fermion limit and the continuum limit are taken under controlled conditions. If the misidentified near-conformal theory with χSB is forced to a small volume where the most basic condition $F \cdot L \gg 1$, set by the Goldstone decay constant F in the chiral limit, is violated and instead the gauge theory is squeezed into the $F \cdot L \ll 1$ condition, the only relevant non-conformal scale F is lost and the theory begins to show confused leading conformal exponents without consistent scaling correction exponent ω, a problem never critically addressed before.

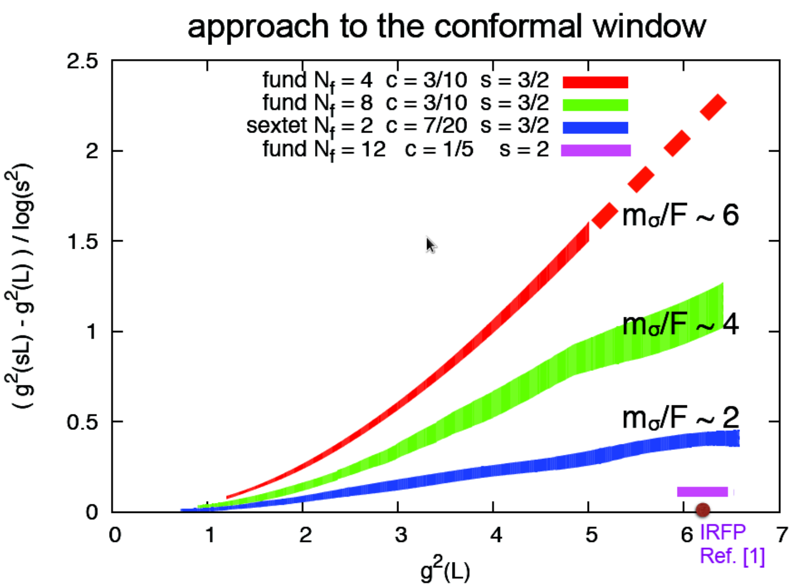

Figure 5.21: The continuum extrapolated discrete β-function for various $SU(3)$ models. Where available also the 0^{++} scalar mass in F units in the chiral limit is also estimated.

5.8 Running coupling summary

Using the finite volume gradient flow scheme the continuum β-functions of the fundamental $N_f = 4, 8, 12$ and the sextet $N_f = 2$ models were obtained. In these models we also have estimates for the m_σ/F ratio in the chiral limit. Here m_σ is the mass of the 0^{++} scalar. A curious correlation between this ratio and the β-function can be observed as summarized on figure 5.21.

As the flavor content approaches the conformal window the β-function becomes smaller smaller and the m_σ/F ratio becomes smaller and smaller as well. At the same time, the m_ϱ/F ratio is largely insensitive to the flavor content and $m_\varrho/F \sim 8$ for $SU(3)$ regardless of N_f and even the representation (fundamental or sextet) as long as the model is outside the conformal window. Hence as the conformal window is approached the ratio m_σ/m_ϱ becomes smaller and smaller. One might argue that the scalar becomes parameterically light relative to the rest of the spectrum as the conformal window is approached and the β-function becomes smaller and smaller. This is precisely the scenario of a dilaton-like scalar although it is not at all clear how the breaking of scale invariance indeed leads to a dilaton-like effective theory for the strongly interacting gauge theories we consider here [17, 18]. Nevertheless the numerical evidence so far seems to favor this scenario.

Bibliography

[1] G. Aad *et al.* [ATLAS Collaboration], Phys. Lett. B **716**, 1 (2012) [arXiv:1207.7214 [hep-ex]].

[2] S. Chatrchyan *et al.* [CMS Collaboration], Phys. Lett. B **716**, 30 (2012) [arXiv:1207.7235 [hep-ex]].

[3] E. Aprile *et al.* [XENON100 Collaboration], Phys. Rev. Lett. **109**, 181301 (2012) [arXiv:1207.5988 [astro-ph.CO]].

[4] D. S. Akerib *et al.* [LUX Collaboration], Phys. Rev. Lett. **112**, 091303 (2014) [arXiv:1310.8214 [astro-ph.CO]].

[5] R. Agnese *et al.* [CDMS Collaboration], Phys. Rev. Lett. **111**, no. 25, 251301 (2013) [arXiv:1304.4279 [hep-ex]].

[6] R. Agnese *et al.* [SuperCDMS Collaboration], Phys. Rev. Lett. **112**, no. 24, 241302 (2014) [arXiv:1402.7137 [hep-ex]].

[7] S. Durr *et al.*, Science **322**, 1224 (2008) [arXiv:0906.3599 [hep-lat]].

[8] S. Weinberg, Phys. Rev. D **19**, 1277 (1979).

[9] L. Susskind, Phys. Rev. D **20**, 2619 (1979).

[10] S. Dimopoulos and L. Susskind, Nucl. Phys. B **155**, 237 (1979).

[11] C. T. Hill and E. H. Simmons, Phys. Rept. **381**, 235 (2003) Erratum: [Phys. Rept. **390**, 553 (2004)] [hep-ph/0203079].

[12] M. E. Peskin and T. Takeuchi, Phys. Rev. D **46**, 381 (1992).

[13] F. Sannino and K. Tuominen, Phys. Rev. D **71**, 051901 (2005) [hep-ph/0405209].

[14] D. D. Dietrich and F. Sannino, Phys. Rev. D **75**, 085018 (2007) [hep-ph/0611341].

[15] Z. Fodor, K. Holland, J. Kuti, D. Nogradi, C. Schroeder and C. H. Wong, Phys. Lett. B **718**, 657 (2012) [arXiv:1209.0391 [hep-lat]].

[16] T. Appelquist and Y. Bai, Phys. Rev. D **82**, 071701 (2010) [arXiv:1006.4375 [hep-ph]].

[17] K. Yamawaki, M. Bando and K. i. Matumoto, Phys. Rev. Lett. **56**, 1335 (1986).

[18] B. Holdom and J. Terning, Phys. Lett. B **200**, 338 (1988).

[19] T. W. Appelquist, D. Karabali and L. C. R. Wijewardhana, Phys. Rev. Lett. **57**, 957 (1986).

[20] B. Holdom, Phys. Lett. B **150**, 301 (1985).

[21] T. Appelquist and L. C. R. Wijewardhana, Phys. Rev. D **36**, 568 (1987).

[22] E. Eichten and K. D. Lane, Phys. Lett. B **90**, 125 (1980).

[23] W. E. Caswell, Phys. Rev. Lett. **33**, 244 (1974).

[24] T. Banks and A. Zaks, Nucl. Phys. B **196**, 189 (1982).

[25] D. K. Hong, S. D. H. Hsu and F. Sannino, Phys. Lett. B **597**, 89 (2004) [hep-ph/0406200].

[26] D. D. Dietrich, F. Sannino and K. Tuominen, Phys. Rev. D **72**, 055001 (2005) [hep-ph/0505059].

[27] A. Belyaev, M. S. Brown, R. Foadi and M. T. Frandsen, Phys. Rev. D **90**, 035012 (2014) [arXiv:1309.2097 [hep-ph]].

[28] R. S. Chivukula, hep-ph/0011264.

[29] K. Lane, hep-ph/0202255.

[30] A. Martin, Subnucl. Ser. **46**, 135 (2011) [arXiv:0812.1841 [hep-ph]].

[31] F. Sannino, Acta Phys. Polon. B **40**, 3533 (2009) [arXiv:0911.0931 [hep-ph]].

[32] M. Piai, Adv. High Energy Phys. **2010**, 464302 (2010) [arXiv:1004.0176 [hep-ph]].

[33] T. DeGrand and A. Hasenfratz, Phys. Rev. D **80**, 034506 (2009) [arXiv:0906.1976 [hep-lat]].

[34] L. Del Debbio, Int. J. Mod. Phys. A **29**, 1445006 (2014).

[35] T. DeGrand, Rev. Mod. Phys. **88**, 015001 (2016) [arXiv:1510.05018 [hep-ph]].

[36] A. Deuzeman, M. P. Lombardo and E. Pallante, Phys. Lett. B **670**, 41 (2008) [arXiv:0804.2905 [hep-lat]].

[37] J. B. Kogut and D. K. Sinclair, Phys. Rev. D **81**, 114507 (2010) [arXiv:1002.2988 [hep-lat]].

[38] J. B. Kogut and D. K. Sinclair, Phys. Rev. D **85**, 054505 (2012) [arXiv:1111.3353 [hep-lat]].

[39] J. B. Kogut and D. K. Sinclair, Phys. Rev. D **84**, 074504 (2011) [arXiv:1105.3749 [hep-lat]].

[40] J. B. Kogut and D. K. Sinclair, Phys. Rev. D **90**, no. 1, 014506 (2014) [arXiv:1406.1524 [hep-lat]].

[41] J. B. Kogut and D. K. Sinclair, Phys. Rev. D **92**, no. 5, 054508 (2015) [arXiv:1507.00375 [hep-lat]].

[42] T. DeGrand, Phys. Rev. D **80**, no. 11, 114507 (2009) [arXiv:0910.3072 [hep-lat]].

[43] T. DeGrand, Phys. Rev. D **84**, 116901 (2011) [arXiv:1109.1237 [hep-lat]].

[44] Z. Fodor, K. Holland, J. Kuti, D. Nogradi, C. Schroeder and C. H. Wong, PoS LATTICE **2012**, 279 (2012) [arXiv:1211.4238 [hep-lat]].

[45] A. Cheng, A. Hasenfratz, Y. Liu, G. Petropoulos and D. Schaich, Phys. Rev. D **90**, no. 1, 014509 (2014) [arXiv:1401.0195 [hep-lat]].

[46] M. P. Lombardo, K. Miura, T. J. Nunes da Silva and E. Pallante, JHEP **1412**, 183 (2014) [arXiv:1410.0298 [hep-lat]].

[47] A. Athenodorou, E. Bennett, G. Bergner and B. Lucini, Phys. Rev. D **91**, no. 11, 114508 (2015) [arXiv:1412.5994 [hep-lat]].

[48] C.-J. D. Lin, K. Ogawa and A. Ramos, JHEP **1512**, 103 (2015) [arXiv:1510.05755 [hep-lat]].

[49] R. C. Brower, G. T. Fleming and H. Neuberger, Phys. Lett. B **721**, 299 (2013) [arXiv:1212.6190 [hep-lat]].

[50] H. Neuberger, Phys. Rev. D **90**, no. 11, 114501 (2014) [arXiv:1410.2820 [hep-lat]].

[51] R. Brower, A. Hasenfratz, C. Rebbi, E. Weinberg and O. Witzel, J. Exp. Theor. Phys. **120**, no. 3, 423 (2015) [arXiv:1410.4091 [hep-lat]].

[52] R. C. Brower, A. Hasenfratz, C. Rebbi, E. Weinberg and O. Witzel, Phys. Rev. D **93**, no. 7, 075028 (2016) [arXiv:1512.02576 [hep-ph]].

[53] Z. Fodor, K. Holland, J. Kuti, S. Mondal, D. Nogradi and C. H. Wong, Phys. Rev. D **94**, no. 9, 091501 (2016) doi:10.1103/PhysRevD.94.091501 [arXiv:1607.06121 [hep-lat]].

[54] A. Cheng, A. Hasenfratz and D. Schaich, Phys. Rev. D **85**, 094509 (2012) [arXiv:1111.2317 [hep-lat]].

[55] A. Patella, Phys. Rev. D **86**, 025006 (2012) [arXiv:1204.4432 [hep-lat]].

[56] A. Cheng, A. Hasenfratz, G. Petropoulos and D. Schaich, JHEP **1307**, 061 (2013) [arXiv:1301.1355 [hep-lat]].

[57] Z. Fodor, K. Holland, J. Kuti, D. Ngrdi and C. H. Wong, PoS LATTICE **2013**, 089 (2014) [arXiv:1402.6029 [hep-lat]].

[58] M. Garca Prez, A. Gonzlez-Arroyo, L. Keegan and M. Okawa, JHEP **1508**, 034 (2015) [arXiv:1506.06536 [hep-lat]].

[59] D. Nogradi, JHEP **1205**, 089 (2012) doi:10.1007/JHEP05(2012)089 [arXiv:1202.4616 [hep-lat]].

[60] L. Del Debbio, B. Lucini, A. Patella, C. Pica and A. Rago, arXiv:1111.4672 [hep-lat].

[61] S. Catterall, L. Del Debbio, J. Giedt and L. Keegan, PoS LATTICE **2011**, 068 (2011) [arXiv:1110.1660 [hep-ph]].

[62] F. Bursa, L. Del Debbio, D. Henty, E. Kerrane, B. Lucini, A. Patella, C. Pica and T. Pickup *et al.*, Phys. Rev. D **84**, 034506 (2011) [arXiv:1104.4301 [hep-lat]].

[63] S. Sint and P. Vilaseca, arXiv:1111.2227 [hep-lat].

[64] T. Appelquist, G. T. Fleming and E. T. Neil, Phys. Rev. D **79**, 076010 (2009) [arXiv:0901.3766 [hep-ph]].

[65] X. -Y. Jin and R. D. Mawhinney, PoS LAT **2009**, 049 (2009) [arXiv:0910.3216 [hep-lat]].

[66] Z. Fodor, K. Holland, J. Kuti, D. Nogradi, C. Schroeder, Phys. Lett. B **703**, 348 (2011) [arXiv:1104.3124 [hep-lat]].

[67] A. Hasenfratz, arXiv:1106.5293 [hep-lat].

[68] V. A. Novikov, M. A. Shifman, A. I. Vainshtein and V. I. Zakharov, Phys. Rept. **116**, 103 (1984) [Sov. J. Part. Nucl. **17**, 204 (1986)] [Fiz. Elem. Chast. Atom. Yadra **17**, 472 (1986)].

[69] A. B. Zamolodchikov and A. B. Zamolodchikov, Annals Phys. **120**, 253 (1979).

[70] J. Balog and A. Hegedus, J. Phys. A A **37**, 1881 (2004) [hep-th/0309009].

[71] J. Balog and A. Hegedus, Nucl. Phys. B **725**, 531 (2005) [hep-th/0504186].

[72] J. Balog and A. Hegedus, Nucl. Phys. B **829**, 425 (2010) [arXiv:0907.1759 [hep-th]].

[73] F. D. M. Haldane, Phys. Lett. A **93**, 464 (1983).

[74] F. D. M. Haldane, Phys. Rev. Lett. **50**, 1153 (1983).

[75] W. Bietenholz, A. Pochinsky and U. J. Wiese, Phys. Rev. Lett. **75**, 4524 (1995) [hep-lat/9505019].

[76] M. Bogli, F. Niedermayer, M. Pepe and U. -J. Wiese, arXiv:1112.1873 [hep-lat].

[77] M. Luscher, Nucl. Phys. B **200**, 61 (1982).

[78] G. Bhanot, R. F. Dashen, N. Seiberg and H. Levine, Phys. Rev. Lett. **53**, 519 (1984).

[79] S. Caracciolo, R. G. Edwards, A. Pelissetto and A. D. Sokal, Nucl. Phys. B **403**, 475 (1993) [hep-lat/9205005].

[80] A. Patrascioiu and E. Seiler, Nucl. Phys. Proc. Suppl. **30**, 184 (1993).

[81] M. Hasenbusch, Phys. Rev. D **53**, 3445 (1996) [hep-lat/9507008].

[82] W. Bietenholz, U. Gerber, M. Pepe and U. -J. Wiese, JHEP **1012**, 020 (2010) [arXiv:1009.2146 [hep-lat]].

[83] F. Niedermayer, Phys. Rev. Lett. **61**, 2026 (1988).

[84] U. Wolff, Phys. Rev. Lett. **62**, 361 (1989).

[85] B. Berg and M. Luscher, Nucl. Phys. B **190**, 412 (1981).

[86] J. Balog, F. Niedermayer and P. Weisz, Nucl. Phys. B **824**, 563 (2010) [arXiv:0905.1730 [hep-lat]].

[87] J. Balog, F. Niedermayer and P. Weisz, Phys. Lett. B **676**, 188 (2009) [arXiv:0901.4033 [hep-lat]].

[88] H. Gies and J. Jaeckel, Eur. Phys. J. C **46**, 433 (2006) [hep-ph/0507171].

[89] D. B. Kaplan, J. -W. Lee, D. T. Son and M. A. Stephanov, Phys. Rev. D **80**, 125005 (2009) [arXiv:0905.4752 [hep-th]].

[90] J. Braun, C. S. Fischer and H. Gies, Phys. Rev. D **84**, 034045 (2011) [arXiv:1012.4279 [hep-ph]].

[91] Y. Aoki *et al.* [LatKMI Collaboration], Phys. Rev. D **89**, 111502 (2014) [arXiv:1403.5000 [hep-lat]].

[92] E. Rinaldi [LSD Collaboration], arXiv:1510.06771 [hep-lat].

[93] T. Appelquist *et al.*, Phys. Rev. D **93**, no. 11, 114514 (2016) [arXiv:1601.04027 [hep-lat]].

[94] Z. Fodor, K. Holland, J. Kuti, D. Nogradi and C. H. Wong, PoS LATTICE **2013**, 062 (2014) [arXiv:1401.2176 [hep-lat]].

[95] Z. Fodor, K. Holland, J. Kuti, S. Mondal, D. Nogradi and C. H. Wong, PoS LATTICE **2014**, 270 (2015) [arXiv:1501.06607 [hep-lat]].

[96] Z. Fodor, K. Holland, J. Kuti, S. Mondal, D. Nogradi and C. H. Wong, PoS LATTICE **2014**, 244 (2015) [arXiv:1502.00028 [hep-lat]].

[97] R. Foadi, M. T. Frandsen and F. Sannino, Phys. Rev. D **87**, no. 9, 095001 (2013) [arXiv:1211.1083 [hep-ph]].

[98] H. Georgi, Phys. Rev. Lett. **98**, 221601 (2007) [hep-ph/0703260].

[99] M. Luscher, Nucl. Phys. B **219**, 233 (1983).

[100] P. van Baal and J. Koller, Annals Phys. **174**, 299 (1987).

[101] H. Leutwyler, Phys. Lett. B **189**, 197 (1987).

[102] L. Del Debbio and R. Zwicky, Phys. Rev. D **82**, 014502 (2010) [arXiv:1005.2371 [hep-ph]].

[103] L. Del Debbio and R. Zwicky, Phys. Lett. B **700**, 217 (2011) [arXiv:1009.2894 [hep-ph]].

[104] J. Gasser and H. Leutwyler, Annals Phys. **158**, 142 (1984).

[105] A. Amato, T. Rantalaiho, K. Rummukainen, K. Tuominen and S. Thtinen, PoS LATTICE **2015**, 225 (2016) [arXiv:1511.04947 [hep-lat]].

[106] L. Del Debbio, B. Lucini, A. Patella, C. Pica and A. Rago, Phys. Rev. D **93**, no. 5, 054505 (2016) [arXiv:1512.08242 [hep-lat]].

[107] I. Caprini, G. Colangelo and H. Leutwyler, Phys. Rev. Lett. **96**, 132001 (2006) [hep-ph/0512364].

[108] R. Contino, C. Grojean, M. Moretti, F. Piccinini and R. Rattazzi, JHEP **1005**, 089 (2010) [arXiv:1002.1011 [hep-ph]].

[109] J. Soto, P. Talavera and J. Tarrus, Nucl. Phys. B **866**, 270 (2013) [arXiv:1110.6156 [hep-ph]].

[110] M. Golterman and Y. Shamir, Phys. Rev. D **94**, no. 5, 054502 (2016) [arXiv:1603.04575 [hep-ph]].

[111] L. Keegan, PoS LATTICE **2015**, 048 (2016) [arXiv:1508.01685 [hep-lat]].

[112] A. J. Hietanen, J. Rantaharju, K. Rummukainen and K. Tuominen, JHEP **0905**, 025 (2009) [arXiv:0812.1467 [hep-lat]].

[113] L. Del Debbio, B. Lucini, A. Patella, C. Pica and A. Rago, Phys. Rev. D **80**, 074507 (2009) [arXiv:0907.3896 [hep-lat]].

[114] L. Del Debbio, B. Lucini, A. Patella, C. Pica and A. Rago, Phys. Rev. D **82**, 014509 (2010) [arXiv:1004.3197 [hep-lat]].

[115] L. Del Debbio, B. Lucini, A. Patella, C. Pica and A. Rago, Phys. Rev. D **82**, 014510 (2010) [arXiv:1004.3206 [hep-lat]].

[116] F. Bursa *et al.*, Phys. Rev. D **84**, 034506 (2011) [arXiv:1104.4301 [hep-lat]].

[117] J. Giedt and E. Weinberg, Phys. Rev. D **85**, 097503 (2012) [arXiv:1201.6262 [hep-lat]].

[118] A. Hietanen, R. Lewis, C. Pica and F. Sannino, JHEP **1407**, 116 (2014) [arXiv:1404.2794 [hep-lat]].

[119] R. Arthur, V. Drach, M. Hansen, A. Hietanen, C. Pica and F. Sannino, arXiv:1602.06559 [hep-lat].

[120] Z. Fodor, K. Holland, J. Kuti, D. Nogradi and C. Schroeder, Phys. Lett. B **681**, 353 (2009) [arXiv:0907.4562 [hep-lat]].

[121] Y. Aoki *et al.* [LatKMI Collaboration], Phys. Rev. D **87**, no. 9, 094511 (2013) [arXiv:1302.6859 [hep-lat]].

[122] T. Appelquist *et al.* [LSD Collaboration], Phys. Rev. D **90**, no. 11, 114502 (2014) [arXiv:1405.4752 [hep-lat]].

[123] T. Appelquist *et al.*, arXiv:1204.6000 [hep-ph].

[124] Y. Aoki *et al.*, Phys. Rev. D **86**, 054506 (2012) [arXiv:1207.3060 [hep-lat]].

[125] Y. Aoki *et al.* [LatKMI Collaboration], Phys. Rev. Lett. **111**, no. 16, 162001 (2013) [arXiv:1305.6006 [hep-lat]].

[126] V. Drach, M. Hansen, A. Hietanen, C. Pica and F. Sannino, PoS LATTICE **2015**, 223 (2016) [arXiv:1508.04213 [hep-lat]].

[127] T. DeGrand, Y. Liu, E. T. Neil, Y. Shamir and B. Svetitsky, Phys. Rev. D **91**, 114502 (2015) [arXiv:1501.05665 [hep-lat]].

[128] A. Hietanen, C. Pica, F. Sannino and U. I. Sondergaard, Phys. Rev. D **87**, no. 3, 034508 (2013) [arXiv:1211.5021 [hep-lat]].

[129] C.-J. D. Lin, K. Ogawa, H. Ohki and E. Shintani, JHEP **1208**, 096 (2012) [arXiv:1205.6076 [hep-lat]].

[130] E. Itou, PTEP **2013**, no. 8, 083B01 (2013) [arXiv:1212.1353 [hep-lat]].

[131] G. de Divitiis *et al.* [Alpha Collaboration], Nucl. Phys. B **437**, 447 (1995) [hep-lat/9411017].

[132] A. Gonzalez-Arroyo, J. Jurkiewicz and C. P. Korthals-Altes, CPT-81-P-1336, C81-09-30-1.

[133] G. C. Rossi and M. Testa, Nucl. Phys. B **163**, 109 (1980).

[134] G. C. Rossi and M. Testa, Annals Phys. **148**, 144 (1983).

dc_1357_16

[135] M. Luscher, R. Sommer, P. Weisz and U. Wolff, Nucl. Phys. B **413**, 481 (1994) [hep-lat/9309005].

[136] K. Symanzik, Nucl. Phys. B **190**, 1 (1981).

[137] M. Luscher, Nucl. Phys. B **254**, 52 (1985).

[138] M. Luscher, R. Narayanan, P. Weisz and U. Wolff, Nucl. Phys. B **384**, 168 (1992) [hep-lat/9207009].

[139] A. D. Kennedy and S. Sint, PoS LATTICE **2015**, 274 (2016) [arXiv:1511.08539 [hep-lat]].

[140] J. Heitger *et al.* [ALPHA Collaboration], Nucl. Phys. Proc. Suppl. **106**, 859 (2002) [hep-lat/0110201].

[141] A. J. Hietanen, K. Rummukainen and K. Tuominen, Phys. Rev. D **80**, 094504 (2009) [arXiv:0904.0864 [hep-lat]].

[142] F. Bursa, L. Del Debbio, L. Keegan, C. Pica and T. Pickup, Phys. Rev. D **81**, 014505 (2010) [arXiv:0910.4535 [hep-ph]].

[143] T. DeGrand, Y. Shamir and B. Svetitsky, Phys. Rev. D **83**, 074507 (2011) [arXiv:1102.2843 [hep-lat]].

[144] J. Rantaharju, T. Rantalaiho, K. Rummukainen and K. Tuominen, Phys. Rev. D **93**, no. 9, 094509 (2016) [arXiv:1510.03335 [hep-lat]].

[145] T. Karavirta, J. Rantaharju, K. Rummukainen and K. Tuominen, JHEP **1205**, 003 (2012) [arXiv:1111.4104 [hep-lat]].

[146] F. Bursa, L. Del Debbio, L. Keegan, C. Pica and T. Pickup, Phys. Lett. B **696**, 374 (2011) [arXiv:1007.3067 [hep-ph]].

[147] T. Appelquist *et al.*, Phys. Rev. Lett. **112**, no. 11, 111601 (2014) [arXiv:1311.4889 [hep-ph]].

[148] T. Appelquist, G. T. Fleming and E. T. Neil, Phys. Rev. Lett. **100**, 171607 (2008) Erratum: [Phys. Rev. Lett. **102**, 149902 (2009)] [arXiv:0712.0609 [hep-ph]].

[149] Y. Shamir, B. Svetitsky and T. DeGrand, Phys. Rev. D **78**, 031502 (2008) [arXiv:0803.1707 [hep-lat]].

[150] T. DeGrand, Y. Shamir and B. Svetitsky, Phys. Rev. D **82**, 054503 (2010) [arXiv:1006.0707 [hep-lat]].

[151] T. DeGrand, Y. Shamir and B. Svetitsky, Phys. Rev. D **87**, 074507 (2013) [arXiv:1201.0935 [hep-lat]].

[152] T. DeGrand, Y. Shamir and B. Svetitsky, Phys. Rev. D **88**, no. 5, 054505 (2013) [arXiv:1307.2425].

[153] T. DeGrand, Y. Shamir and B. Svetitsky, Phys. Rev. D **85**, 074506 (2012) [arXiv:1202.2675 [hep-lat]].

[154] M. Lscher, JHEP **1008**, 071 (2010) Erratum: [JHEP **1403**, 092 (2014)] [arXiv:1006.4518 [hep-lat]].

[155] Z. Fodor, K. Holland, J. Kuti, D. Nogradi and C. H. Wong, JHEP **1211**, 007 (2012) [arXiv:1208.1051 [hep-lat]].

[156] M. Luscher and P. Weisz, JHEP **1102**, 051 (2011) [arXiv:1101.0963 [hep-th]].

[157] O. Bar and M. Golterman, Phys. Rev. D **89**, no. 3, 034505 (2014) Erratum: [Phys. Rev. D **89**, no. 9, 099905 (2014)] [arXiv:1312.4999 [hep-lat]].

[158] A. Cheng, A. Hasenfratz, Y. Liu, G. Petropoulos and D. Schaich, JHEP **1405**, 137 (2014) [arXiv:1404.0984 [hep-lat]].

[159] A. Hasenfratz, D. Schaich and A. Veernala, JHEP **1506**, 143 (2015) [arXiv:1410.5886 [hep-lat]].

[160] Z. Fodor, K. Holland, J. Kuti, S. Mondal, D. Nogradi and C. H. Wong, JHEP **1506**, 019 (2015) [arXiv:1503.01132 [hep-lat]].

[161] J. Rantaharju, Phys. Rev. D **93**, no. 9, 094516 (2016) [arXiv:1512.02793 [hep-lat]].

[162] A. Hasenfratz, Y. Liu and C. Y. H. Huang, arXiv:1507.08260 [hep-lat].

[163] Z. Fodor, K. Holland, J. Kuti, S. Mondal, D. Nogradi and C. H. Wong, JHEP **1509**, 039 (2015) [arXiv:1506.06599 [hep-lat]].

[164] G. 't Hooft, Nucl. Phys. B **153**, 141 (1979).

[165] W. J. Marciano, Phys. Rev. D **21**, 2425 (1980).

[166] Z. Fodor, K. Holland, J. Kuti, D. Nogradi, C. Schroeder and C. H. Wong, PoS LATTICE **2012**, 024 (2012) [arXiv:1211.6164 [hep-lat]].

[167] Z. Fodor, K. Holland, J. Kuti, S. Mondal, D. Nogradi and C. H. Wong, Phys. Rev. D **94**, no. 1, 014503 (2016) [arXiv:1601.03302 [hep-lat]].

[168] K. Kainulainen, K. Tuominen and J. Virkajarvi, Phys. Rev. D **75**, 085003 (2007) [hep-ph/0612247].

[169] R. Foadi, M. T. Frandsen, T. A. Ryttov and F. Sannino, Phys. Rev. D **76**, 055005 (2007) [arXiv:0706.1696 [hep-ph]].

[170] M. Antola, M. Heikinheimo, F. Sannino and K. Tuominen, JHEP **1003**, 050 (2010) [arXiv:0910.3681 [hep-ph]].

[171] K. Kainulainen, J. Virkajarvi and K. Tuominen, JCAP **1002**, 029 (2010) [arXiv:0912.2295 [astro-ph.CO]].

[172] E. Witten, Phys. Lett. B **117**, 324 (1982).

[173] S. L. Adler and W. A. Bardeen, Phys. Rev. **182**, 1517 (1969).

[174] R. S. Chivukula and T. P. Walker, Nucl. Phys. B **329**, 445 (1990).

[175] P. Langacker and G. Steigman, Phys. Rev. D **84**, 065040 (2011) [arXiv:1107.3131 [hep-ph]].

[176] S. Borsanyi *et al.*, Science **347**, 1452 (2015) [arXiv:1406.4088 [hep-lat]].

[177] W. J. Lee and S. R. Sharpe, Phys. Rev. D **60**, 114503 (1999) [hep-lat/9905023].

[178] C. Aubin and C. Bernard, Phys. Rev. D **68**, 034014 (2003) [hep-lat/0304014].

[179] S. R. Sharpe and R. S. Van de Water, Phys. Rev. D **71**, 114505 (2005) [hep-lat/0409018].

[180] G. Cacciapaglia and F. Sannino, JHEP **1404**, 111 (2014) [arXiv:1402.0233 [hep-ph]].

[181] S. Di Chiara, R. Foadi, K. Tuominen and S. Thtinen, Nucl. Phys. B **900**, 295 (2015) [arXiv:1412.7835 [hep-ph]].

[182] C. Morningstar and M. J. Peardon, Phys. Rev. D **69**, 054501 (2004) [hep-lat/0311018].

[183] R. Narayanan and H. Neuberger, JHEP **0603**, 064 (2006) [hep-th/0601210].

[184] M. Luscher, Commun. Math. Phys. **293**, 899 (2010) [arXiv:0907.5491 [hep-lat]].

[185] M. Luscher, PoS LATTICE **2010**, 015 (2010) [arXiv:1009.5877 [hep-lat]].

[186] R. Lohmayer and H. Neuberger, PoS LATTICE **2011**, 249 (2011) [arXiv:1110.3522 [hep-lat]].

[187] Z. Fodor, K. Holland, J. Kuti, D. Nogradi and C. H. Wong, PoS LATTICE **2012**, 050 (2012) [arXiv:1211.3247 [hep-lat]].

[188] P. Fritzsch and A. Ramos, JHEP **1310**, 008 (2013) [arXiv:1301.4388 [hep-lat]].

[189] P. Fritzsch and A. Ramos, PoS Lattice **2013**, 319 (2014) [arXiv:1308.4559 [hep-lat]].

[190] A. Ramos, PoS Lattice **2013**, 053 (2014) [arXiv:1308.4558 [hep-lat]].

[191] J. Rantaharju, PoS Lattice **2013**, 084 (2014) [arXiv:1311.3719 [hep-lat]].

[192] M. Lscher, JHEP **1406**, 105 (2014) [arXiv:1404.5930 [hep-lat]].

[193] A. Ramos, JHEP **1411**, 101 (2014) [arXiv:1409.1445 [hep-lat]].

[194] S. Borsanyi *et al.*, JHEP **1209**, 010 (2012) [arXiv:1203.4469 [hep-lat]].

[195] M. Asakawa *et al.* [FlowQCD Collaboration], Phys. Rev. D **90**, no. 1, 011501 (2014) Erratum: [Phys. Rev. D **92**, no. 5, 059902 (2015)] [arXiv:1312.7492 [hep-lat]].

[196] H. Suzuki, PTEP **2013**, 083B03 (2013) Erratum: [PTEP **2015**, 079201 (2015)] [arXiv:1304.0533 [hep-lat]].

[197] J. Koller and P. van Baal, Nucl. Phys. B **273**, 387 (1986).

[198] J. Koller and P. van Baal, Nucl. Phys. B **302**, 1 (1988).

[199] P. van Baal, Nucl. Phys. B **307**, 274 (1988) Erratum: [Nucl. Phys. B **312**, 752 (1989)].

[200] P. van Baal, Acta Phys. Polon. B **20**, 295 (1989).

[201] C. P. Korthals Altes, CPT-85/P-1806.

[202] A. Coste, A. Gonzalez-Arroyo, J. Jurkiewicz and C. P. Korthals Altes, Nucl. Phys. B **262**, 67 (1985).

[203] A. Coste, A. Gonzalez-Arroyo, C. P. Korthals Altes, B. Soderberg and A. Tarancon, Nucl. Phys. B **287**, 569 (1987).

[204] C. P. Korthals Altes, Nucl. Phys. Proc. Suppl. **10A**, 284 (1989).

[205] C. Bernard, Phys. Rev. D **71**, 094020 (2005) [hep-lat/0412030].

[206] C. Bernard, Phys. Rev. D **73**, 114503 (2006) [hep-lat/0603011].

[207] C. Bernard, M. Golterman and Y. Shamir, Phys. Rev. D **73**, 114511 (2006) [hep-lat/0604017].

[208] S. R. Sharpe, PoS LAT **2006**, 022 (2006) [hep-lat/0610094].

[209] Y. Shamir, Phys. Rev. D **75**, 054503 (2007) [hep-lat/0607007].

[210] C. Bernard, M. Golterman, Y. Shamir and S. R. Sharpe, Phys. Lett. B **649**, 235 (2007) [hep-lat/0603027].

[211] C. Bernard, M. Golterman and Y. Shamir, Phys. Rev. D **77**, 074505 (2008) [arXiv:0712.2560 [hep-lat]].

[212] K. Symanzik, Nucl. Phys. B **226**, 187 (1983).

[213] M. Luscher and P. Weisz, Commun. Math. Phys. **97**, 59 (1985) Erratum: [Commun. Math. Phys. **98**, 433 (1985)].

[214] Z. Fodor, K. Holland, J. Kuti, S. Mondal, D. Nogradi and C. H. Wong, JHEP **1409**, 018 (2014) [arXiv:1406.0827 [hep-lat]].

[215] J. A. M. Vermaseren, S. A. Larin and T. van Ritbergen, Phys. Lett. B **405**, 327 (1997) [hep-ph/9703284].

[216] C. Pica and F. Sannino, Phys. Rev. D **83**, 035013 (2011) [arXiv:1011.5917 [hep-ph]].

[217] M. Luscher, P. Weisz and U. Wolff, Nucl. Phys. B **359**, 221 (1991).

[218] F. Tekin *et al.* [ALPHA Collaboration], Nucl. Phys. B **840**, 114 (2010) [arXiv:1006.0672 [hep-lat]].

[219] D. Nogradi, Z. Fodor, K. Holland, J. Kuti, S. Mondal and C. H. Wong, PoS LATTICE **2014**, 328 (2014) [arXiv:1410.8801 [hep-lat]].

[220] C. Aubin and C. Bernard, Phys. Rev. D **68**, 074011 (2003) [hep-lat/0306026].

[221] J. Gasser and H. Leutwyler, Nucl. Phys. B **307**, 763 (1988).

[222] F. C. Hansen and H. Leutwyler, Nucl. Phys. B **350**, 201 (1991).

[223] M. Gell-Mann, R. J. Oakes and B. Renner, Phys. Rev. **175**, 2195 (1968).

[224] A. Deuzeman, M. P. Lombardo and E. Pallante, Phys. Rev. D **82**, 074503 (2010) [arXiv:0904.4662 [hep-ph]].

[225] T. Banks and A. Casher, Nucl. Phys. B **169**, 103 (1980).

[226] E. V. Shuryak and J. J. M. Verbaarschot, Nucl. Phys. A **560**, 306 (1993) [hep-th/9212088].

[227] P. H. Damgaard, Nucl. Phys. Proc. Suppl. **128**, 47 (2004) [hep-lat/0310037].

[228] J. J. M. Verbaarschot and T. Wettig, Ann. Rev. Nucl. Part. Sci. **50**, 343 (2000) [hep-ph/0003017].

[229] Z. Fodor, K. Holland, J. Kuti, D. Nogradi and C. Schroeder, PoS LATTICE **2008**, 066 (2008) [arXiv:0809.4890 [hep-lat]].

[230] U. M. Heller, Nucl. Phys. Proc. Suppl. **63**, 248 (1998) [hep-lat/9709159].

[231] J. Kripfganz and C. Michael, Nucl. Phys. B **314**, 25 (1989).

[232] M. Creutz, Phys. Rev. D **21**, 2308 (1980).

[233] E. Bilgici *et al.*, Phys. Rev. D **80**, 034507 (2009) [arXiv:0902.3768 [hep-lat]].

[234] U. M. Heller and F. Karsch, Nucl. Phys. B **251**, 254 (1985).

[235] G. P. Lepage and P. B. Mackenzie, Phys. Rev. D **48**, 2250 (1993) [hep-lat/9209022].

[236] P. Perez-Rubio and S. Sint, PoS LATTICE **2010**, 236 (2010) [arXiv:1011.6580 [hep-lat]].

[237] S. Duane, A. D. Kennedy, B. J. Pendleton and D. Roweth, Phys. Lett. B **195**, 216 (1987).

[238] J. C. Sexton and D. H. Weingarten, Nucl. Phys. B **380**, 665 (1992).

[239] T. Takaishi and P. de Forcrand, Phys. Rev. E **73**, 036706 (2006) [hep-lat/0505020].

[240] J. Kuti, PoS LATTICE **2013**, 004 (2014).

[241] T. A. Ryttov and R. Shrock, Phys. Rev. D **83**, 056011 (2011) [arXiv:1011.4542 [hep-ph]].

[242] G. Ferretti, JHEP **1606**, 107 (2016) [arXiv:1604.06467 [hep-ph]].

[243] L. Vecchi, arXiv:1506.00623 [hep-ph].

[244] T. Ma and G. Cacciapaglia, JHEP **1603**, 211 (2016) [arXiv:1508.07014 [hep-ph]].

[245] P. van Baal, Nucl. Phys. B **264**, 548 (1986).

[246] U. Wolff [ALPHA Collaboration], Comput. Phys. Commun. **156**, 143 (2004) Erratum: [Comput. Phys. Commun. **176**, 383 (2007)] [hep-lat/0306017].

[247] T. Appelquist, A. G. Cohen and M. Schmaltz, Phys. Rev. D **60**, 045003 (1999) [hep-th/9901109].

[248] L. Del Debbio, B. Lucini, A. Patella, C. Pica and A. Rago, Phys. Rev. D **82**, 014510 (2010) [arXiv:1004.3206 [hep-lat]].